IOWA STATE UNIVERSITY
Digital Repository

2009

Pressure distribution on the roof of a model low-rise building tested in a boundary layer wind tunnel

Matthew Robert Goliber
Iowa State University

Pressure distribution on the roof of a model low-rise building tested in a boundary layer wind tunnel

By

Matthew Robert Goliber

A thesis submitted to the graduate faculty

in partial fulfillment of the requirements for the degree of

MASTER OF SCIENCE

Major: Civil Engineering (Structural Engineering)

Program of Study Committee:

Sivalingam Sritharan, Co-major Professor
Partha Sarkar, Co-major Professor
Thomas Rudolphi
Terry Wipf

Iowa State University
Ames, Iowa
2009

Dedication

To my family

TABLE OF CONTENTS

Nomenclature

B……..Characteristic dimension of the structure

C_L…… Static aerodynamic force coefficient of lift

C_p…….Pressure coefficient

C(t)….. Dynamic pressure coefficient

$\overline{F}_L$ …... Mean lift force

P…….. Absolute pressure

$P_{ref.}$….. Reference pressure $= \frac{1}{2}\rho u^2$

P_i……..Dynamic pressure (i = 1 to n)

P_0…….Static pressure

P_s……. Static pressure

p(t)…...Dynamic pressure less static pressure $(P_i - P_0)$

R……..Specific gas constant

T…….. Absolute temperature

U….....Reference velocity at a reference height

U(t)….. Velocity at a reference height

ρ……...Air density = PR/T

Abstract

With three of the largest metropolitan areas in the United States along the Gulf coast (Houston, Tampa, and New Orleans), residential populations ever increasing due to the subtropical climate, and insured land value along the coast from Texas to the Florida panhandle greater than $500 billion, hurricane related knowledge is as important now as ever before. This thesis focuses on model low-rise building wind tunnel tests done in connection with full-scale low-rise building tests. Mainly, pressure data collection equipment and methods used in the wind tunnel are compared to pressure data collection equipment and methods used in the field.

Although the focus of this report is on the testing of models in the wind tunnel, the low-rise building in the field is located in Pensacola, Florida. It has a wall length of 48 feet, a width of 32 feet, a height of 10 feet, and a gable roof with a pitch of 1:3 and 68 pressure ports strategically placed on the surface of the roof. Built by Forest Products Laboratory (FPL) in 2002, the importance of the test structure has been realized as it has been subjected to numerous hurricanes. In fact, the validity of the field data is so important that the following thesis was necessary.

The first model tested in the Bill James Wind Tunnel for this research was a rectangular box. It was through the testing of this box that much of the basic wind tunnel and pressure data collection knowledge was gathered. Knowledge gained from Model 1 tests was as basic as how to: mount pressure tubes on a model, use a pressure transducer, operate the wind tunnel, utilize the pitot tube and reference pressure, and measure wind velocity. Model 1 tests also showed the importance of precise construction to produce precise pressure coefficients.

Model 2 was tested in the AABL Wind Tunnel at Iowa State University. This second model was a 22 inch cube which contained a total of 11 rows of pressure ports on its front and top faces. The purpose of Model 2 was to validate the tube length, tube diameter, port diameter, and pressure transducer used in the field. Also, Model 2 was used to study the effects of surface roughness on pressure readings.

A partial roof and wall of the low-rise building in the field was used as the third model. Similar to the second model, Model 3 was tested in the AABL Wind Tunnel. Initially, the objectives of the third model were to validate the pressure port protection device (PPPD) being used in the field and test the possibility of interpolating between pressure ports. But in the end, Model 3 was best used to validate the inconsistencies of the full-scale PPPD, validate the transducers used in the field, and prove the importance of scaling either all or none of the model.

Fourthly, Model 4 was a 1:16 model of the low-rise building itself. Based on the three previous model tests, Model 4 was instrumented with 202 pressure transducers to better understand: 1) the pressure distribution on the roof of the structure, 2) the affects of the fundamental test variables such as tube length, tube diameter, port diameter, transducer type, and surface roughness, 3) the affects of a scaled

PPPD, 4) the importance of wind angle of attack, and 5) the possibility of measuring pressure data and load data simultaneously.

In the end, the combination of all four model tests proved to be helpful in understanding the pressure data gathered on the roof of the low-rise building in the field. The two main recommendations for the field structure are for reevaluation of the PPPD design and slight redistribution of the pressure ports. The wind tunnel model tests show a need for these two modifications in order to gather more accurate field pressure data. Other than these two adjustments, the model tests show that the remaining data gathering system is currently accurate.

Chapter 1: Introduction

1.1 HURRICANE FACTS

The term "hurricane" is regionally specific and refers to a strong "tropical cyclone" located in the North Atlantic Ocean, the Northeast Pacific Ocean east of the dateline, or the South Pacific Ocean east of 160° east longitude. A "tropical cyclone" is "the generic term for a non-frontal synoptic scale low-pressure system over topical or subtropical waters with organized convection (i.e., thunderstorm activity) and definite cyclonic surface wind circulation" (NHC, 2009). A tropical cyclone becomes a tropical storm when it reaches winds of 39 mph. Depending on the region of the world, a tropical storm becomes a hurricane, typhoon, severe tropical storm, severe cyclonic storm, or tropical cyclone when it reaches winds of 74 mph or greater.

Once a tropical storm becomes a hurricane, it is classified using one of five different categories, according to the Saffir-Simpson hurricane scale as shown in Table 1.1. Note the description, the drop in barometric pressure, the increase in wind speed, and the potential damage from Category 1 to Category 5. As stated above, Hurricane Camille was classified as a Category 5 hurricane. This was the only Category 5 hurricane to reach the Gulf coast between 1900 and 2007. Of the remaining 39 major hurricanes to reach the Gulf coast, seven were of category 4 intensity, including the Galveston Hurricane (Geocities, 2009). Hurricane Katrina was classified as a Category 3 hurricane.

Table 1.1. Saffir-Simpson hurricane scale (NHC, 2009)

Category	Description	Barometric Pressure		Wind Speed		Storm Surge		Damage Potential
		(mb)	(in)	(km/hr)	(mph)	(m)	(ft)	
5	Devastating	<920	<27	>250	>150	>5.5	>18	Catastrophic Damage to Structures
4	Very Strong	920 - 944	27.00 - 27.90	211 - 249	131 - 155	4.0 - 5.5	13 - 18	Extreme Structural Damage
3	Strong	945 - 964	27.91 - 28.49	179 - 210	111 - 130	2.7 - 3.9	9 - 12	Extensive Structural Damage
2	Moderate	965 - 979	28.50 - 28.93	154 - 178	96 - 110	1.8 - 2.6	6 - 8	Moderate Damage to Houses
1	Weak	≥980	≥28.94	120 - 153	74 - 95	1.2 - 1.7	4 - 5	Minimal Damage to Vegetation

1.2 IMPACT OF HURRICANES

With three of the largest metropolitan areas in the United States along the Gulf coast (Houston, Tampa, and New Orleans), residential populations ever increasing due to the subtropical climate, and insured land value along the coast from Texas to the Florida panhandle greater than $500 billion (Geocities, 2009), hurricane related knowledge is as important now as ever before. Since 1900, forty

major hurricanes (category 3, 4, and 5 on the Saffir-Simpson scale as shown in Table 1.1) have affected the Gulf coast with the three most devastating being the Galveston Hurricane, Hurricane Camille, and Hurricane Katrina (Geocities, 2009). In the year 1900, the Galveston Hurricane wiped out the city of Galveston, Texas and claimed 6,000 lives. In 1969, Hurricane Camille (category 5 hurricane) reached measured wind gusts of 172 mph and it was believed to reach unrecorded wind gusts as high as 220 mph. Although small, Hurricane Camille remains the strongest hurricane to ever enter the United States mainland (Geocities, 2009). Finally, a few months after the 2005 devastation caused by Hurricane Katrina, it was estimated that the hurricane had claimed 1,336 lives and done $75 billion worth of damage.

Table 1.2. Summary of three gulf coast hurricanes (Wikepedia, 2009)

Hurricane	Season	Category	Lives Lost	Cost (2005 USD)
Galveston	1900	4	6,000	$99.4 billion
Camille	1969	5	296	$21.2 billion
Katrina	2005	3	1,336	$81 billion

1.3 HURRICANES AFFECTING PENSACOLA, FL

As of 2007, the city of Pensacola, located in the western panhandle region of Florida, had an estimated population of 54,283 (Citi-data, 2009). The major hurricanes which have made landfall near Pensacola in recent years include Hurricane Ivan in 2004 and Hurricane Dennis in 2005. Figure 1.1 illustrates the paths of Hurricanes Ivan and Dennis. Note the 65 mile radius of Pensacola shown on Figures 1.1 and 1.2. Hurricane Ivan destroyed 10,000 homes, heavily damaged another 27,000, and caused six billion dollars worth of damage in and around Pensacola. The following year, Hurricane Dennis routed itself just east of Pensacola, limiting the city to moderate damage (Wikipedia, 2009). Also note Figure 1.2, which illustrates the reoccurring tropical cyclone, tropical storm, and hurricane events that affected the Pensacola area from 2000 to 2007.

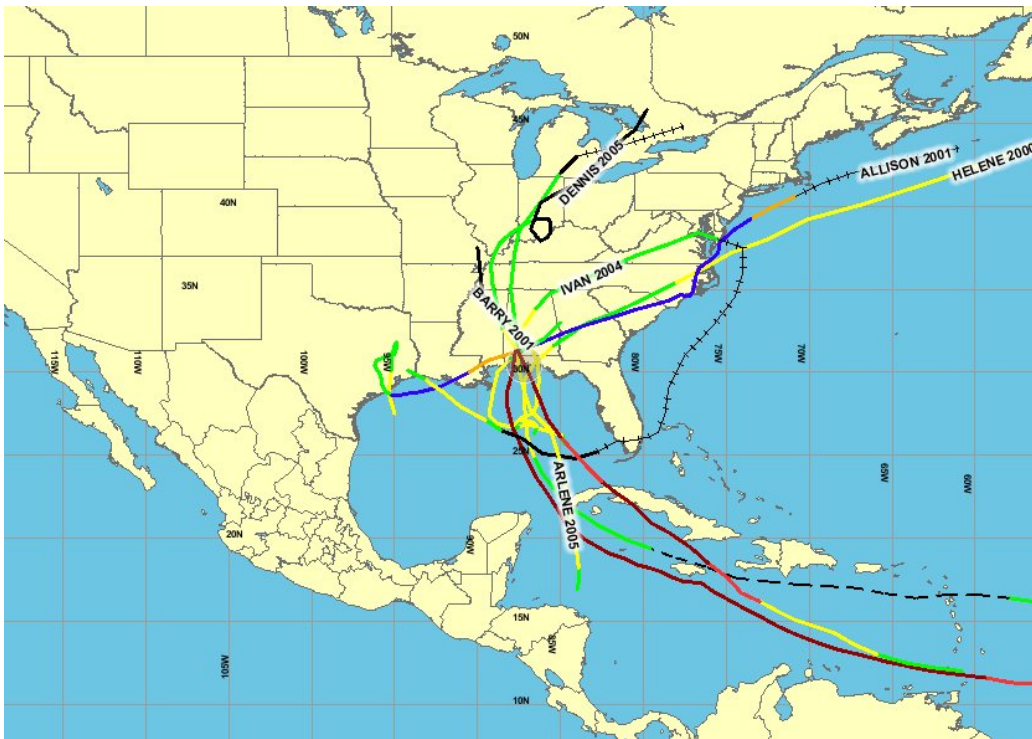**Figure 1.1. Hurricane paths of Ivan and Dennis through Pensacola, FL (NHC, 2009)**

Figure 1.2. Storm paths near Pensacola, FL from 2000 to 2007 (NHC, 2009)

1.4 PRELUDING RESEARCH

The numerous storm paths shown in Figure 1.2 reinforce the 21st century decision made by Forest Products Laboratory (FPL) to construct a low-rise building near Pensacola, Florida and research hurricane induced pressures and loads on the building. Following the initial construction of the building, the research sponsored by FPL can be separated into two phases. Phase I of the research was completed in 2007. In brief, the goal of phase I was to utilize finite element analysis to model the roof of the low-rise building and match pressure data as measured in the field with load cell data as measured in the field. It was hypothesized that a quality finite element model of the roof could bridge the gap between surface pressures on the roof and structural loads.

Unfortunately, when the pressures, as measured in the field, were applied to the finite element model, the finite element output load data did not match the load cell data measured in the field. The problem that surfaced pertained to the collected pressures on the roof. It was hypothesized that either the pressure ports in the field were spaced too far apart or the ports were collecting inaccurate data. Thus, phase II of the research began and will be presented in the following paper. The main goal of phase II was to determine the number of pressure ports needed in the field to accurately quantify the pressure distribution on the roof.

1.5 SCOPE OF RESEARCH

The initial task for this research project was to understand the method of measuring pressure at different pressure port locations on a structure. Lab pressure transducers, field pressure transducers, a rectangular-shaped test model, strategically placed pressure ports on the test model, the AABL Wind and Gust Tunnel, and the Bill James Wind Tunnel located in the WiST Laboratory at Iowa State University were used to accomplish the tasks. Although collecting pressure data in wind tunnels seems to be a routine task, it was important to demonstrate an understanding of the WiST Lab's measurement system and wind tunnels before moving forward with the tests because each experiment setup is unique.

While viewing results of the first task, it was clear that different variables could be affecting lab pressure readings. Thus, a second task was formulated. The physical aspect of this task was to construct and instrument a cube-shaped test model with various pressure tube lengths, tube diameters, port diameters, surface roughness, and types of transducers. The test model was subjected to a suburban boundary layer wind flow in the wind tunnel. The numerical aspect of this task was to quantify the affect of the following five different variables on pressure readings; port diameter, tube diameter, tube length, transducer type, and surface roughness. It was thought that these variables may be causing inaccurate pressure readings on the low-rise building in the field.

Thirdly, a partial roof and wall model was constructed and the pressure port hardware used in the field was mounted on the roof. Similar to the five variables stated above, it was thought that the pressure port protection device (PPPD) used to protect the pressure measuring system from moisture, was adversely affecting the pressure readings. Like the cube-shaped test model, the partial roof and wall model was subjected to a suburban boundary layer wind flow in the wind tunnel. As secondary objectives for this third task, the effects of shingles on pressure readings and the difference between the lab pressure transducer and field transducer were studied, but the main objective was to study the influence of the PPPD on pressure readings on the test roof.

To accomplish the fourth task and main research goal, a scaled version of the low-rise building itself was built and instrumented to better understand the pressure distribution on the roof. The model was subjected to a coastal boundary layer wind flow to model the wind flow in the field. To verify the conclusions made during the tests for tasks two and three, four pressure ports on the model had various tube lengths, tube diameters, port diameters, and transducers. Also, a scaled version of the PPPD was mounted on the model. Secondary objectives of the fourth test model were to reaffirm the affects of the tube length, tube diameter, port diameter, transducer types, and pressure port protection device, but the main goal of the fourth model was to study the pressure distribution on the roof of the model.

Chapter 2: Literature Review

The literature review presented in this chapter examines past research in the following topics: pressure measurements on low-rise buildings, the significance of reference (static) pressure, model testing and full-scale testing and the importance of proper scaling, properly instrumented and placed pressure taps, and possible ways to interpolate between measured pressure points on a structure. This review also summarizes previously studied wind pressures on hip roofs and low-rise building walls through verification of pressure measurements at critical points, mainly corners and edges.

2.1 PREDICTING PRESSURE

2.1.1 Pressure Prediction Methods

A few methods used to predict wind pressure for design purposes are: database-assisted design (DAD), the quasi-steady theory, orthogonal decomposition, and Equivalent Static Wind Load (ESWL) modeling.

Kopp et al. (2006) discuss the advantages and disadvantages (through a field study conducted at the University of Western Ontario) of database-assisted design for low-rise buildings. DAD's purpose is to directly utilize archived wind pressure time series on building envelopes from wind tunnel experiments for "structural analysis software for the building design (Kopp et al., 2006)." DAD analyzes structures beyond those obtained in the database through a series of interpolation. A data handling system is used to perform this interpolation. While significant advances have been made in data handling systems and storage capacity in the past 25 years, the complexity of wind turbulence and geometry of structures make it difficult to relate wind tunnel surface pressures to field surface pressures (Kopp et al., 2006).

Quasi-steady theory also predicts wind pressures on low-rise buildings. The theory states that pressure fluctuations produced by longitudinal turbulence are dominantly proportional to the pressure coefficient. Meanwhile, pressure fluctuations produced by lateral turbulence are secondarily proportional to the pressure coefficient with respect to the wind direction (Holmes, 1990). More specifically, eigenvalues and eigenvectors were used to show that "turbulence generated by flow separation" is the parameter of secondary importance for fluctuating pressures (Letchford et al., 1993). Also, experiments have shown that the quasi-steady theory "can only be applied for the prediction of aerodynamic forces in stagnation regions" where the mean pressure coefficient is greater than zero (Tieleman, 2003). These findings limit the certainty of the quasi-steady theory.

Orthogonal decomposition is a technique which builds a covariance matrix using calculated eigenvectors and eigenvalues. The method involves determining wind loads normal and tangent to the structure and using these components (i.e., eigenvectors and eigenvalues) to construct a matrix that illustrates the relationship between the two components. A proper orthogonal decomposition can be used

to understand "fluctuating wind pressure fields on low-rise buildings (Holmes et al., 1996)." In Australia, Holmes et al. (1996) studied orthogonal decomposition using center-line pressures and pressures on a transverse line along the roof. Results show that the orthogonal decomposition method is "an economical form for describing the spatial and temporal wind pressure variations on a building."

An ESWL model to predict wind pressures on low-rise structures was studied by Chen et al. (2007) on the full-scale Texas Tech building. The ESWL method uses orthogonal decomposition of wind and regards dynamic wind loads as "quasi-static (background) loads with negligible dynamic amplification (resonant) effects" (Chen et al., 2007). The approach uses this equivalent static load to analyze wind load effects on a structure at any instant in time. In ESWL modeling, dynamic external pressures on the model structure are simultaneously measured using Eq. 2.1.

$$p(t) = \frac{1}{2}\left(\rho\{U(t)\}^2 C_p\right)$$
(Eq. 2.1)

ρ = air density

$U(t)$ = velocity at a reference height

C_p = pressure coefficient

These pressure model results are then used to determine ESWL values on low-rise buildings.

2.1.2 Interpolation of Pressure Data

Interpolation of pressure coefficients on low-rise buildings was studied by Chen et al. (2002) in Ontario, Canada. In this study, an artificial neural network (ANN) was used to capture the complex variations of the pressure time series and then predict them over a long time. Experiments were done with both low and high resolution data for the input. Results indicated good performance for the prediction of pressure time series for most locations under a single wind direction in a single terrain. Unfortunately, the ANN approach is much more computationally time-consuming than linear interpolation and more work must be done to incorporate wind angle and building geometry as input parameters and simplify the technique to be more user friendly (Chen et al., 2002) for the ANN approach to be more effective than linear interpolation.

Further research was done by Chen et al. (2003) in the field of interpolation of measured pressure on low-rise buildings. This time focus was on the DAD method, whereby archived pressure time series from wind tunnel experiments were used directly in structural analysis software for the design of a structure (Chen et al., 2003). In order for DAD to be useful, simple interpolation schemes were used to cover the wide range of low building geometries a designer may need since relatively few, geometries, can be included in any database (Chen et al., 2003). Results show an accurate methodology to interpolate pressure time series to building geometries, for which no data are available. This interpolation is done by correcting pressure time series from an aerodynamically and climatologically similar building tested in

the wind tunnel to mean and rms pressure coefficients suitable for the "unknown" building. The flaw in this approach occurs when there is not an aerodynamically similar building, but further work may be performed to define the boundaries of the approach.

Jungman (2007) writes that in his low-rise building research at Iowa State University for the purpose of utilizing finite element modeling to correlate roof pressure to roof load on the wall, the external pressure coefficients for the hip roof were linearly interpolated using the data table in ASCE 7-02 Standard. The variables used in this process were: 1) values of the angle the roof makes with the horizontal, 2) building height divided by wall length parallel with the wind direction, and 3) wall length parallel with the wind direction divided by the wall length perpendicular to the wind direction. Jungman advises that linear interpolation should only be carried out between values of the same sign. He also claims that two pressure coefficients listed in the same data table indicates that the windward roof slope was subjected to either positive or negative pressures.

2.2 MEASURING PRESSURE

While all three of the above pressure prediction methods are satisfactory for estimating pressure on low-rise buildings, conducting direct measurements using instrumentation helps evaluate the accuracy of the methods and is the most certain way to know actual pressures caused by wind loads. Unfortunately, instrumentation and data gathering and interpretation are expensive and tedious. Thus, instrumentation is used on select low-rise buildings, data is gathered and studied, and methods such as those stated above are then developed and used to predict wind pressures on other low-rise buildings. Note the accuracy of each design method is based on the quality of instrumentation and interpretation.

Equation 2.2 is applied to the measuring tube system to obtain the pressure coefficient. With properly installed and functioning equipment, the tubing system can provide highly accurate pressure coefficients.

$$C_p = \frac{p_i - p_0}{\frac{1}{2}\rho U^2} \qquad\qquad (Eq.\ 2.2)$$

p_i = dynamic pressure (i=1 to n)

p_0 = static pressure

ρ = air density

U = reference velocity at reference height.
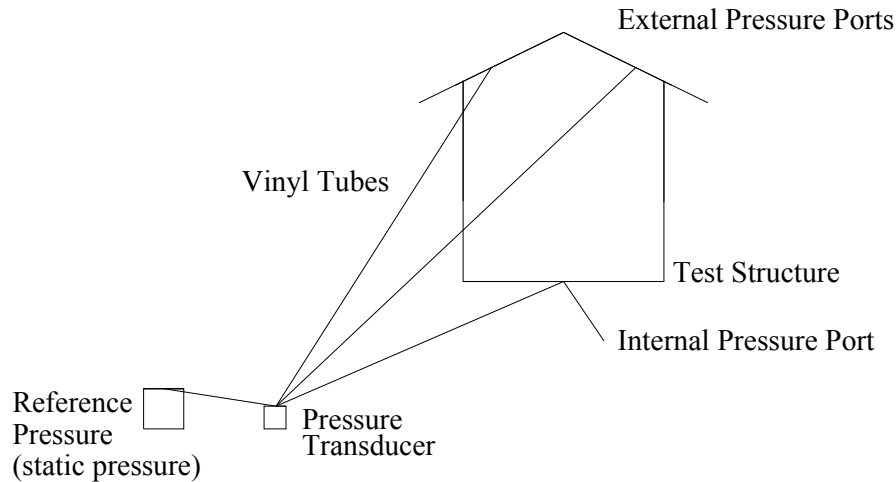
Figure 2.1. Illustration of instrumentation set-up used to determine pressure coefficients (Hitomitsu, 2007)

A specific device that is used to measure wind pressure is the pressure transducer, such as the Setra Systems 265 pressure transducers. These transducers sense either differential or gauge (static) pressure and convert this pressure difference to a proportional electrical output. Positive pressure moves the diaphragm toward the electrode, increasing the capacitance, while a decrease in pressure moves the diaphragm away from the electrode, decreasing the capacitance. The change in capacitance is detected and converted to a linear direct current electrical signal by Setra's unique electronic circuit (Setra, 2008).
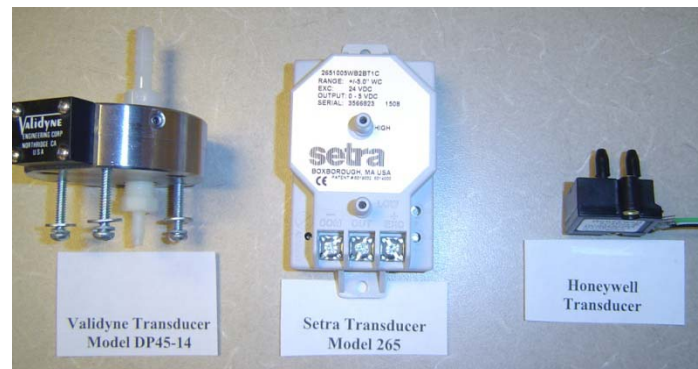
Figure 2.2. Three different transducers which input wind speed from pressure tubes and output a corresponding voltage

2.2.1 Reference Pressure

Reference pressure is the static pressure of the uninterrupted wind flow which is the atmospheric pressure at the ground level. Building surface pressures fluctuate because the flow over a building surface is turbulent while the internal pressure inside the building (Mehta et al., 2004) is usually constant. If large enough, this inequality of external and internal pressures (i.e., differential surface pressure) can

damage building components including the roof. The differential surface pressure is defined as the difference between wind-induced pressures on a structure and the reference static pressure.

The most important measurement in determining wind pressure is the reference static pressure measurement. It is more important at full-scale because wind-induced pressures are very small as compared to atmospheric pressure. For example, the stagnation pressure associated with 45 m/s wind is approximately 1.2 kPa while the standard atmospheric pressure is 101 kPa (Mehta et al., 2004). An incorrect atmospheric pressure measurement of just 1 kPa would alter a surface pressure of 1.2 kPa to 2.2 kPa or by 83.3 percent. The accuracy of reference static pressure is directly related to the ability to measure small variations of pressure.

Reference static pressure is a difficult measurement in the field because it must not be affected by the wind. However, change in atmospheric pressure does occur due to the passage of a thunderstorm or tornado so it should be recorded (Cook, 2001; Levitan et al., 1991). At Texas Tech University, ambient pressure is obtained from a box below ground, which has a smooth lid with a small hole of 1.3 mm. The box is located about 23 m from the test building and even with it being located underground, it is necessary to use tubing of 0.8 mm diameter and 1 m long with restrictors, to reduce fluctuating reference pressure (Mehta et al., 2004). The difficulty remains, from test to test, in measuring atmospheric pressure not affected by the wind, but still affected by storms.

2.2.2 Pressure Taps and Frequency

Pressure taps are smooth holes on the surface of a building where building surface pressure is measured. It is common practice to mount pressure taps flush with the surface and also to use relatively small diameter taps. The tubing length of pressure taps needs to be short to avoid resonance in pressure waves and attenuation in the fluctuating pressures (Mehta et al., 2004). Ahmad et al. (2002) instrumented model structures at Aligarh Muslim University in India, with 3/8 in. long and 1/32 in. internal diameter stainless steel tubing. The full-scale Texas Tech building of Levitan et al. (1991) contained taps 5/16 in. internal diameter and 2 in. long. One year prior to this field test, taps of 3/8 in. internal diameter were mounted on the building and it was discovered that a sampling rate of 10 Hz was sufficient to record peak pressures on the windward wall (Levitan et al., 1991). For the Texas Tech field test, as shown in Figure 2.6, more than 100 pressure taps, mounted flush with the outside building surface, have been installed on the test building (Levitan et al., 1992).
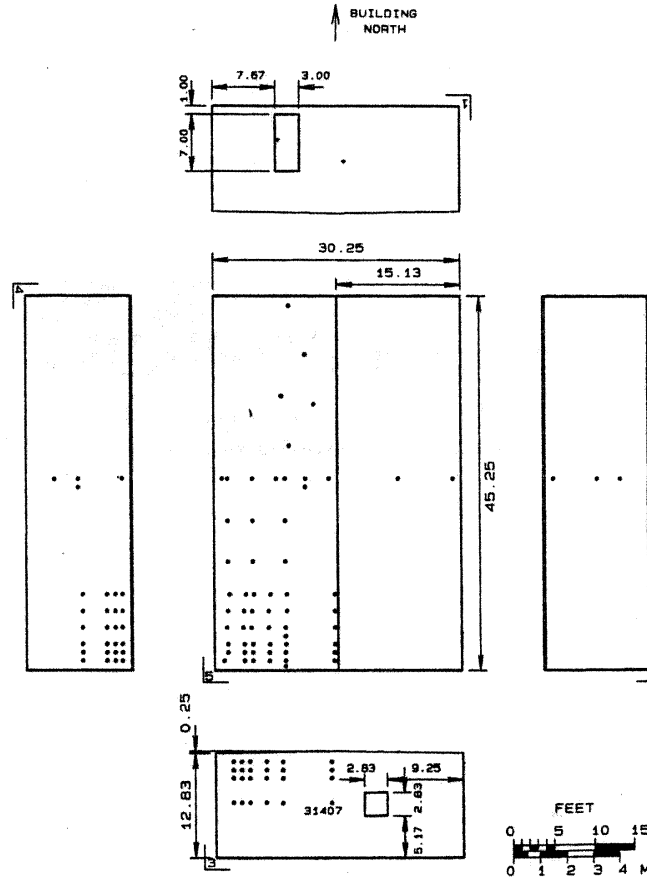
Figure 2.3. Building roof and wall dimensions in feet and pressure tap locations used for Texas Tech building (Levitan et al., 1992)

Okada et al. (1992) used two tube systems to transmit pressure from the pressure taps of the building models to pressure transducers. The 50 Hz system consisted of 16 inch vinyl tubes and Scanivalve pressure scanners (Okada et al., 1992). The 125 Hz system consisted of 16 inch vinyl tubes, restrictors, 4 inch vinyl tube and Scanivalve pressure scanners. Restrictors were 3/16 inch in length with an internal diameter of 3/256 inches. Pressure measurements were recorded to verify presumptions about the two systems' different frequency response characteristics. It was concluded that the mean wind-pressure coefficients with the 50 Hz system were, on an average, 0.99 times those of the 125 Hz system. On the other hand, root-mean-square (rms) and peak wind-pressure coefficients of the 125 Hz system were 1.06 and 1.26 times greater than those of the 50 Hz system, respectively (Okada et al., 1992). These findings imply that sampling frequency of the data has a large effect on peak pressure coefficients and a smaller effect on mean and rms pressure coefficients.

Although mounting and size of pressure taps do not vary significantly from test to test, placement of pressure taps varies between tests generated by different researchers. For example, researchers at

Colorado State University placed 184 pressure taps closely in one corner region of the windward roof. The taps were arranged so that the taps existing on the full-scale building were represented in the model. Additional taps were added in between the locations of the full-scale taps and also very close to the roof edge (Bienkiewicz et al., 1992). In a test at the Tokyo Polytechnic Institute, 512 and 416 pressure taps were uniformly distributed on the roof and walls. The wall taps were placed at heights of 7H/8, 5H/8, 3H/8, and H/8, where H represents the height of the wall (Tamura et al., 2001). The above two examples illustrate a need for numerous pressure taps to better understand local pressure on a building.
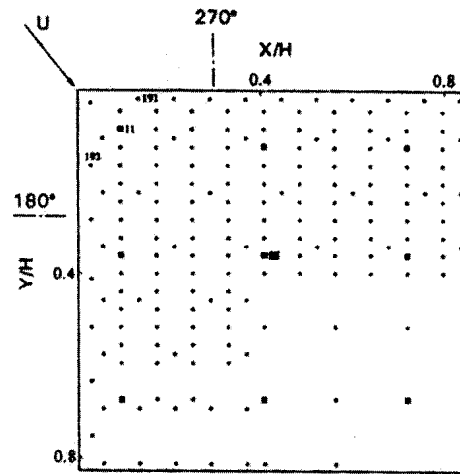
Figure 2.4. Arrangement of 184 pressure taps used by researchers at Colorado State University in one corner region of a low rise building roof (Bienkiewicz et al., 1992)

2.3 WIND TUNNEL TESTING

2.3.1 Scaling Wind Tunnel Models

Minimal research has been done to address the issue of scaling low-rise building tests from the model level to the full-scale level and vise versa. It is envisioned that model tests should be scaled replicas of full-scale tests to account for building geometry as well as the building's surroundings. The main challenge in scaling low-rise building tests is accurately duplicating the wind profile. When performing tests of scaled low-rise buildings, attention must also be given to negative pressure coefficients, the Reynolds number effect, flow reattachment points, extreme peak pressure coefficients, and the scaling ratio. Consideration of these factors assists in the accuracy of data from scaled low-rise building tests.

In March of 2002, researchers at the Silsoe Research Institute in the U.K., compared surface pressures on a model cube and a 6 m full-scale cube. Researchers reported that full-scale coefficients were more negative than any of the wind-tunnel results (Hoxey et al., 2002). Also, Okada et al. (1992) made model and full-scale test comparisons of the Texas Tech building. Findings show that mean wind-

pressure coefficients of wind tunnel tests were in fairly good agreement with those of the on-site measurements except with respect to the high negative pressures on the roof (Okada et al., 1992). Based on scant evidence of delayed flow reattachment in the wind-tunnel studies, researchers at the Silsoe Research Institute concluded that wind tunnel pressure coefficients being less negative is indicative of a Reynolds number effect (Hoxey et al., 2002). This is all information that needs to be considered when attempting to correlate wind tunnel pressure coefficients to field pressure coefficients.

Researchers at the Silsoe Research Institute write that analysis of the full-scale data for the roof has shown that the mean wind reattachment point on the roof varies with wind speed. The trend was for the pressure coefficients to decrease and the reattachment point to move toward the wind with increasing wind speed. This full-scale reattachment point, as illustrated in Figure 2.5, causes an observable difference in pressure coefficients between the average of a number of wind-tunnel results and the full-scale results on the roof (Hoxey et al., 2002). Tests at Virginia Polytechnic Institute and State University (Virginia Tech) showed similar results. Tieleman et al. (1980) concluded that on the basis of the full-scale/model comparisons, natural wind has a significant effect on the mean, rms, and peak pressure coefficients. In addition, full-scale extreme peak coefficients may be as much as 5 times the wind-tunnel values (Tieleman et al., 1980).

To compensate for such large differences between wind-tunnel and full-scale pressure values, research was done separately by the University of Western Ontario (UWO), Virginia Tech, and Texas Tech to establish an acceptable scaling ratio for wind tunnel and full-scale tests. Tests performed at UWO compared pressure coefficients on a building model scale of 1:500 while Virginia Tech compared coefficients on a building model scale of 1:50 with full-scale data. It was found that in a carefully simulated boundary layer, pressure coefficients based on mean velocity show that there is little difference between mean or fluctuating coefficients obtained from a model at 1:500 scale and those from a model at 1:50 scale (Tieleman et al., 1980). Twelve years later, in 1992, researchers at Texas Tech studied models on a scale of 1:65, 1:100 and 1:150. Their results showed that the size reduction ratio of the models had almost no effects on the mean wind-pressure coefficients (Okada et al., 1992). But in 2003, studies at Virginia Tech concluded that in order to satisfy the duplication of small-scale turbulence of the incident flow, it is recommended to utilize models of low-rise buildings no larger than 2% (1:50) of the full-scale building (Tieleman, 2003) and thus 1:10 would not be acceptable.

2.3.2 Model Testing

As previously stated, precise data is the greatest factor in wind tunnel tests. With the mean pressure coefficient being the most important pressure coefficient for design purposes (Hoxey et al., 1993), precise conditions are needed in the wind tunnel to replicate the pressure coefficient in the field.

In fact, model mean, rms, and peak pressure coefficients are likely to be in agreement with full-scale results if the following conditions are met: 1) local pressure coefficients are used, 2) the streamwise turbulence intensity is modeled adequately up to an elevation of at least two building-heights, 3) the streamwise turbulence integral scale is at least as large as the largest model dimension, 4) changes in nearby surface elevation are modeled adequately, and 5) the full-scale data records do not exhibit non-stationary character such as low-frequency components and/or short-duration gusts (Tieleman et al., 1980). There also exists the importance of comparing peak pressure coefficients of the same probability of occurrence. A comparison of pressure measurements requires that both the sampling rate, which depends on velocity and geometric scale, and record length be properly matched in model and full-scale.

For atmospheric flows at high Reynolds numbers, the separation of the large and the small wavelengths of the velocity fluctuations in the frequency domain is farther than for the wind tunnel flows at much lower Reynolds numbers. Sharp-edged scaled models of the order of 1:50 or greater can relax the mean-flow Reynolds number, provided it does not fall below 50,000. Lower Reynolds numbers are not recommended because they lead to the reduction of the incident small-scale turbulence that would fail to initiate the proper vortex development associated with the interaction process between flow and model. Past research conclusions have stated that equality of the Jensen number from model to full-scale test is sufficient to simulate the flow in the surface layer for ideal terrain, and obtain reliable estimates for the wind loads. However, equality of the pressure coefficients between model and full-scale can only be guaranteed if the turbulence Reynolds number is also duplicated (Tieleman, 2003).

2.4 FULL-SCALE TESTS

2.4.1 Previous Full-Scale Tests

Similar to prior model tests, although limited, previous full-scale, low-rise building tests have given rise to important information for future full-scale tests. Jungmann (2007) suggests a more heavily instrumented hip roof in future tests to better determine if the test roof is experiencing a suction or pressure during a hurricane event. It is suggested that a denser distribution of pressure taps would create a better understanding of the wind load on the roof. Of greater importance than the number of instruments is the quality and distribution of instrumentation. In previous tests, difficulties with instrumentation have led to the discrediting of results (Letchford et al., 1993). In fact, researchers are still hoping for advances to be made in the instrumentation so that past difficulties can be overcome.

Suggestions have also been made for collecting full-scale data. For example, in order to capture turbulence characteristics, it is recommended to use a length of record at least 10 to 15 minutes long. Otherwise the wind characteristic measurements may not be reliable and the wind effects data would then be useless (Mehta et al., 2004). At Texas Tech, the data collection system on the full-scale building

begins automatically and runs continuously when the one-minute mean speed at the height of the building reaches 20 mph. Also for the full-scale Texas Tech building, ten samples are averaged to find the mean, rms, maximum, and minimum pressure coefficients (Chen et al., 2007).

On the full-scale, low-rise building, mean and maximum pressures were represented by positive values on the windward wall and negative values on the roof and leeward wall (Chen et al., 2007). In addition, mean and peak pressure coefficients on the full-scale building were greater on the windward roof for wind at a 60° angle-of-attack than for a 90° angle (Levitan et al., 1991). Full-scale tests at Texas Tech have also been used to "investigate the distribution and correlation of fluctuating pressures on a low rise building (Letchford et al., 1993)." Analysis showed that most of the pressure fluctuations were caused by longitudinal and lateral turbulence (Wu et al., 2001). However, flow normal to the roof edges is responsible for the "rollup and discrete shedding of the separation bubble (Letchford et al., 1993)." For illustrative purposes, note the separation bubble between the separation point 1 and the reattachment point in Figure 2.5(b).

(a)   (b)
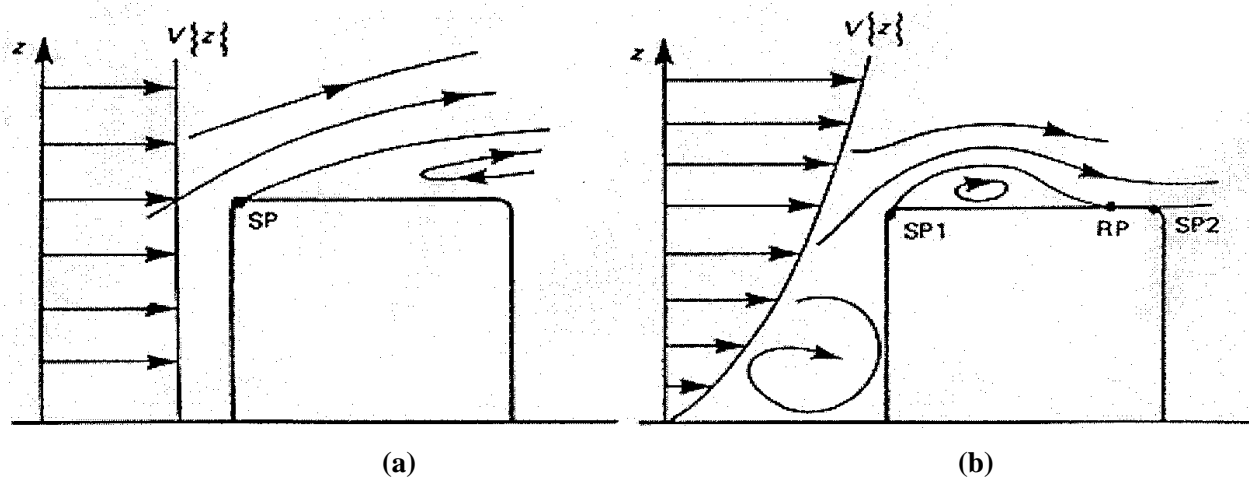
Figure 2.5. Separation and reattachment of wind flow on roofs subjected to (a) uniform and (b) boundary layer wind profiles (Cook, 1990; SP: separation point, RP: reattachment point, z: height, V{z}: wind velocity with respect to height)

In reality, a limited number of full-scale wind pressure tests to collect surface pressure data have been studied. Reasons for this include: lack of reliable measuring devices, high costs of tests, and overall difficulty in conducting the tests. Despite these obstacles, full-scale tests are necessary to validate wind tunnel testing and because scaling effects prevent some important pressure data from being obtained in the wind tunnel (Mehta et al., 2004). The preceding information suggests that it is vital to utilize any opportunity to concurrently test a structure in the field and a model of the structure in the wind tunnel to compare the data collected from each unit.

2.4.2 Wind Pressure on Roofs and Walls

Ahmad et al. (2002) studied wind load effects on seven hip roof, low-rise building models of 10, 15, 20, 25, 30, 35, and 40° roof pitch. Each building, tested in the wind tunnel at the University of Roorkee in India, had a roof overhang of 1.1 m. Post disaster investigations for wind induced damage show that hip roofs outperform gable roofs during catastrophic cyclones while studies by Ahmad et al. (2002) show, more specifically, that lower pitched hip roofs outperform those of greater pitch. Plots by Ahmad et al. illustrate that peak suction is sensitive to wind direction for the roof pitch ranging from 20° to 40° and a change in wind direction, for these roof pitches, by 5 to 10° from the critical loading direction causes a significant reduction in maximum pressure.
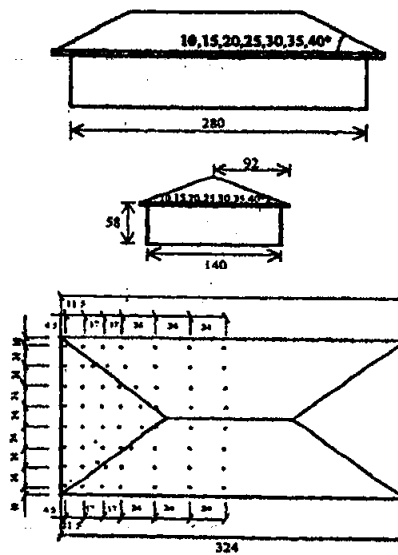
Figure 2.6. Dimensions and pressure tap locations on a hip roof model (Ahmad, 2002)

Noting that peak pressure factors are used for design pressure coefficients, Ahmad et al. (2002) also elaborated on peak pressures in different zones of the roof. Except for the extremes, peak pressure results follow the normal distribution, which is a continuous probability function used to approximate a binomial distribution. Recorded data show that the greatest peak pressures are directly related to the greatest mean pressures, especially in the separator flow region (Ahmad et al., 2002).

In addition to pressures on roofs, wind pressures on free-standing walls have been studied by Robertson et al. (1996). Full-scale free standing walls vary from prison walls, to noise barriers along high volume roads, to garden boundary walls. Results from a three year study, beginning in 1993, show severe loads at the wall toes and that wind direction, wall length, position on the wall, and the presence of return corners significantly affect load measurements on the wall (Robertson et al., 1996).
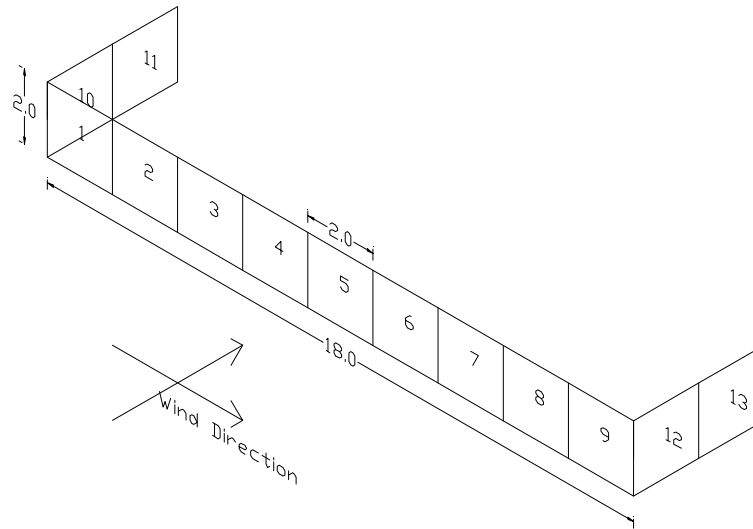
Figure 2.7. Free standing wall with return corners used by Robertson et al. (1996) (All dimensions are in meters)

2.4.3 Verifying Pressure Measurements

There are three important entities that affect pressure measurements on a low-rise building. Wind direction, geometry of the building, and turbulence, together, generate peak pressures on low-rise buildings.

In 1991, 2001, and 2007 tests were performed by various researchers, which showed that maximum pressure coefficients occur when wind direction is at an angle between 0° and 90°. Tests by Levitan et al. (1991) on the Texas Tech building revealed that the average mean and peak pressure coefficients on the windward roof were greater for wind direction of 60° than for wind direction of 90° relative to the test building. Results from Tamura et al. (2001) on research from the Tokyo Polytechnic Institute state that large negative pressures appear near the leading edge of a side wall. It was concluded that "maximum drag is generated when the wind direction is slightly inclined to one side (Tamura et al., 2001)."

It is known that the geometry of a low-rise building affects wind pressure coefficients. The wind pressure distribution is determined mainly by the shape of the building, which has four important parameters: height, span, length, and roof pitch (Hoxey et al., 1993). Despite knowing these critical parameters, "understanding the influence that each of these parameters has on wind loads remains elusive and, consequently, design codes are unable to account properly for the effect of building geometry (Hoxey et al., 1993)." For example, research by Tieleman (2003) at Virginia Tech shows that an increase in the structure's height, in the same boundary layer flow, increases the value of the roof pressure coefficients (Tieleman, 2003). Stathopoulos (1980) studied these varying geometries and claimed that

"probability density functions of wind pressures can be used to estimate the number of occurrences of a particular pressure level within a given time period (Stathopoulos, 1980)."

Stathopoulos (1980) also credits wind turbulence for creating design havoc on low-rise structures and claims that peak pressure factors are greater than those expected by the normal distribution (Okada et al., 1992). Tieleman (2003) noted that an increase in longitudinal turbulence creates smaller mean pressure coefficients, but larger fluctuating pressure coefficients (Tieleman, 2003). Prior to Tieleman's (2003) studies, Letchford et al. (1993) used "eigenvalue analysis of the covariances" and claimed that longitudinal and lateral turbulence are the cause of most pressure fluctuations (Letchford et al., 1993). However, wind direction, wind speeds, structure geometry, and turbulence all increase the uncertainty of pressure values and, therefore, the difficulty in designing a low-rise building for wind loads.

2.4.4 Corners and Edges

Most frequently, peak pressures on low-rise buildings occur at the roof at corners, windward edges, and ridges (Tieleman, 2003). In some cases, these pressures can be as many as three times the pressure observed on the rest of the structure. Although this knowledge is useful, gauging this pressure is extremely difficult. The reason pressures are high near the corners, edges and ridges is because of flow separation and vortex formation (Chen et al., 2007). It is challenging to interpolate pressures between ports in these areas because it is difficult to predict the location of the vortex region and where the flow will reattach.

Vortex formation is caused by "rotational vortex flow and axial velocity in the core of the vortex (Tieleman, 2003)." Together, flow separation and vortex formation are capable of generating large "suction pressures near upstream corners (Tieleman, 2003)." The problem in current wind loading design is that local factors must be determined before using the quasi-static design approach to predict "peak pressures where flow separation and vortex formation take place (Ginger et al., 1995)." Ginger et al. (1995) studied the Texas Tech building and determined a pressure factor of 3.0 at edge locations of 0.2 times the mean roof height for the worst wind directions (Ginger et al., 1995) as illustrated in Figure 2.8. Prior to these findings, Letchford et al. (1993) showed that flow reattachment on the walls occurred beyond 1.0 times the height of the building (Letchford et al., 1993). Their work reiterates the significance of the flow reattachment point.
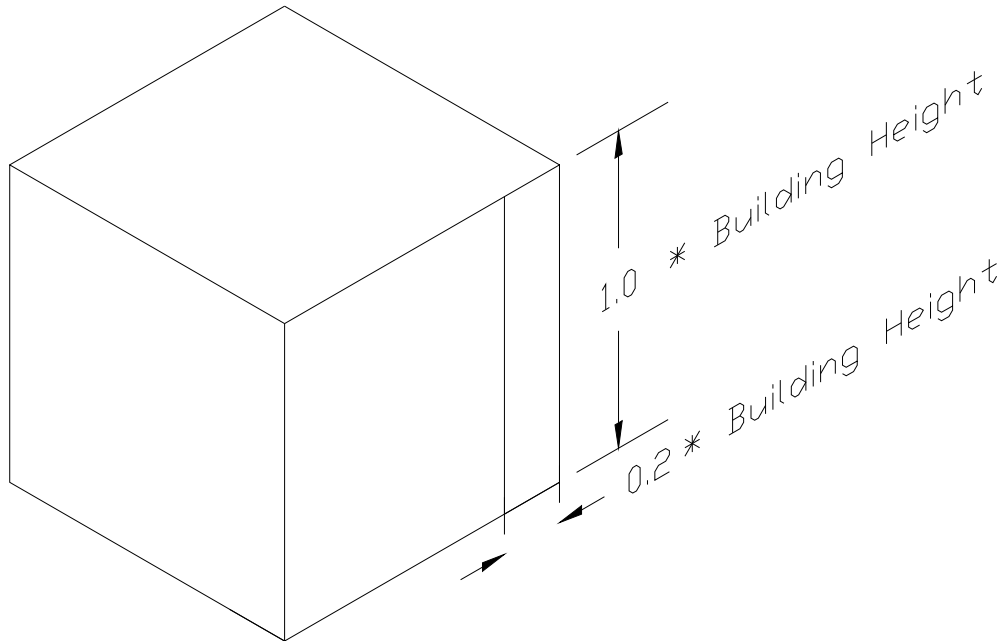
Figure 2.8. Illustration of the critical pressure region located a distance of 0.2 times the mean building height from the edge

Most codes suggest that pressures on low-rise buildings are the highest at the roof corners (Stathopoulos, 1980). Despite this claim, past research shows that even while overloading the structure with pressure taps, quantifying suction pressures near the corners and edges of low-rise buildings remains elusive. The Artificial Neural Network of Chen et al. (2002) illustrated this point when it had trouble quantifying the magnitude of a pressure tap located at the corner of the structure. For their research, pressure taps were placed at high resolution, but correlation between adjacent corner taps was low, alluding to the possibility that greater unknown suction pressures could be taking place between pressure taps.

Past research has shown that not just edges, corners, and ridges are susceptible to high suction pressures, but mainly windward edges, corners, and ridges are especially susceptible to large suction pressure. Bienkiewicz et al. (1992) used the wind tunnel to study pressures in the windward corner of a 1:25 scale model of the Texas Tech building at Colorado State University in 1992 and found that greater turbulence produces greater pressure fluctuations, especially in windward roof corners. Results also showed peak suction always took place near the windward side of roof edges (Bienkiewicz et al., 1992). Okada et al., (1992) write that windward corners on the Texas Tech building are "sensitive to the angle of attack (Okada et al., 1992)."

Chapter 3: Wind Tunnel Test 1 for Verification of Wind Pressure Measurements

To develop a basic understanding of the wind tunnel, pressure measuring devices, wind tunnel instrumentation techniques, and pressure port interpolation possibilities, a rectangular box shaped test model was designed, built, and tested first in this study. All tests for this model were conducted in the Bill James Wind Tunnel (Figure 3.1) located in the Wind Simulation and Testing (WiST) Laboratory corresponding to a uniform and smooth upstream flow. Pressure data from ports located at carefully selected locations on the test model was collected and pressure coefficients were calculated at these port locations. The coefficients were then compared to theoretical coefficients found in the literature for uniform flow to verify that the wind tunnel tests were being conducted correctly and that the pressure measurement system in this and upcoming tests will perform accurately.

Figure 3.1. Bill James Wind Tunnel located in the WiST Lab at Iowa State University

3.1 TEST MODEL

The test chamber at ISU's Bill James Wind Tunnel has a width of 3 feet and a height of 2.5 feet. The first test model was built according to this cross sectional area of 1260 square inches, with a wind tunnel blockage limitation set at eight percent of the cross sectional area for any orientation of the model.

3.1.1 Dimensions and Materials

The model was constructed with 1/4 in. thick plywood on the four side faces and the top face, the bottom face has no plywood, and the four corners contain a dimension lumber 2 x 4, with its actual dimensions being 1.5 in. x 3.5 in. The plywood connection seams were filled with wood putty to ensure smooth wind flow over the seams. As illustrated in Figure 3.1, L-shaped metal brackets allowed the test model to be fastened to the floor of the wind tunnel. The pre-drilled holes in the horizontal legs of the brackets provided for the use of bolts, nuts, and washers and thus, easy access to the inner portion of the model.
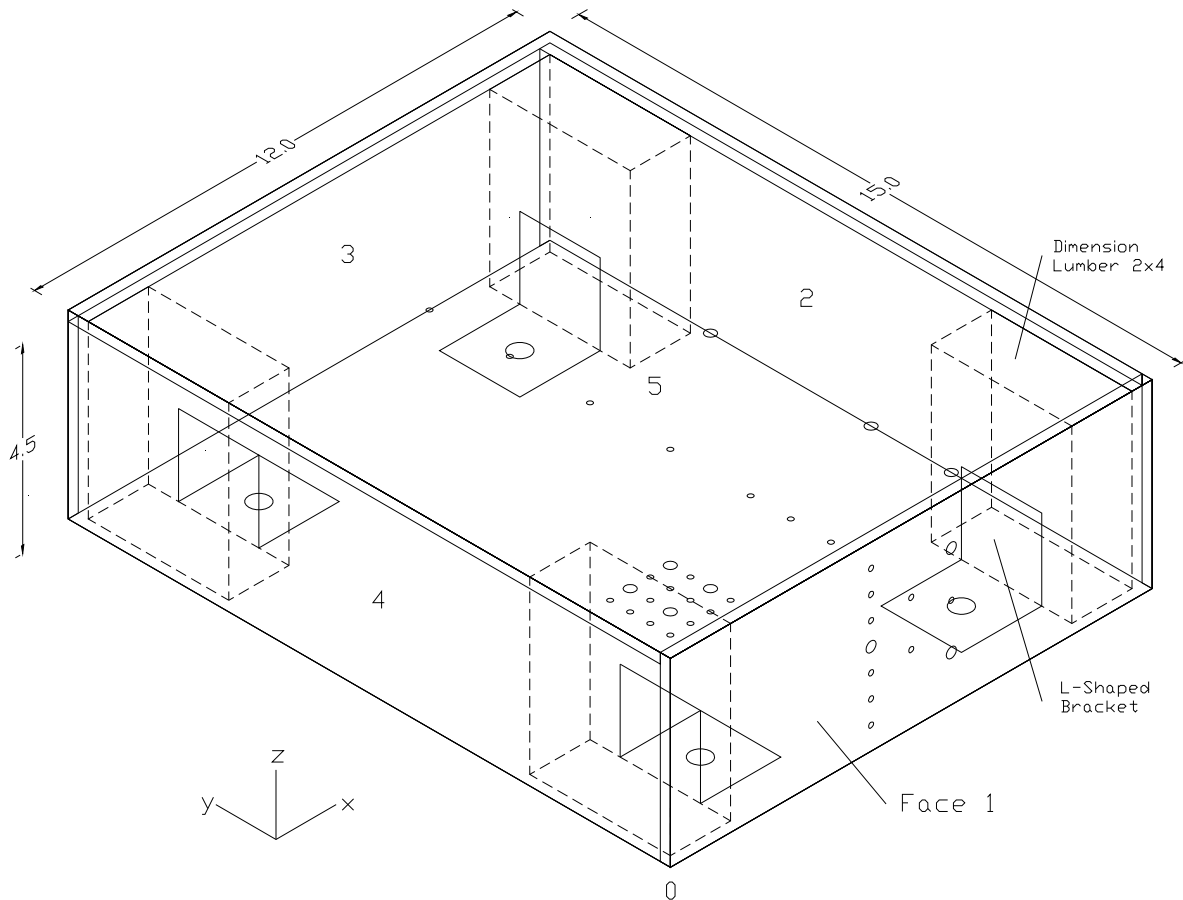
Figure 3.2. Three dimensional schematic of the first wind tunnel model and locations of 38 pressure ports (All dimensions are in inches)

3.1.2 Pressure Port Locations

As identified in Figure 3.2, the front face of Model 1 was referred to as Face 1 and the top as Face 5. Face numbers increase in the counterclockwise direction around the structure. Thus, if viewing the front of the model, Face 2 is the right side of the model, Face 3 is the back side, and Face 4 is the left side. Pressure taps were labeled 1 through 38, beginning with Face 1 of the model and ending with Face 5. Pressure tap locations are summarized in Table 3.1. Beginning with Face 1, the pressure taps increase

from left to right (x direction), front to back (y direction), and bottom to top (z direction). For example, pressure tap number 3 is located on Face 1 at the x, y, and z coordinates of 7 in., 0 in., and 1.125 in. The origin (0, 0, 0) is located at the bottom and leftmost point of Face 1.

Table 3.1. Pressure port numbers and locations for Model 1

Pressure Port Number	Model Face Number	Location (in.)		
		x	y	z
1	1	5.00	0.00	0.56
2	1	5.00	0.00	1.13
3	1	7.00	0.00	1.13
4	1	5.00	0.00	1.69
5	1	6.00	0.00	1.69
6	1	5.00	0.00	2.25
7	1	7.00	0.00	2.25
8	1	5.00	0.00	2.81
9	1	6.00	0.00	2.81
10	1	5.00	0.00	3.38
11	1	7.00	0.00	3.38
12	1	5.00	0.00	3.94
13	5	0.50	0.50	4.50
14	5	1.00	0.50	4.50
15	5	1.50	0.50	4.50
16	5	2.00	0.50	4.50
17	5	4.50	0.50	4.50
18	5	7.50	0.50	4.50
19	5	0.50	1.00	4.50
20	5	1.00	1.00	4.50
21	5	1.50	1.00	4.50
22	5	2.00	1.00	4.50
23	5	0.50	1.50	4.50
24	5	1.00	1.50	4.50
25	5	1.50	1.50	4.50
26	5	2.00	1.50	4.50
27	5	4.50	1.50	4.50
28	5	0.50	0.02	4.50
29	5	1.00	2.00	4.50
30	5	1.50	2.00	4.50
31	5	2.00	2.00	4.50
32	5	4.50	2.50	4.50
33	5	7.50	2.50	4.50
34	5	4.50	4.50	4.50
35	5	4.50	6.50	4.50
36	5	7.50	6.50	4.50
37	5	4.50	8.50	4.50
38	5	4.50	10.50	4.50

As illustrated in Figure 3.3, Face 1 has a width of 12.0 inches and a height of 4.5 inches. There were three vertical sections of pressure ports. The middle vertical section was located at the horizontal center of Face 1. The other two vertical sections were located at 1.0 inch off center from the middle vertical section.

There were three vertical rows of pressure ports located on Face 1 of the model. The outer two rows were designed equidistant from the vertical centerline of the face. In theory, a wind load at 0 degrees would produce an equal pressure profile along the two outer, vertical rows. The same is true of the two vertical rows of pressure ports equidistant from the vertical center of Face 5. The middle row of pressure ports on Face 1 was designed to better understand the distribution of pressure between two ports. In this case, pressure port 5 is located at the center of the area defined by ports 2, 3, 6, and 7. Pressure port 9 was located at the center of the area defined by ports 6, 7, 10, and 11.
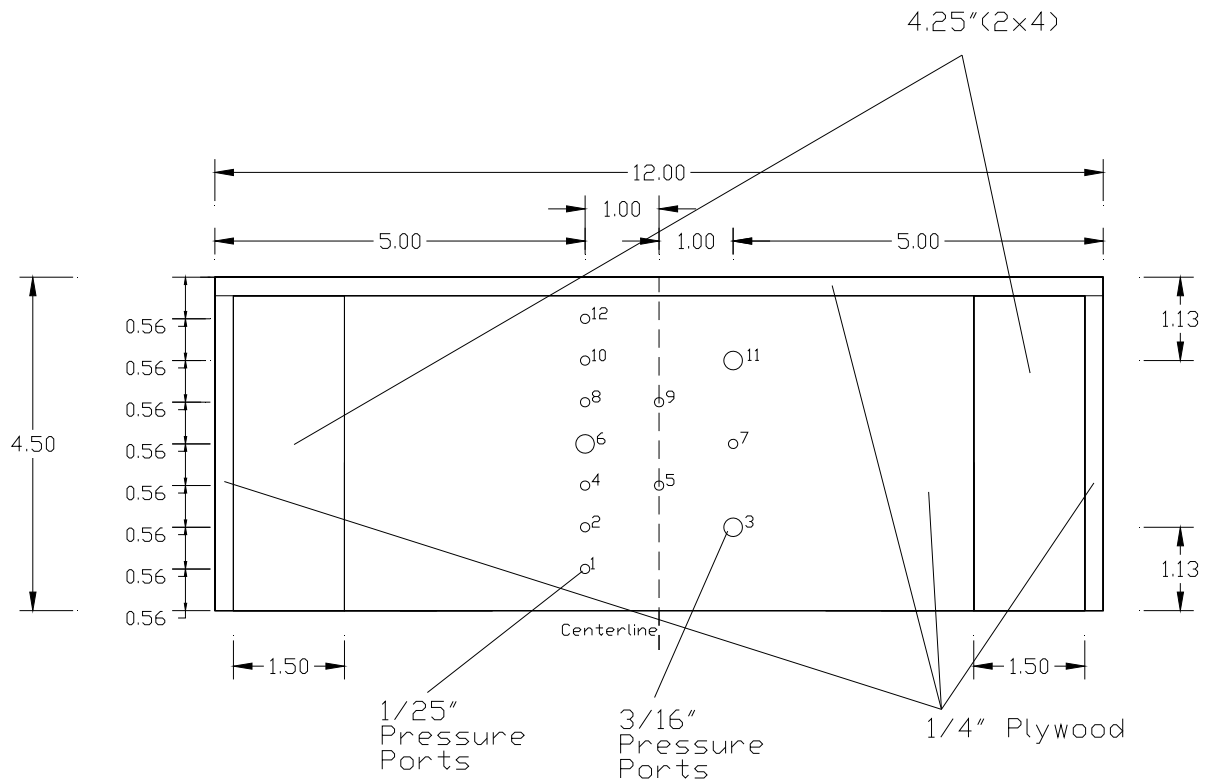
Figure 3.3. Face 1 of Model 1 with 12 pressure ports (All dimensions are in inches)

Face 5 of the test model contained 26 pressure ports, as shown in Figure 3.4. One corner section of Face 5 contained 4 pressure ports with an inner diameter of 3/16 inch and 12 pressure ports with an inner diameter of 1/25 in. Two longitudinal pressure port rows existed 1.5 inches off center on Face 5 of

the first model, with the left row containing 1/25 inch ports and the right row containing 3/16 inch ports. Separate wind loads were applied to the first model at 0 degrees and 45 degrees.

Sixteen pressure ports were erected at the corner of Face 5 of the rectangular box. The goal of these sixteen ports was to compare pressure results with other published results as well as study the interpolation possibility. In the corner, there were numerous ports at the midpoints of two other ports. Also, the literature review revealed that a building with a flat roof experiences its largest pressures near its edges and corners. Thus, it seemed obvious to place a conglomeration of pressure ports at the corner of Face 5, especially for the wind load tests of 45 degrees.
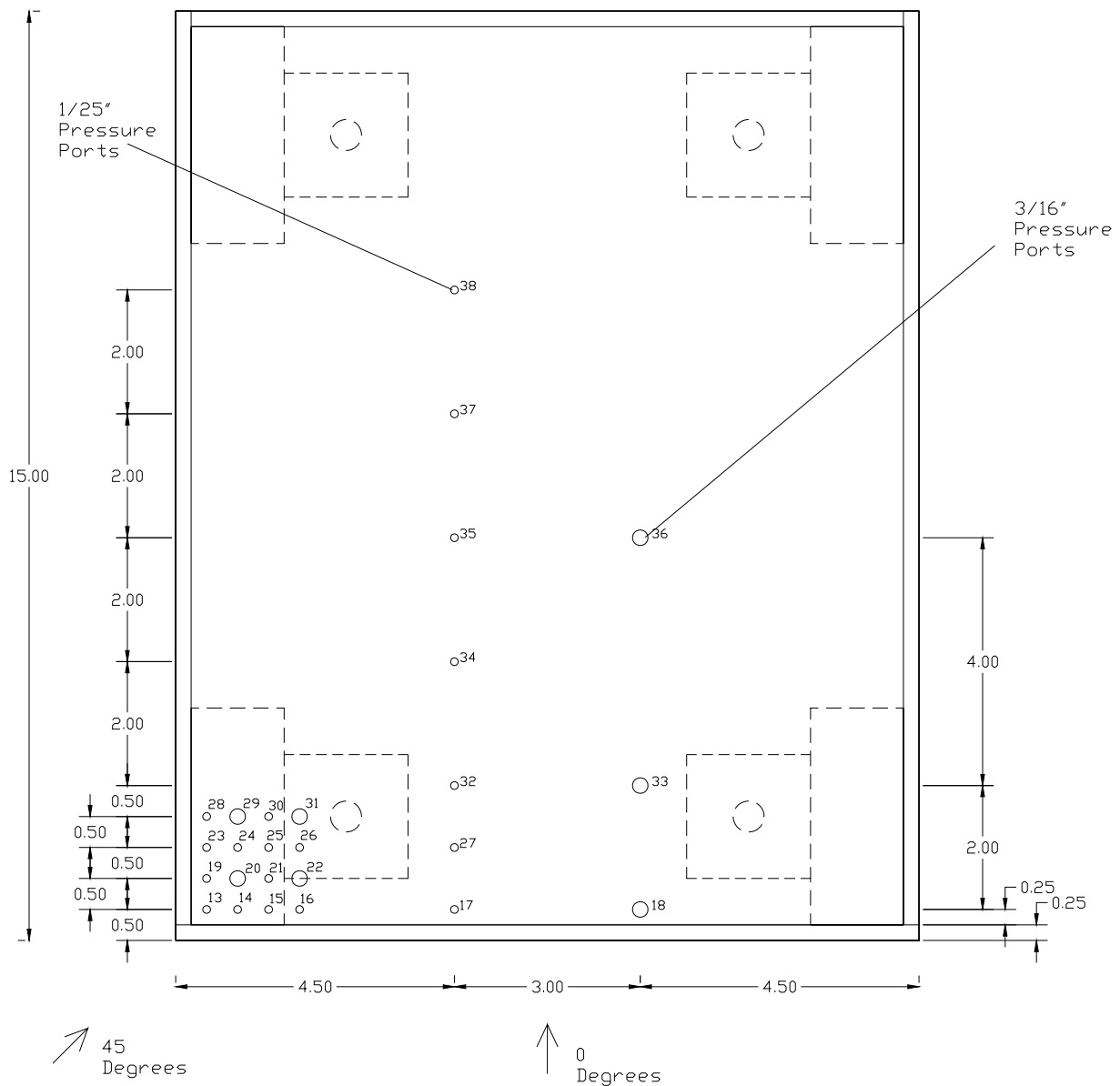
Figure 3.4. Face 5 of the first model with 26 pressure ports (All dimensions are in inches)
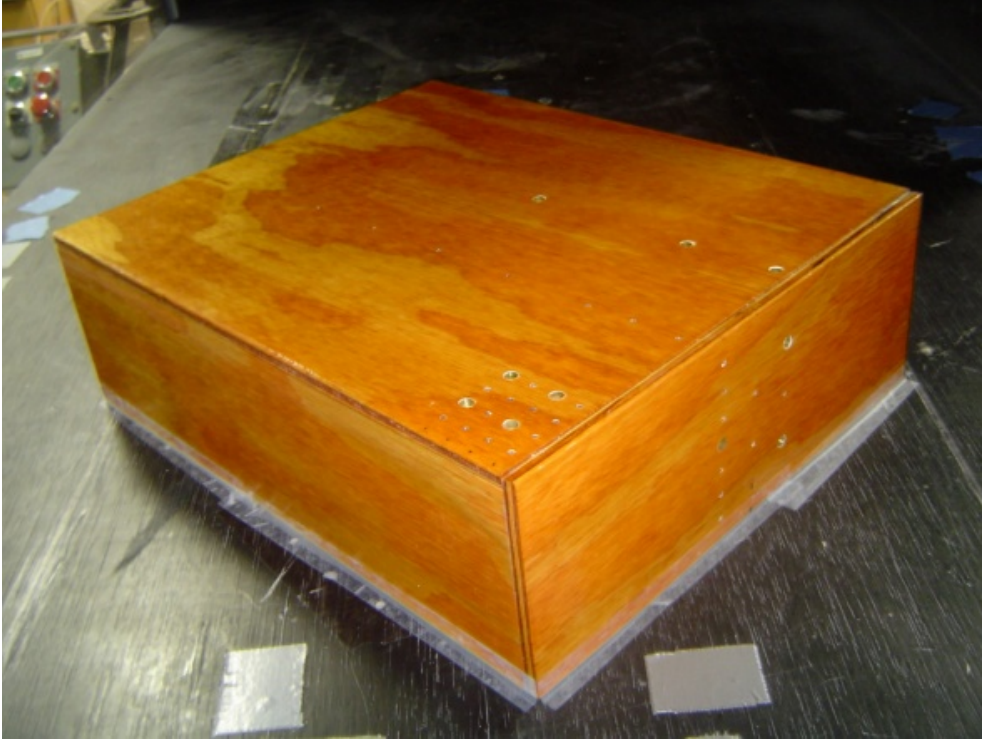
Figure 3.5. Rectangular box shaped test model in the wind tunnel for wind loading direction of 45°

3.2 INSTRUMENTATION SCHEME

Pressure port locations, pressure port diameter, transducer type, and wind angle were the four factors considered during the design and wind tunnel testing of this model. The locations of pressure ports were selected to better understand the possibility of interpolating pressures between ports. Two different pressure port diameters were used to determine if a difference in port diameter causes a difference in pressure readings. Three different pressure transducers were used to compare the measurements of each transducer.

3.2.1 Pressure Port Diameters

Pressure port diameters of 3/16 in. and 1/25 in. were used for the model tests. Relative to the typical port sizes used in the lab, larger diameter ports are used to measure pressure in the field. In the lab, typical port diameters range between 1/48 in. and 1/25 inches. Thus, the model was constructed using field and laboratory size ports to compare the port size effect on pressure readings. As shown in Figures 3.3 and 3.4, smaller and larger pressure ports were strategically located on the rectangular box model such that a 3/16 in. diameter port (i.e., Port 6), in theory, should produce a pressure reading equivalent to a 1/25 in. diameter port (i.e., Port 7) during the 0 degree wind load case.

3.2.2 Transducer Types

Two different pressure transducers were used during the model 1 tests. Scanivalve's Digital Sensor Array (DSA), as shown in Figure 3.6, was used as the primary pressure transducer. It houses 16 pressure ports and is considered one of the most accurate lab pressure transducers. A single pressure port transducer, manufactured by Honeywell, was used to compare the accuracy of single port transducers to the DSA. For the particular low-rise building being studied in the field, single pressure port transducers are much more cost effective to use than multiple DSAs.
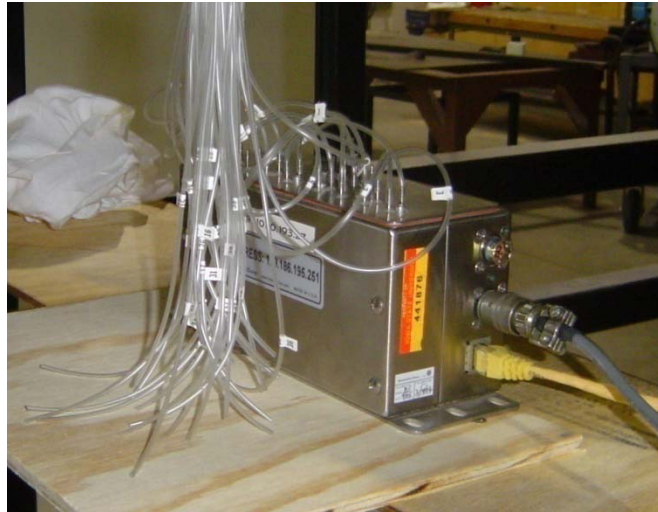
Figure 3.6. Scanivalve's Digital Sensor Array with 16 pressure ports and vinyl tubing

Each transducer port receives pressure input through a vinyl tube attached to a port on the model and then outputs a corresponding value that can be converted by the user into the desired measurement unit (e.g., pounds per square inch). Similar to pressure port diameter, the vinyl tubing diameter and length that connects the pressure port on the building to the transducer can vary significantly between lab and field tests. In the case of the model, the tube diameter (1/25 in.) and length (26 in.) were kept constant at for each port. For the 3/16 inch ports, an adapter, as shown in Figure 3.7, was manufactured using varying brass pipe diameters and super glue to connect the 3/16 in. port to the 1/25 in. inner diameter tubing.

Figure 3.7. Adapter used to connect the 3/16 inch pressure port to the 1/25 inch vinyl tubing

3.3 TESTING

Wind angles of 0 and 45 degrees, as shown in Figure 3.4, were used to test the rectangular box model during the wind tunnel tests. Both cases were compared to better understand the pressure distribution on the model due to the wind direction. The practicality of interpolating pressure data between pressure ports for the 0 and 45 degree cases was also studied. Table 3.2 shows the test plan followed during testing of Model 1. Note that both the transducer and the wind angle were changed throughout the twelve tests.

Table 3.2. Model 1 test plan displaying test number, wind angle of attack, and recommended pressure ports for the twelve tests

Test	Angle	1	2	3	4	5	6	7	8	9	10	11	12	13	14	15	16	17	18	19	20	21	22	23	24	25	26	27	28	29	30	31	32	33	34	35	36	37	38	Total Ports
1	0	x	x	x	x	x	x	x	x	x	x	x	x																											12
2	0																	x	x									x					x	x	x	x	x	x	x	10
3	0			x		x	x	x		x		x						x	x									x					x	x	x	x	x	x	x	16
4	0													x	x	x	x			x	x	x	x	x	x	x	x		x	x	x	x								16
5	45	x	x	x	x	x	x	x	x	x	x	x	x																											12
6	45																	x	x									x					x	x	x	x	x	x	x	10
7	45			x		x	x	x	x			x						x	x									x					x	x	x	x	x	x	x	16
8	45													x	x	x	x			x	x	x	x	x	x	x	x		x	x	x	x								16
9*	0		x			x				x																														3
10*	45		x			x				x																														3
11*	0													x		x			x																					3
12*	45													x		x			x																					3

*Honeywell Transducers

3.4 RESULTS AND DISCUSSION

As explained in Chapter 2, portal pressure data is generally displayed as a pressure coefficient. Pressure coefficients are developed by performing data manipulation. For the rectangular box tests, the DSA and Honeywell transducers output the difference between the total port pressure and the system static pressure. That output is then divided by the reference pressure (P_{ref}). Dividing the transducer output by the reference pressure removes the velocity factor from the data, enabling the computation of the pressure coefficient (Eq. 2.2).

Tables 3.3 through 3.5 show the pressure coefficients for all the pressure ports located on Model 1. Ports 3, 5, 6, 7, 9, 11, 17, 18, 27, and 32 through 38 were tested twice at the same angle to check the consistancy of the wind load throughout the twelve tests. Note the small difference in Port 3 coefficients between Test 1 and Test 3 to be 0.01. Similar readings for each of the aforementioned ports prove that a relatively constant wind load was maintained throughout the twelve tests. Also note the minimal difference between the Honeywell and DSA pressure coefficients for ports 2, 10, 14, and 19 in Tables 3.3 and 3.4. These results show the accuracy of a single-port pressure transducer such as the Honeywell transducer. It was discovered after the tests that the Honeywell transducers connected to Ports 6 and 16, which did not supply data, were damaged by the soldering gun when the input, output, and voltage wires were soldered to the transducer. Other interesting and expected observations for the pressure coefficients are: the ports on Face 1 were subjected entirely to positive pressure, the ports on Face 5 were subjected entirely to negative, suction pressures, and ports 16 and 28 were subjected to relatively large pressures for the 45 degree case.

Table 3.3. Pressure coefficients for Face 1 of Model 1

Test	Angle	Face 1 Pressure Ports											
		1	2	3	4	5	6	7	8	9	10	11	12
1	0	0.503	0.407	0.438	0.360	0.370	0.459	0.616	0.541	0.599	0.600	0.827	0.501
2	0	-	-	-	-	-	-	-	-	-	-	-	-
3	0	-	-	0.428	-	0.356	0.451	0.590	-	0.571	-	0.804	-
4	0	-	-	-	-	-	-	-	-	-	-	-	-
5	45	0.392	0.381	0.288	0.414	0.361	0.417	0.346	0.389	0.348	0.294	0.232	0.095
6	45	-	-	-	-	-	-	-	-	-	-	-	-
7	45	-	-	0.289	-	0.362	0.418	0.346	-	0.349	-	0.232	-
8	45	-	-	-	-	-	-	-	-	-	-	-	-
9*	0	-	0.408	-	-	-	NA	-	-	-	0.590	-	-
10*	45	-	0.383	-	-	-	NA	-	-	-	0.294	-	-
11*	0	-	-	-	-	-	-	-	-	-	-	-	-
12*	45	-	-	-	-	-	-	-	-	-	-	-	-

*Honeywell Transducers

Table 3.4. Pressure coefficients for the corner ports on Face 5 of Model 1

Test	Angle	Face 5 Corner Pressure Ports															
		13	14	15	16	19	20	21	22	23	24	25	26	28	29	30	31
1	0	-	-	-	-	-	-	-	-	-	-	-	-	-	-	-	-
2	0	-	-	-	-	-	-	-	-	-	-	-	-	-	-	-	-
3	0	-	-	-	-	-	-	-	-	-	-	-	-	-	-	-	-
4	0	-1.255	-1.260	-1.260	-1.258	-1.263	-1.267	-1.287	-1.279	-1.263	-1.271	-1.278	-1.291	-1.228	-1.234	-1.256	-1.253
5	45	-	-	-	-	-	-	-	-	-	-	-	-	-	-	-	-
6	45	-	-	-	-	-	-	-	-	-	-	-	-	-	-	-	-
7	45	-	-	-	-	-	-	-	-	-	-	-	-	-	-	-	-
8	45	-1.056	-0.854	-0.679	-2.623	-0.930	-0.758	-0.710	-0.618	-0.793	-0.685	-0.641	-0.641	-2.669	-0.536	-0.577	-0.603
9*	0	-	-	-	-	-	-	-	-	-	-	-	-	-	-	-	-
10*	45	-	-	-	-	-	-	-	-	-	-	-	-	-	-	-	-
11*	0	-	-1.141	-	NA	-1.252	-	-	-	-	-	-	-	-	-	-	-
12*	45	-	-0.863	-	NA	-0.840	-	-	-	-	-	-	-	-	-	-	-

*Honeywell Transducers

Table 3.5. Pressure coefficients for the center ports on Face 5 of Model 1

Test	Angle	Face 5 Center Pressure Ports									
		17	18	27	32	33	34	35	36	37	38
1	0	-	-	-	-	-	-	-	-	-	-
2	0	-1.351	-1.108	-1.281	-1.154	-1.202	-0.824	-0.578	-0.570	-0.394	-0.305
3	0	-1.353	-1.121	-1.281	-1.156	-1.199	-0.826	-0.575	-0.568	-0.391	-0.308
4	0	-	-	-	-	-	-	-	-	-	-
5	45	-	-	-	-	-	-	-	-	-	-
6	45	-2.343	-1.682	-0.292	-0.479	-0.367	-0.472	-0.494	-0.469	-0.346	-0.294
7	45	-2.347	-1.685	-0.291	-0.478	-0.366	-0.470	-0.493	-0.467	-0.346	-0.294
8	45	-	-	-	-	-	-	-	-	-	-
9	0	-	-	-	-	-	-	-	-	-	-
10	45	-	-	-	-	-	-	-	-	-	-
11	0	-	-	-	-	-	-	-	-	-	-
12	45	-	-	-	-	-	-	-	-	-	-

The graphs in Figures 3.8 through 3.15 show the pressure distribution near the vertical center of Face 1 and Face 5 for the 0° case, the pressure distribution near the corner of Face 5 for the 0 and 45° cases, the effects of port diameter on pressure readings, and the practicality of interpolating pressure between ports.

Figures 3.8 and 3.9 illustrate the distribution of pressure near the centerline of Faces 1 and 5 of the model for the 0° wind load case. Figures 3.8 and 3.9 illustrate the measured pressure distribution in a uniform flow as compared to that of a boundary-layer wind flow. Since Model 1 was subjected to a uniform wind flow, the pressure distribution is somewhat different from that of a boundary layer flow

although they follow a similar trend as shown in Figures 3.8 and 3.9. Figure 3.10 illustrates the pressure distribution in a uniform flow. While the measured pressures on Face 5 resemble that of Figure 3.10, those on Face 1 do not. The similarities and differences between the measured pressure distributions and those available in the literature show that the wind tunnel setup and the instrumentation used to measure pressure were functioning well.
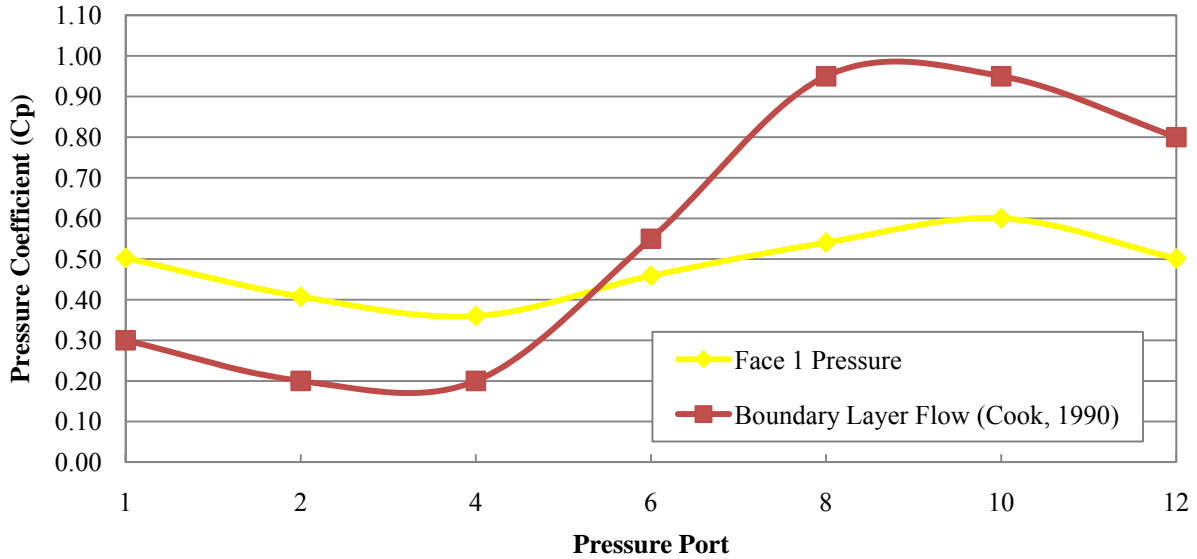
Figure 3.8. Comparison of pressure distributions on Face 1 of Model 1 in uniform flow and boundary-layer flow at 0° wind angle (Cook, 1990)
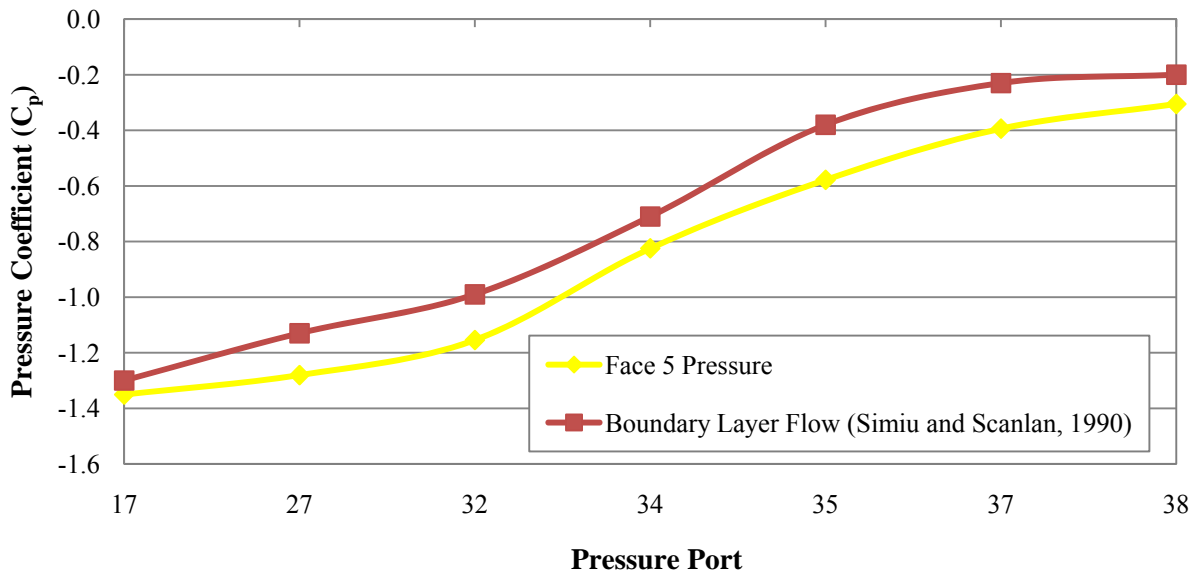
Figure 3.9. Comparison of pressure distributions on Face 5 of Model 1 in uniform flow and boundary-layer flow at 0° wind angle (Simiu and Scanlan, 1996)
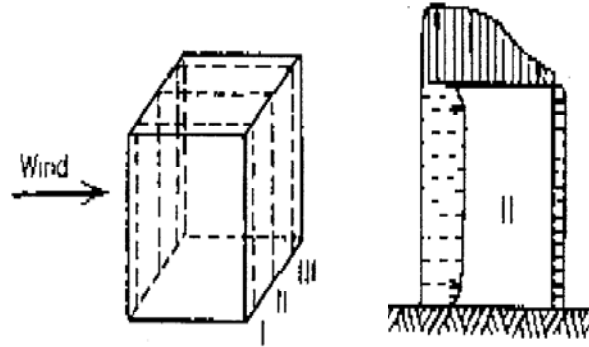
Figure 3.10. Pressure distribution on the windward, roof, and leeward surfaces of a flat roof model subjected to a uniform wind flow (Simiu and Scanlan, 1996)
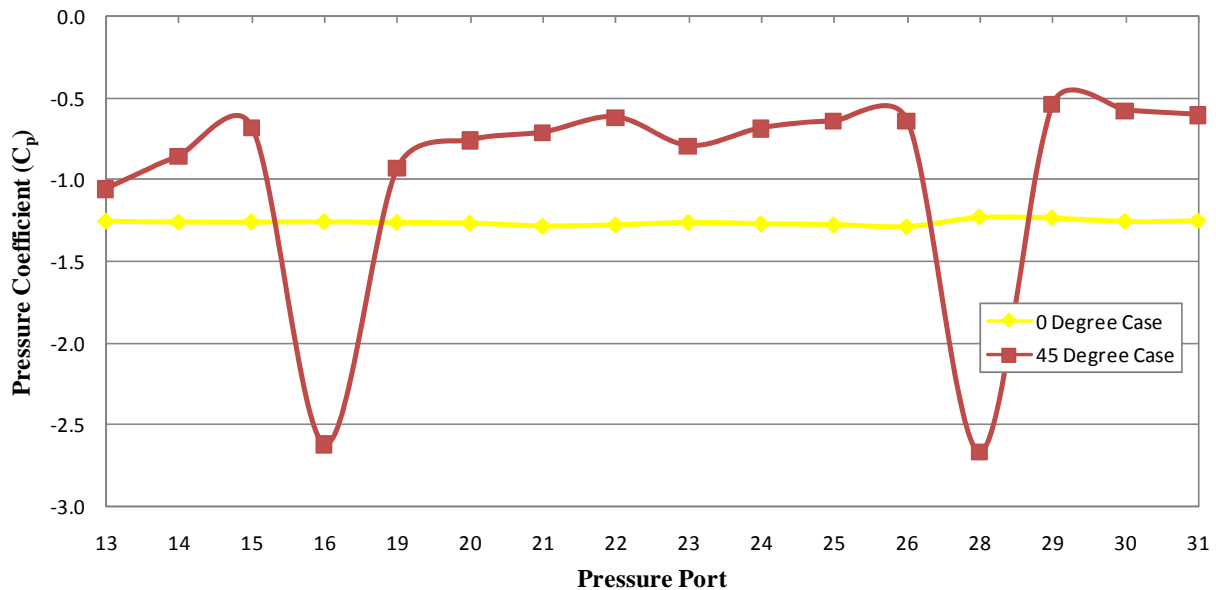
Figure 3.11 depicts the pressure distribution near the corner of Face 5 for the 0 and 45° cases. Notice the relatively uniform pressure distribution for the 0° case compared to the pressure distribution for the 45° case. Also, refer to Figure 3.4 and note the location of ports 16 and 28. Interestingly, the two ports are the farthest from the corner along the edge. This reiterates the information in Chapter 2 regarding large magnitude pressures near the corners and along the edges of structures and also alludes to a delta-wing vortex phenomenon, which can cause damage near the corners of low rise buildings, as discussed in Section 2.4.4. Again, obtaining expected data encourages the utilization of similar testing methods for the next three models.


Figure 3.11. Pressure distribution near the corner of Face 5 of Model 1

The effects of pressure port diameter are illustrated in Figures 3.12 and 3.13. As stated previously, the two ports compared in the figures should have similar pressure readings. For each pair of data, the right column represents the 1/25 in. (1.0 mm) diameter port and the left column represents the

3/16 in. (4.8 mm) diameter port. As the figures show, in some cases, the larger port produces greater pressure readings and in other cases, the smaller port produces greater pressure readings. Based on the data, no conclusions can be reached regarding the effect of port size on pressure readings. Thus, it was decided to build and study Model 4 to further investigate this issue.
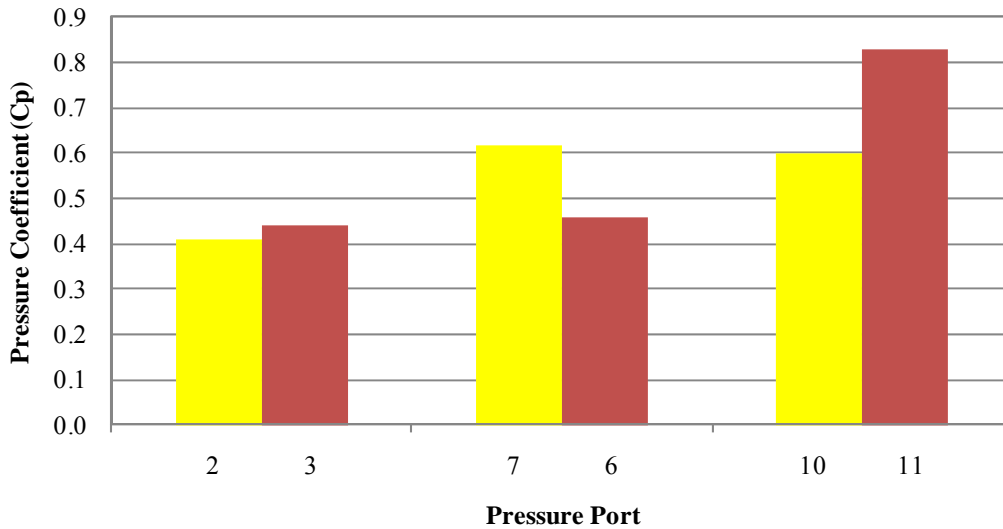
Figure 3.12. Pressure coefficients for ports equidistant from the vertical center on Face 1
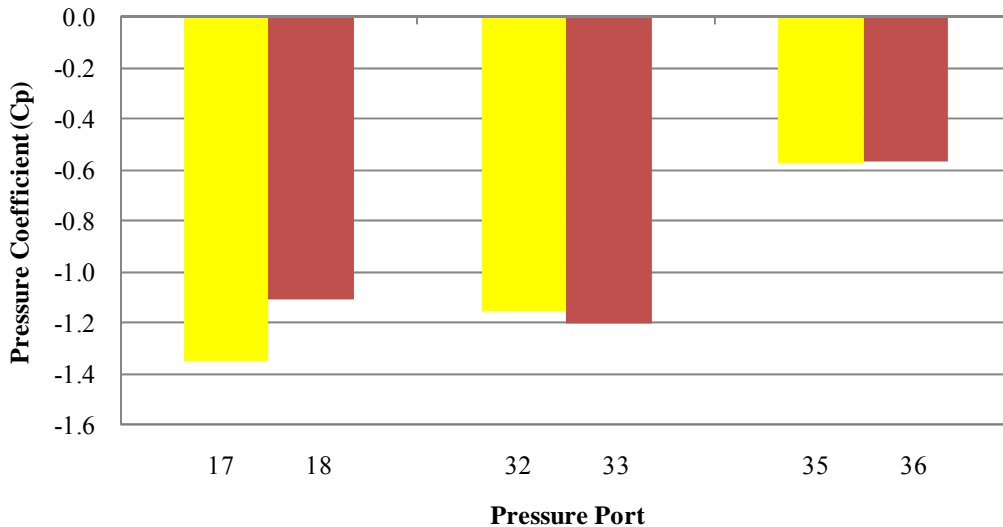
Figure 3.13. Pressure coefficients for ports equidistant from vertical center on Face 5

Figures 3.14 and 3.15 illustrate the difficulty of interpolating pressure data between ports. As shown in Figures 3.8 through 3.15, the pressure pattern between ports depends on the geometry of the structure, port location, and wind angle of attack. Based on these facts, it should be noted that a model of

the actual structure must be studied to determine the actual pressure distribution between ports for any given structure. Interpolating between ports will be addressed further using Model 3.
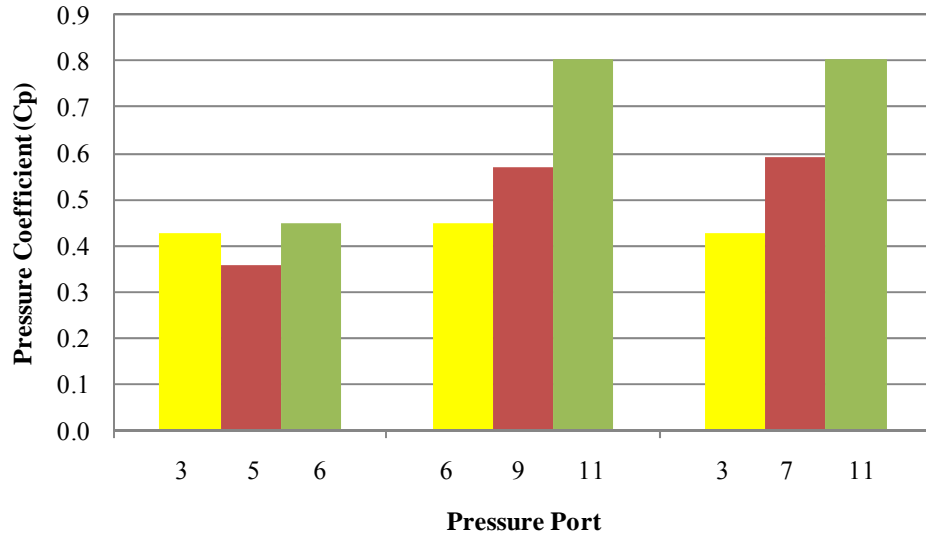
Figure 3.14. Pressure coefficients for interpolation ports on Face 1 due to 0° wind load
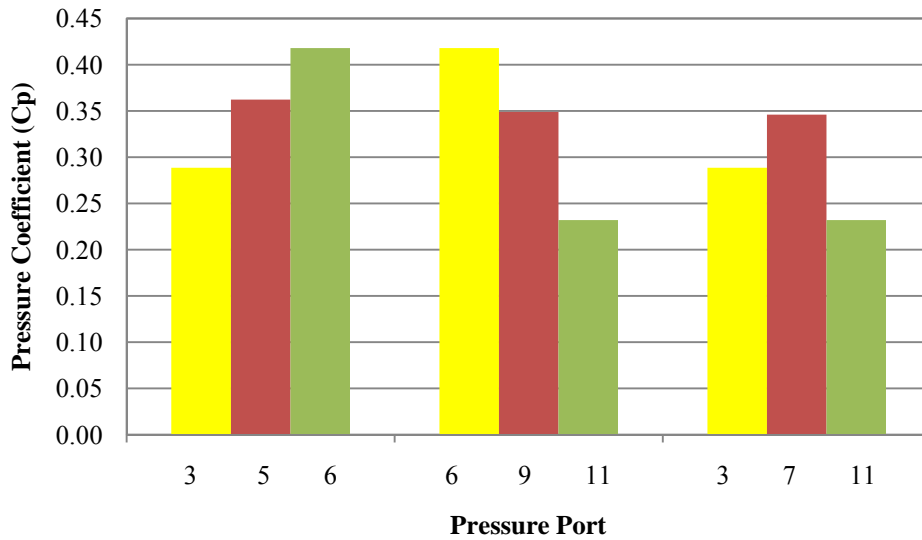
Figure 3.15. Pressure coefficients for interpolation ports on Face 1 due to 45° wind load

After the completion of Model 1 tests and analysis, it was concluded that there is a basic understanding of accurate testing and data analysis procedures, the single-port pressure transducers are accurate, the effect of pressure port diameter on pressure readings needs to be studied further, and the possibility of interpolating pressure data between ports needs further studying.

Chapter 4: Wind Tunnel Test 2 of Basic Pressure Instrumentation Tests on a Cube in Boundary Layer Flow

To further study the effects of transducer type and port diameter on pressure measurements as in Model 1 and to better understand the effects of pressure port diameter, vinyl tube diameter, vinyl tube length, transducer type, and surface roughness on experimental pressure readings, Model 2, a 22 in. cube was built and tested in the AABL Wind and Gust Tunnel located in the WiST Lab at Iowa State University. This model was designated as Model 2. The instrumentation scheme for the front and top faces of the cube was strategically chosen to allow for optimal evaluation of the aforementioned test variables. To increase the usability of the test data, the cube was subjected to a suburban boundary layer flow, and reference barometric pressure, temperature, and velocity values were recorded accordingly. The goal of the fundamental tests was to quantify the effects of port diameter, tube diameter, tube length, transducer type, and surface roughness on pressure readings.

4.1 TEST MODEL

Iowa State University's AABL Wind and Gust Tunnel has a width of 8 feet and a height of 7.5 feet at the location of the boundary-layer test section designated for performing wind tunnel tests on buildings. The 22 in. cube was dimensioned according to the wind tunnel test section cross sectional area of 8352 square inches, with a wind tunnel blockage limitation of the test unit set at eight percent of the test section cross sectional area for the wind load case normal to the cube.

4.1.1 Dimensions and Materials

As stated above, the basic test model was a 22 in. cube. It was constructed with 1/4 in. thick plywood, and four 21.75 x 1.5 x 3.5 in. vertical braces attached on the interior at the corners with wood glue. To improve the aesthetics, wood stain was applied to the surface of the cube. For a smooth surface and thus an optimal wind flow over the cube, four layers of polyurethane clear gloss varnish were applied over the stain and light sanding was done after applying each of the first three layers. The clear gloss varnish is advertised as the smoothest of the four varnish finishes available. Figure 4.1 shows the finished version of the 22 in. cube. Because of the cube's relatively large size and smooth texture, it served as an optimal model for distributing numerous pressure ports and collecting accurate pressure data.
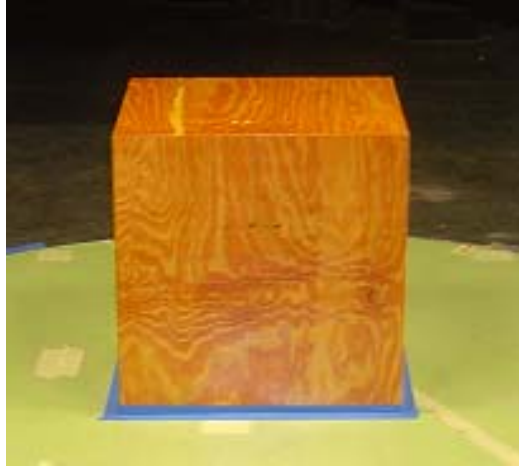
Figure 4.1. Finished version of the 22 in. cube in the AABL Wind and Gust tunnel

4.1.2 Instrumentation Scheme

As shown in Figure 4.2, eleven horizontal rows of seven pressure ports each were constructed on the surface of the cube adding to a total of 77 pressure ports. Five rows of pressure ports were located on the front face of the cube and six on the top face as illustrated in Figures 4.3 and 4.4. The ports on the front face were located at 0.591, 0.636, 0.682, 0.727, and 0.773 of the cube height. The ports on the top face were located at 0.023, 0.068, 0.114, 0.159, 0.2045, and 0.4545 of the cube length. Pressure port test rows were numbered 1 through 4 on the front, 5 through 9 on the top, and a control row was housed on both the front and the top face.

As shown in Figures 4.2 through 4.5, each test row contains seven pressure ports. Row control ports are located at the row ends and in the middle. The remaining four ports varied across the row according to the variable tested. Any fluctuating pressure data across the row was attributed to the distance the port was off-center and the tested variable. Comparing the test row port to its equivalent column control port accounted for the distance the port was off-center. The remaining fluctuating pressure was attributed entirely to the tested variable.

As illustrated in Figures 4.3 and 4.4, all pressure ports were strategically located within the middle third region of the cube. It was hypothesized that if the cube is normal to the wind flow, then each row of pressure ports within the middle third region of the cube should read relatively similar pressure data. Two end ports and a center port were constructed in each row to verify the normality of the cube and the above stated hypothesis.
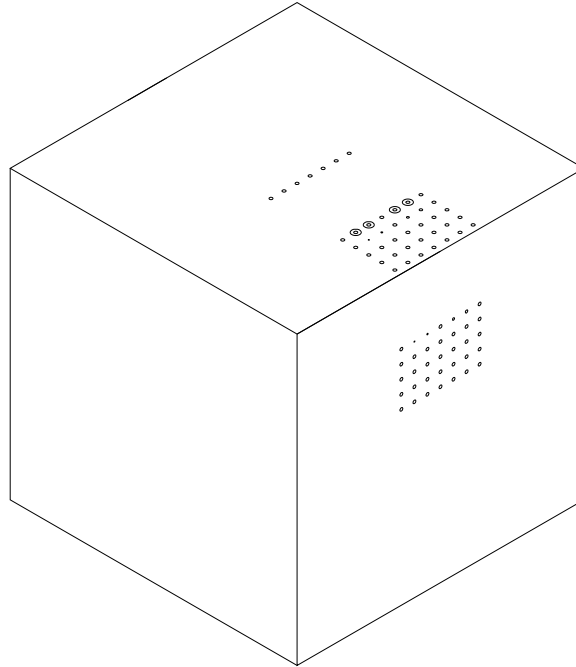
Figure 4.2. Three dimensional schematic of Model 2 and locations of the 77 pressure ports

Row 4 o · · o o o o   Port Size Test
Row 3 o o o o o o o   Tube Length Test
Row 2 o o o o o o o   Transducer Test
Row 1 o o o o o o o   Tube Diameter Test
       o o o o o o o   Front Control Row
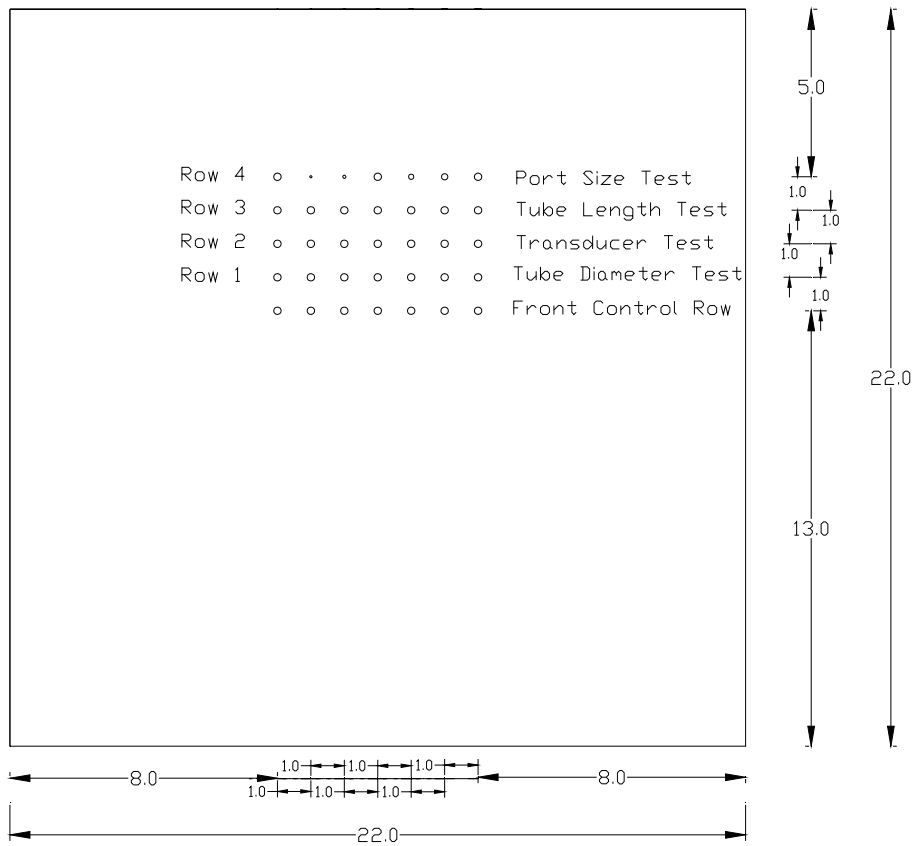
Figure 4.3. Front face schematic of Model 2 (All dimensions are in inches)
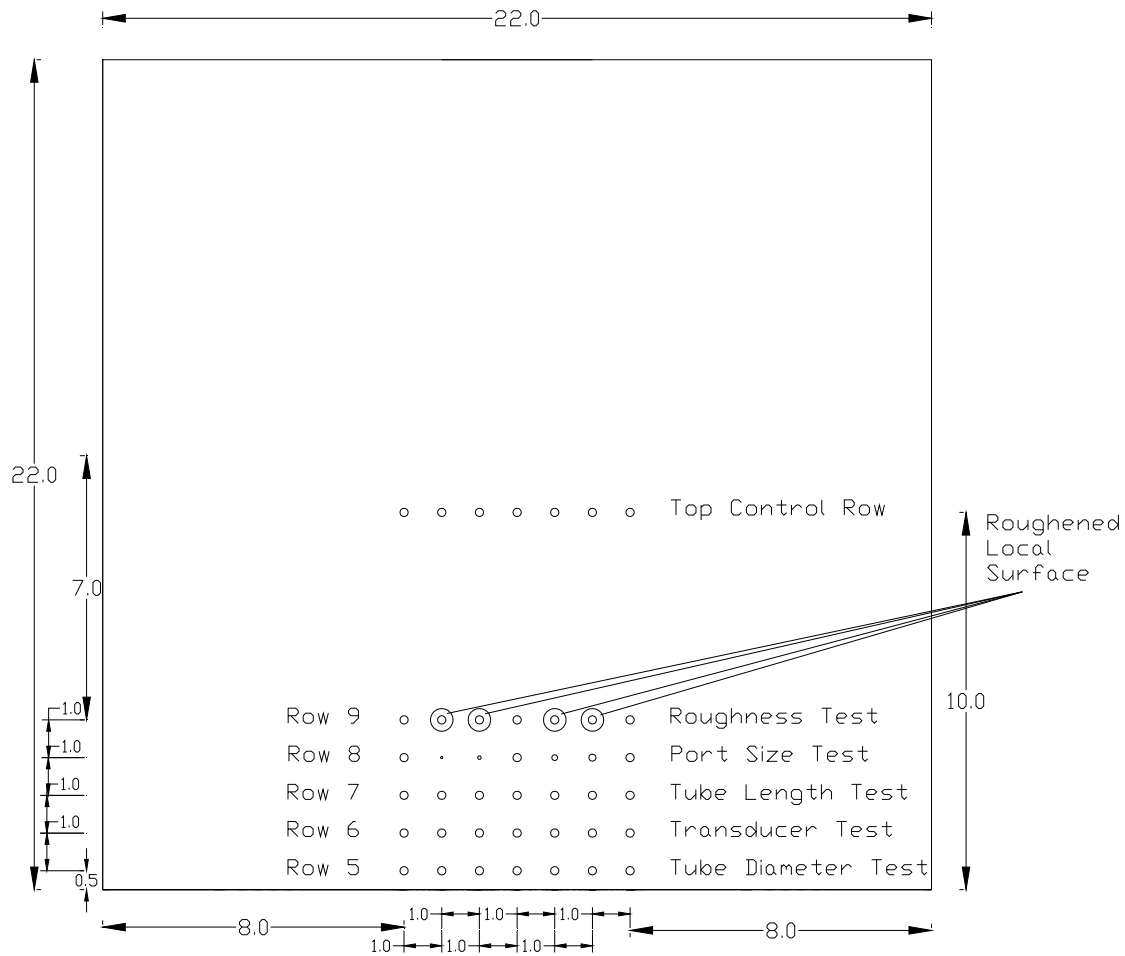
Figure 4.4. Top face schematic of Model 2 (22-in. Cube)

4.2 TESTING

In an attempt to quantify the affects of the test variables discussed in Section 4.1.2 and shown in Figures 4.3 and 4.4, the following test set up was conducted. A suburban boundary layer wind flow was directed perpendicular (i.e., 0°) to the front face of the cube and pressure was measured at all 77 ports using the DSA pressure transducer. Collected DSA results were then divided by the "dynamic pressure" to give the corresponding pressure coefficient. As explained in Section 2.2, "dynamic pressure" is a reference value based on air density and a reference velocity at the time of the test.

4.2.1 Boundary Layer

To produce the turbulent suburban boundary layer wind flow in the AABL Wind and Gust Tunnel, four spires and a series of wood blocks were used (Jones, 2008). Figure 4.5 depicts the terrain

upstream of the cube. As shown, the wind first interacts with the four spires. Next the wind encounters the wood blocks and finally, the wind interacts with the cube. Note that the cube is not pictured in Figure 4.5, but the pitot tube, which is used to measure the static and dynamic wind pressures and located upstream of the cube, is shown.
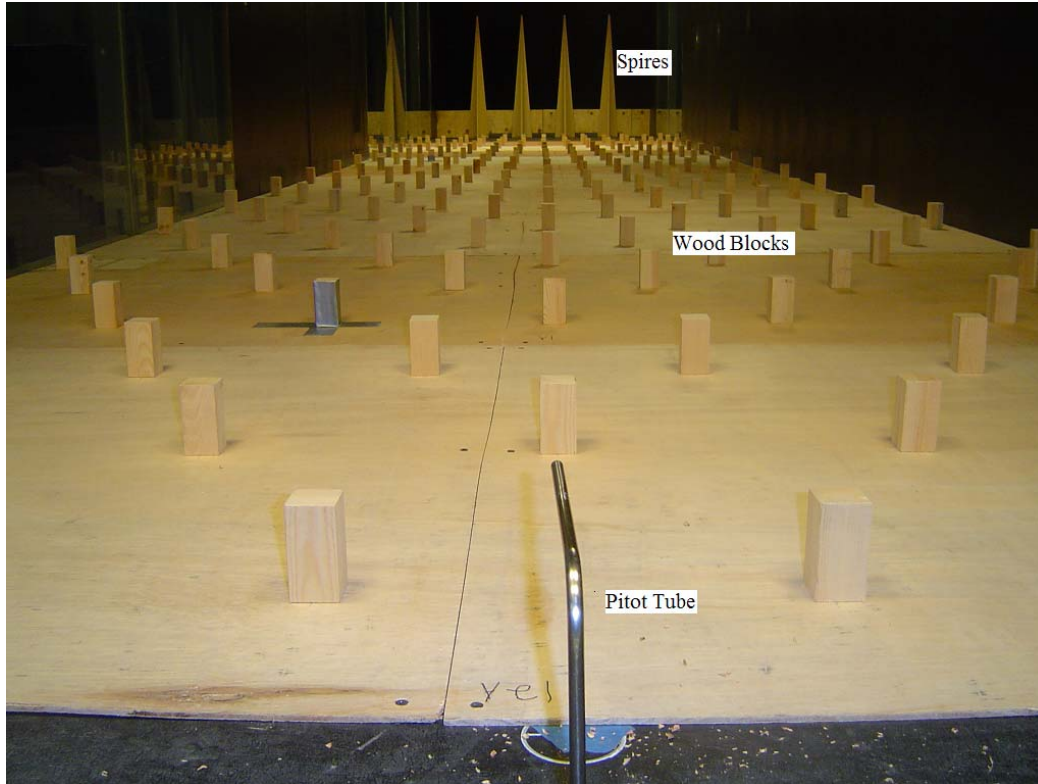
Figure 4.5. Seen here are four spires and wood blocks used to generate a suburban boundary layer wind flow in the AABL Wind and Gust Tunnel as well as the pitot tube used to measure static and dynamic pressures

The wind profile generated at the test section location due to its interaction with the roughness elements and spires in Figure 4.5 is shown in Figure 4.6. An instrument used to measure turbulent flow, known as the Cobra Probe, was used to measure the wind profile. The Power Law Exponent (α) of the velocity profile in Figure 4.6 was estimated to be approximately 0.28, which corresponds to the Power Law Exponent (α) of a suburban terrain as mentioned in Simiu and Scanlan (1996).
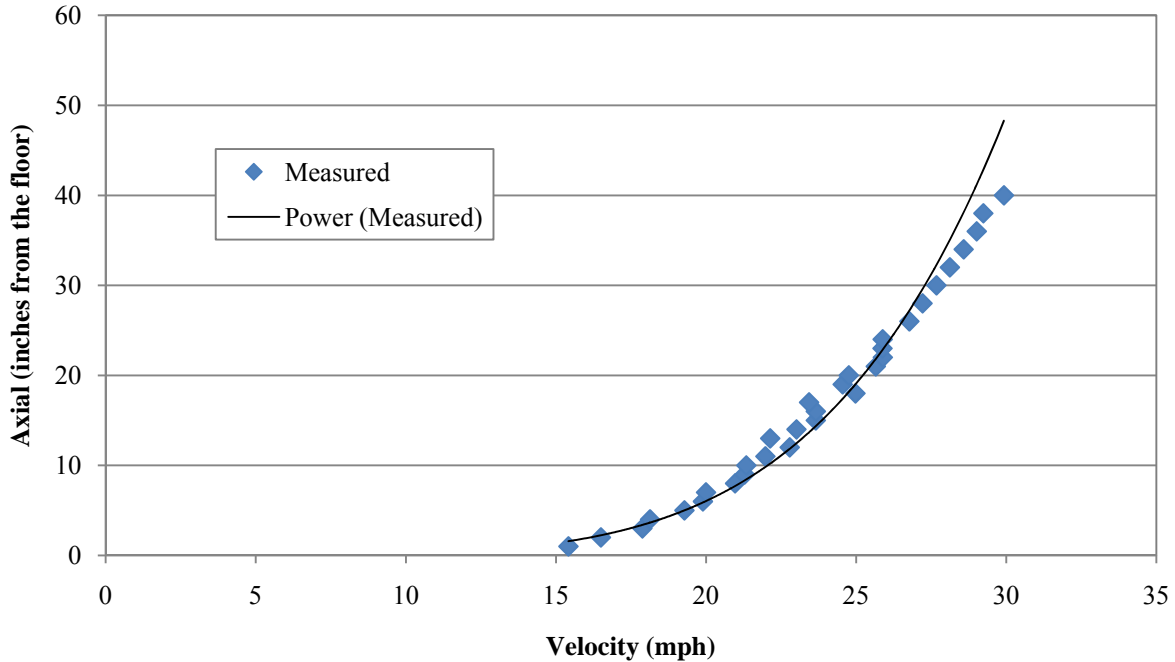
Figure 4.6. Suburban boundary layer profile as measured in the wind tunnel by the Cobra probe

4.2.2 Miscellaneous Reference Values

In all the tests, the DSA transducer outputs the total port pressure less a reference pressure. The static pressure from the pitot tube was used as the reference pressure for the DSA. The static pressure coefficient as calculated from the pitot tube data is shown in Eq. 4.1. An alternative way to measure static pressure was used by taking an average readings of pressure ports installed on the floor, ceiling, and wall surfaces of the wind tunnel at the location of the test section. In theory, only static pressure exists at the surfaces of the wind tunnel because the surface wind velocity is zero. As shown in the following calculations, each method used to measure static pressure produced similar results. For no particular reason, the pitot tube was chosen to input static pressure inside the wind tunnel at a location upstream of the model to the DSA.

Pitot Tube Static Pressure Coefficient:

$$C_p = \frac{p_s - p_0}{\frac{1}{2}\rho U^2}$$

(Eq. 4.1)

$p_s - p_0 = 5.46791$ Pa

$P = 101072$ Pa

$R = 287.05$ J/(kg·K)

$T = 293°$ K

$U = 11.57$ m/s

$C_p = 0.068$

Wall and Floor Static Pressure Coefficient:

$$C_p = \frac{p_s - p_0}{\frac{1}{2}\rho U^2}$$

(Eq. 4.2)

$p_s - p_0 = 5.262547$ Pa

$P = 101072$ Pa

$R = 287.05$ J/(kg·K)

$T = 293°$ K

$U = 11.57$ m/s

$C_p = 0.065$

The reference barometric pressure (P) at the time of the Model 2 tests was 29.85 in. Hg (101072 Pascal). Reference temperature in the tunnel was 67. 7º F (293º K). The gas constant used in the dynamic pressure equation was 124.71 J/(mol·K) (287.05 J/(kg·K)). Because the height of the cube is almost equal to the thickness of the boundary layer as shown in Figure 4.6, the velocity of 25.86 mph (11.57 m/s), at the eave height, was used as the reference velocity.

4.2.3 Test Variables

After verifying the suburban boundary layer wind profile and the static pressure input as discussed above, Model 2 was tested. Figure 4.7 shows an internal Model 2 view of all 77 pressure ports as well as the ZOC pressure transducer (Scanivalve). At the beginning, the plan was to use the ZOC to measure pressure, but after inconsistent test readings were obtained from the ZOC, it was replaced by the DSA. For ease of comprehension, the front face test variables, as shown in Figure 4.3, will be thoroughly discussed below. Other than the surface roughness variable, which is also discussed below, test variable

rows on the top face, as shown in Figure 4.4, were set up exactly like the front face rows. The reason for testing the variables on both the front and top faces was to study the consistency of the results for both positive and negative pressures.

Figure 4.7. An inside view of the model showing the tube connections between the ports and the ZOC transducer

For the tube length test, vinyl tube lengths varied across Row 3. From left to right port, lengths of 20, 5, 10, 20, 30, 35, and 20 inches were used to connect the pressure ports to the DSA pressure transducer. The three 20-inch tubes were connected to the DSA as reference ports. These reference ports were studied to determine the variability of pressure across the row. The other four ports in Row 3 were connected to the DSA and used to compare pressure values produced by different tube lengths. Typical diameter size (1/25 in. inner diameter) tubing was used to connect the seven "tube length test" ports to the DSA. Also, all seven port diameters were 1/48 in. Data collected from the ports in Row 3 was used to compare the affect of tube length on pressure measurements.

To test the effects of port diameter, the ports in Row 4, from left to right, were constructed of diameters 1/48, 1/32, 1/16, 1/48, 3/32, 1/8, and 1/48 inch. The three 1/48 inch pressure ports in Row 4 were connected to the DSA using 1/25 in. inner diameter tubing and were used as reference ports. The four larger ports in Row 4 were tapered down at the port end of the tube over a span of 1.5 inches to 1/25 in. inner diameter tubing. The total length of adapters and tubing from each pressure port to the DSA was 20 inches. Data collected from the ports in Row 4 was used to compare the affect of port size on pressure measurements.

For the tube diameter test, vinyl tube diameters varied across Row 1. Similar to the port diameter test, there were five different pressure tube diameters. From left to right, the tube diameters were 1/25, 1/32, 1/25, 1/48, 3/32, 1/8, and 1/25 in. The three 1/25 in. ports in Row 1 were connected to the DSA as reference ports, while the other four ports were tapered at both ends and connected to the DSA. Total length of adapters and tubing from each pressure port to the DSA was, again, 20 inches. Port diameter remained constant at 1/48 in. for all seven ports. Data collected from Row 1 was used to compare the effect of tube diameter on pressure measurements.

To test the effects of different transducers, the ports in Row 2, from left to right, were connected to the DSA, ZOC, Honeywell, DSA, Setra, ZOC, and DSA pressure transducers. The two outer and one middle DSA ports in Row 2 served as reference ports. Port diameter and tube length was a constant 1/48 in. and 20 in., respectively, for all seven ports in Row 2. Inner tube diameter for the DSA and ZOC transducers was 1/25 in., while the inner tube diameter for the Honeywell and Setra transducers was 1/8 in., as recommended by the manufacturers. Data collected from Row 2 was used to compare the effects of transducers on pressure measurements.

For the surface roughness test on the top face of the model (i.e., Row 9), the ports, from left to right, were surrounded by no sand paper, grade 320 sand paper, grade 220 sand paper, no sand paper, grade 120 sand paper, grade 80 sand paper, and no sand paper. Grade 80 is the roughest and grade 320 is the smoothest of these sand papers. All seven pressure ports were connected to the DSA with the outer two ports and middle port serving as the reference ports. Port diameter, tube diameter, and tube length was a constant 1/48 in., 1/25 in., and 20 in., respectively, for all seven ports. Figure 4.8 illustrates the sand paper used to create surface roughness on the cube. Data collected for Row 9 was used to compare the affects of surface roughness on pressure measurements.

Figure 4.8. Top face of the 22 in. cube illustrating the five test rows

4.3 RESULTS AND DISCUSSION

Figures 4.9 and 4.10 show graphs of the mean pressure coefficients measured within the middle third section on the front and top faces of the 22 in. cube. Figures 4.11 and 4.12 show the wind flow and pressure distribution on a cube as mentioned in Cook (1990) and Simiu and Scanlan (1996). Note the difference between the uniform and boundary-layer wind flows' interaction with the cube as shown in Figure 4.11. Also, comparison of Figures 4.9, 4.10, and 4.12 reveal that the pressure coefficients as mentioned in Simiu and Scanlan are larger than those measured on the 22 in. cube. One reason for this discrepancy is because the 22 in. cube is large relative to the boundary layer profile and thus, the reference velocity at eave height is relatively large, producing a relatively small pressure coefficient value.

For Model 2 pressure coefficient data, five test runs were performed with each test run consisting of the collection of 10,000 data points over a time interval of 20 seconds. The average (mean) and root-mean-square (rms) of the 50,000 data points were calculated and are displayed in Figures 4.13 through 4.19. The rms is the square root of the mean of each data point squared.
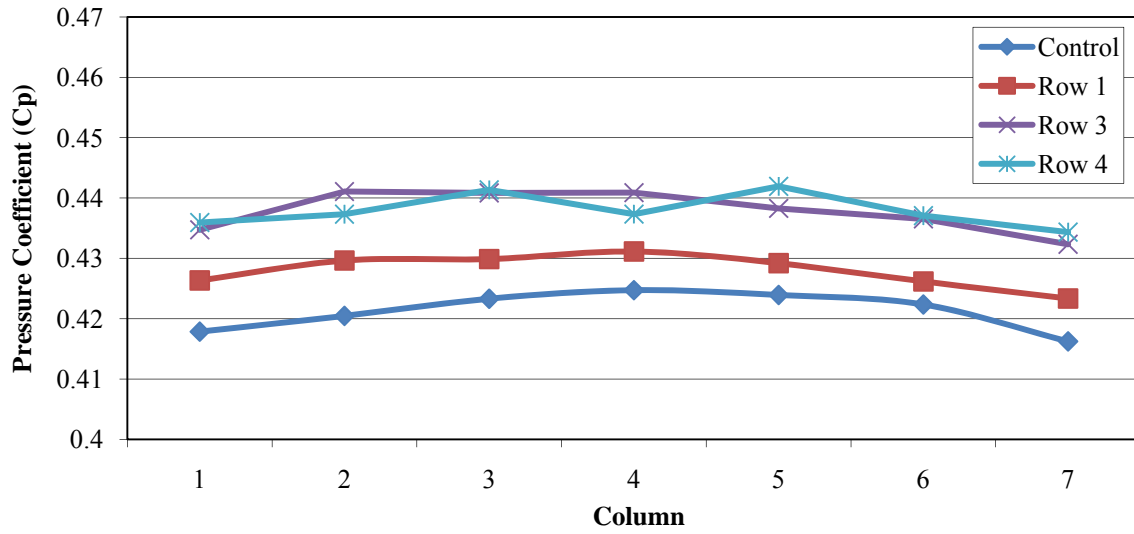
Figure 4.9. Mean pressure coefficients measured on the front face of the 22 in. cube
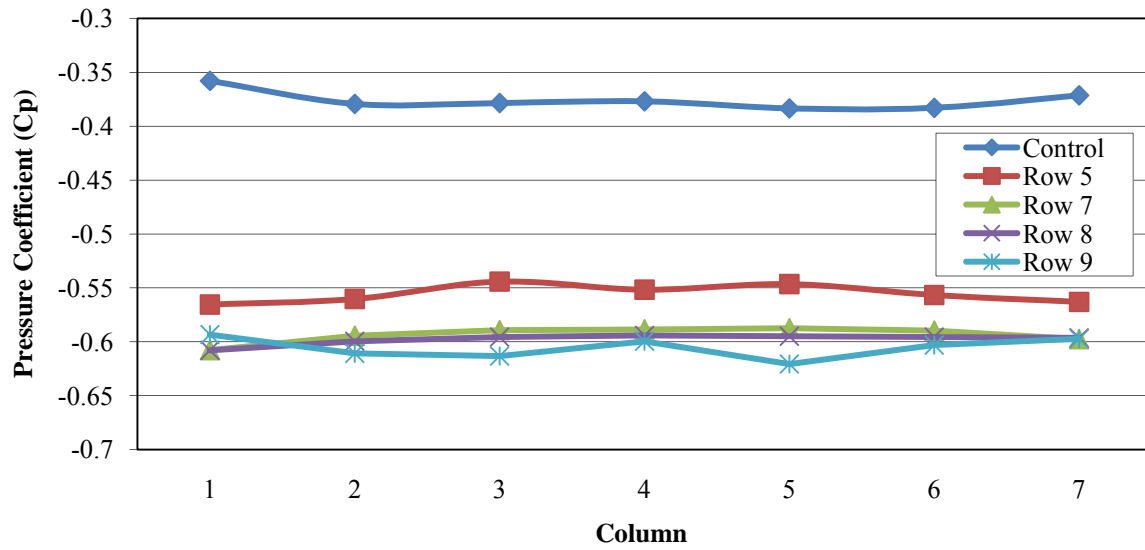
Figure 4.10. Mean pressure coefficients measured on the top face of the 22 in. cube

(a) Uniform wind profile   **(b) Boundary layer profile**
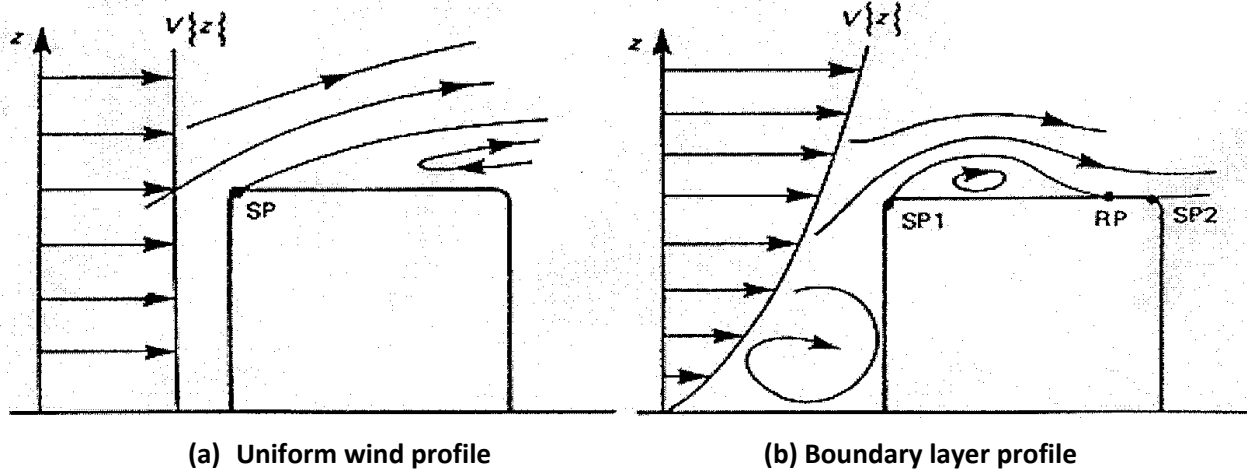
Figure 4.11. Separation and reattachment of wind flow on roofs subjected to (a) uniform and (b) boundary layer wind profiles (Cook, 1990; SP: separation point, RP: reattachment point, z: height, V{z}: wind velocity with respect to height)
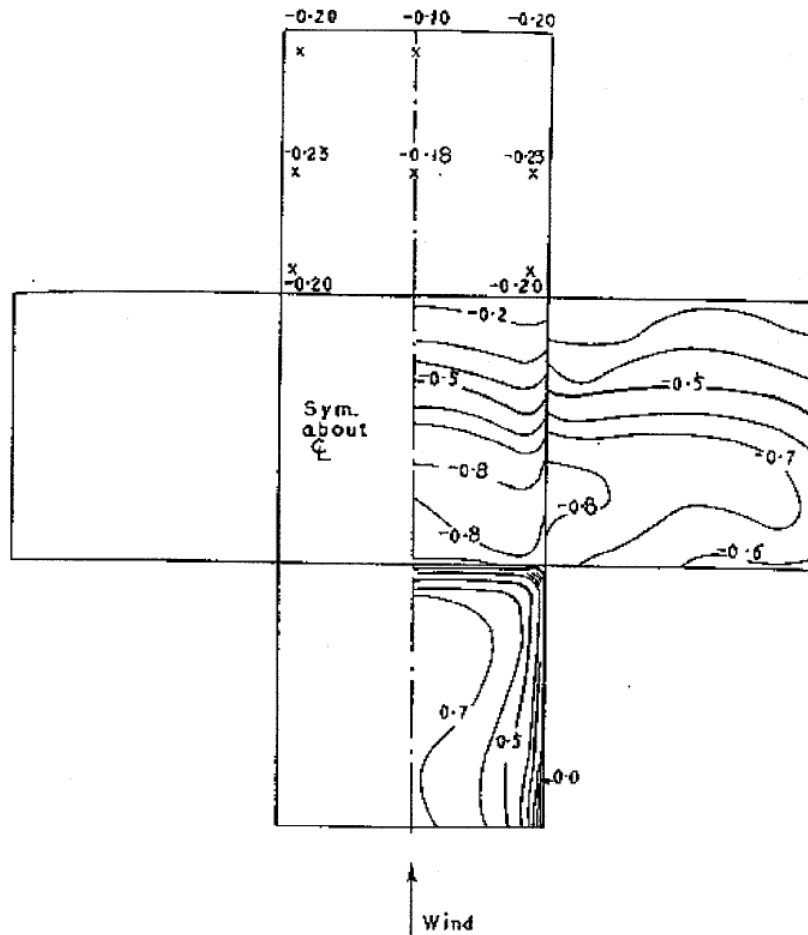
Figure 4.12. Pressure distribution on the surface of a cube subjected to a boundary-layer wind flow (Simiu and Scanlan, 1996)

Because of the slight variation of pressure across each row as shown in Figures 4.9 and 4.10, the pressure coefficient at each pressure port in rows one through four was divided by the pressure coefficient at the matching column port in the front control row. For example, the pressure coefficient at the leftmost port of row 1 was divided by that of the leftmost port of the front control row. For the top face, pressure coefficient at each port in rows five through nine was divided by the pressure coefficient at the matching column port in the top control row. In the end, the ratios across each row were compared to determine any pressure result affects due to the five different test variables. Sections 4.3.1 through 4.3.5 discuss the test variable ratio results.

4.3.1 Pressure Port Diameter

In regards to port diameter affecting pressure readings, Figure 4.14 illustrates that an increase in port diameter coincides with a decrease in measured pressure. Note that this trend occurs only on the top face of the cube. On the front face, as shown in Figure 4.13, one port larger than the reference port of 1/48 in. measures an increase in pressure, one port shows the same, and the other two ports measure a decrease in pressure. Based on the two figures, no trend conclusion can be affirmed, but it can be stated that the pressure fluctuation due to a change in port diameter is no greater than 5 percent for the given port diameters measured. Also, because the variation shown in Figure 4.13 is smaller than 0.8 percent, the trend in Figure 4.14 should be noted for future fundamental tests. Also note a possible Reynolds Number effect in Figure 4.13 in that pressure magnitude decreases, then increases, and then decreases as port diameter increases.
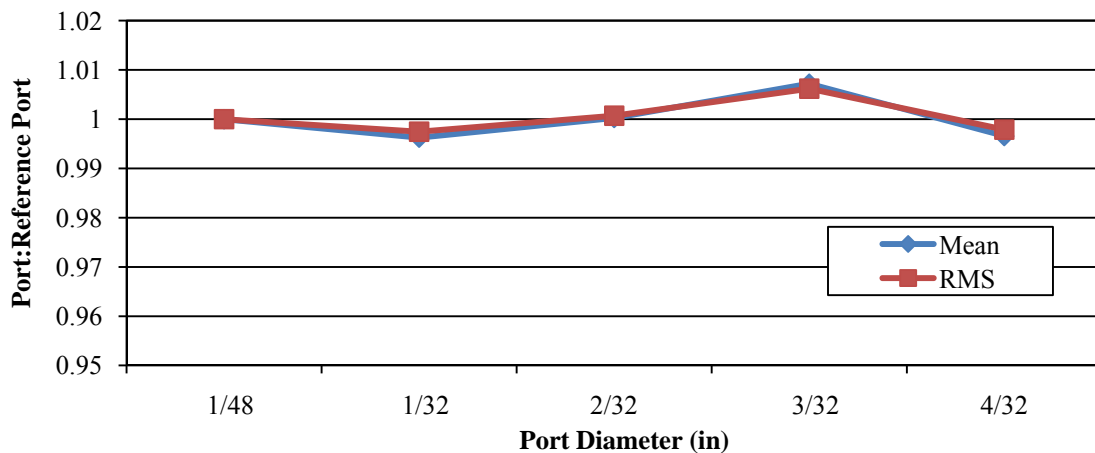
Figure 4.13. Port diameter trend on the front face with respect to the pressure value for the reference port diameter of 1/48 in.
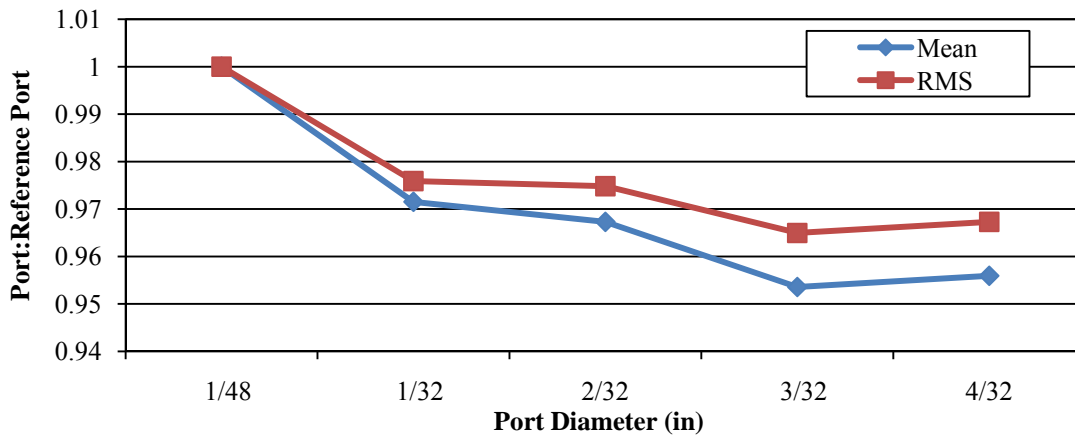
Figure 4.14. Port diameter trend on the top face with respect to the pressure value for the reference port diameter of 1/48 in.

4.3.2 Tube Diameter

For the tube diameter affects on pressure readings, Figure 4.15 illustrates that an increase in tube diameter coincides with a decrease in the mean and rms of pressures. Note that this trend occurs only on the front face of the cube. On the top face, as shown in Figure 4.16, the smaller and larger tube diameters, with respect to the reference tube diameter of 1/25 in., measure a decrease in pressure. Based on the two figures, no trend conclusion can be affirmed, but it can be stated that the pressure fluctuation due to a change in tube diameter is no greater than 6.0 percent for the given tube diameters measured. The trend in Figure 4.15 should be noted for future fundamental tests. Also note a possible Reynolds Number effect in Figure and 4.16 in that the pressure magnitude increases, then decreases, and then increases as the tube diameter increases.
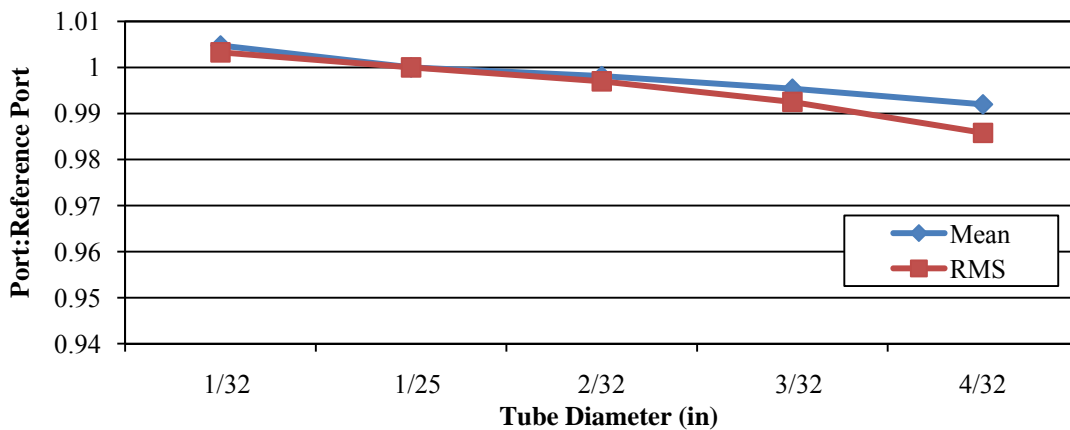
Figure 4.15. Tube diameter trend on the front face with respect to the pressure value for the reference tube diameter of 1/25 in.
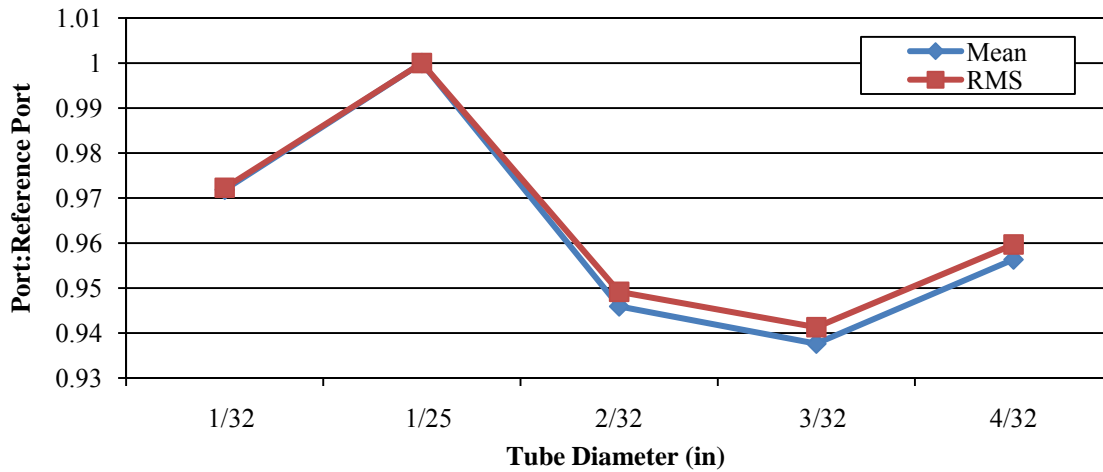
Figure 4.16. Tube diameter trend on the top face with respect to the pressure value for the reference tube diameter of 1/25 in.

4.3.3 Tube Length

In regards to tube length effects on pressure readings, Figure 4.17 illustrates that an increase in tube length coincides with a decrease in measured pressure. Note that this trend occurs only on the front face of the cube. On the top face, as shown in Figure 4.18, the smaller and larger tube lengths, with respect to the reference tube length of 20 in., measure a decrease in pressure. Based on the two figures, no trend conclusion can be affirmed, but it can be stated that the pressure fluctuation due to a change in tube length is no greater than 5.5 percent for the given tube lengths measured. The trend in Figure 4.17 should be noted for future fundamental tests. Also note a possible Reynolds Number effect in Figure 4.18.
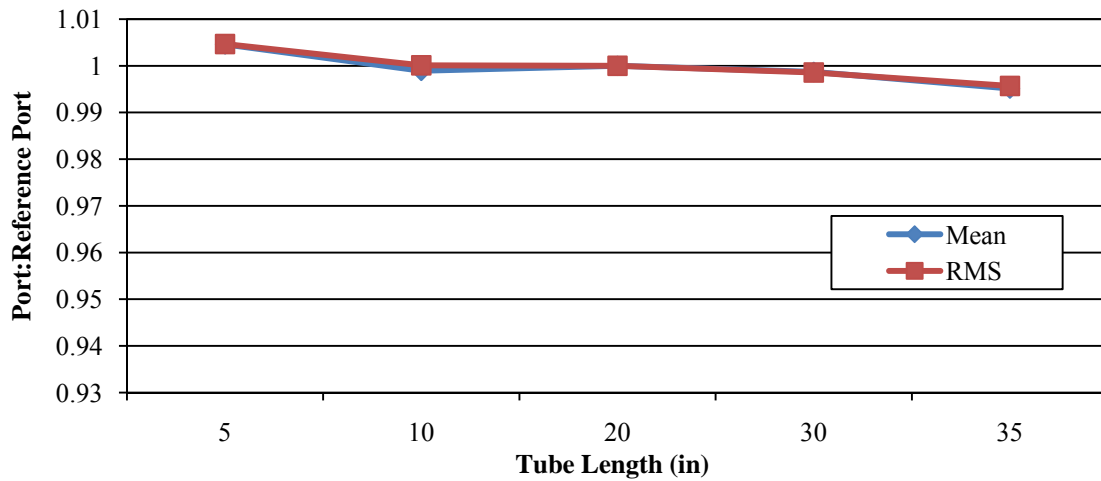
Figure 4.17. Tube length trend on the front face with respect to the pressure value for the reference tube length of 20 in.
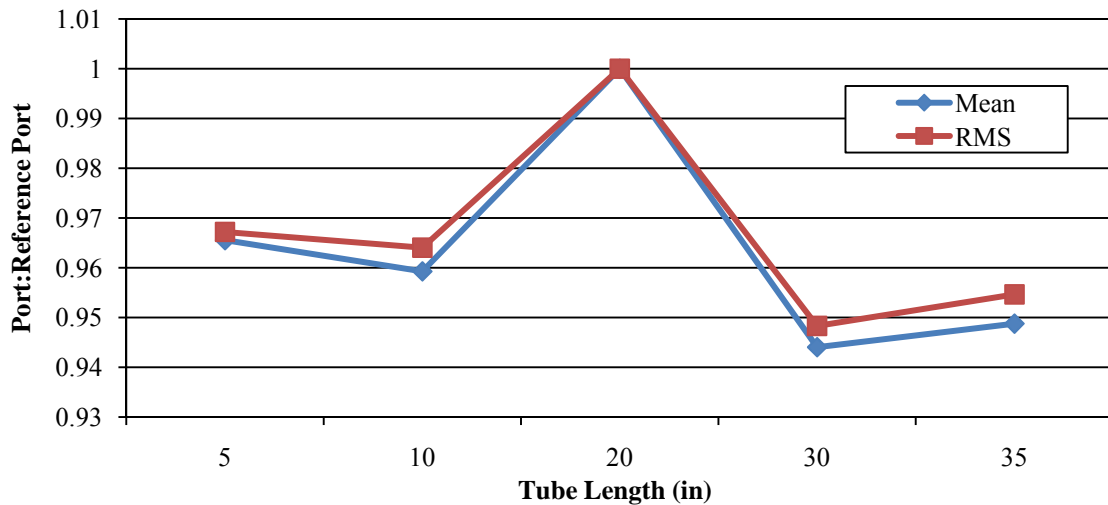
Figure 4.18. Tube length trend on the top face with respect to the pressure value for the reference tube diameter of 20 in.

4.3.4 Transducer Type

For the transducer affects on pressure readings, ZOC malfunctions were experienced during testing. The ZOC transducer was measuring pressure coefficients equal to half the magnitude of the DSA, Setra, and Honeywell coefficients. Much time and effort was put into fixing the ZOC, but by the time it worked properly, the suburban boundary layer set-up had been disassembled and the fourth model was being tested. It was decided that enough information on the performance of the transducers was gathered during the first model tests and also that the transducers would be tested during the fourth model tests. Thus, research was able to continue despite no reliable transducer type results on pressure readings.

4.3.5 Surface Roughness

Regarding the surface roughness effects on pressure readings, Figure 4.19 illustrates a general trend that an increase in surface roughness can produce an increase in measured pressure (not including Grade 80 data). Note that this trend occurs on the top face of the cube. It can be stated that the pressure fluctuation is no greater than 1.5 percent for the roughness surfaces measured.
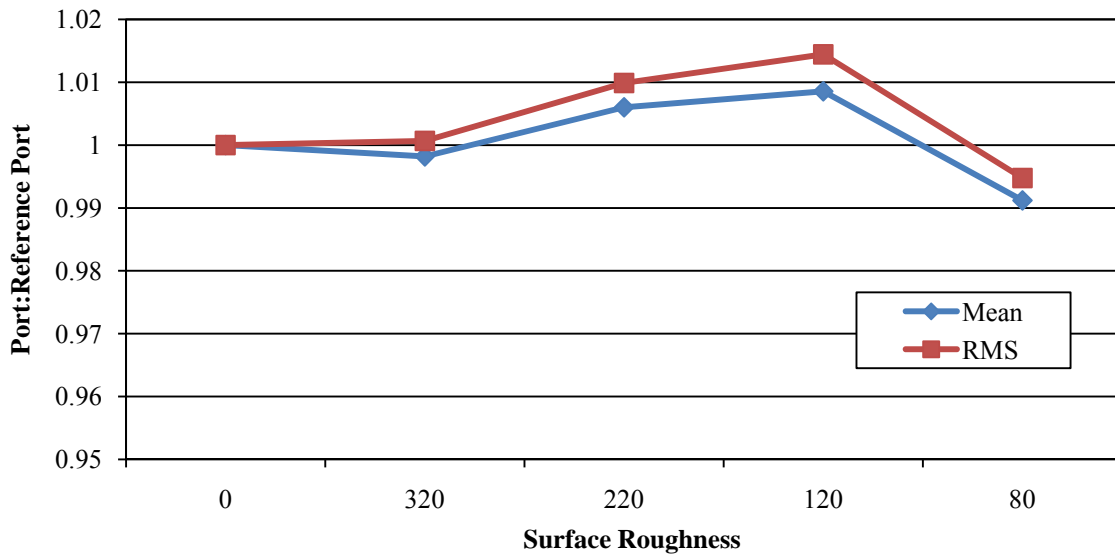
Figure 4.19. Surface roughness trend on the top face with respect to the pressure value for the reference roughness of no sand paper

Chapter 5: Wind Tunnel Test 3 to Understand the Pressure Port Protection Device Using a Partial Roof and Wall Test Model

To develop a basic understanding of the pressure port protection device (PPPD) currently used in the field on the test house, a partial roof and wall model of the field structure was constructed and tested in the AABL Wind and Gust Tunnel at Iowa State University. One non-shingled roof and one shingled roof model were first instrumented with lab pressure collection hardware and tested separately. Then the two models were instrumented with field pressure collection hardware, including a single-port transducer and PPPD, and tested separately. The goals in testing the two models were to: 1) reaffirm the conclusion made after the first model test that the single-port pressure transducer used in the field is as accurate as the lab pressure transducers; 2) determine the effect of surface roughness on pressure readings; 3) determine the effect of field hardware, including the PPPD, on pressure readings; and 4) determine whether pressure data can be recorded at strategic locations to study the possibility of interpolating pressure readings between the ports.

5.1 TEST MODEL

As stated in Chapter 4.1, Iowa State University's AABL Wind and Gust Tunnel has a width of 8 feet and a height of 7.25 feet at the location designated for performing wind tunnel tests involving a boundary layer. The partial roof and wall test model was built according to the cross sectional area of 8352 square inches of the wind tunnel test region, with a wind tunnel blockage limitation set at approximately eight percent of the cross sectional area for any orientation of the model.

5.1.1 Dimensions and Materials

A two foot section at the center of the low rise building in the field was used to create the design for the partial roof and wall model. As illustrated in Figures 5.1 through 5.5, the two models were identical, except one partial roof and wall model was constructed with roof shingles and roofing felt and the other was not. Both models had widths of 24 in., roof slopes of 1:3, and leeward heights of 20 in. Each model was braced with dimension lumber and rafter plates as shown in Figures 5.2 and 5.3. The interior of the models contained 1/2 in. gypsum board and they were enclosed on the exterior with 1/2 in. plywood.

    (a) With shingles   **(b) Without shingels**
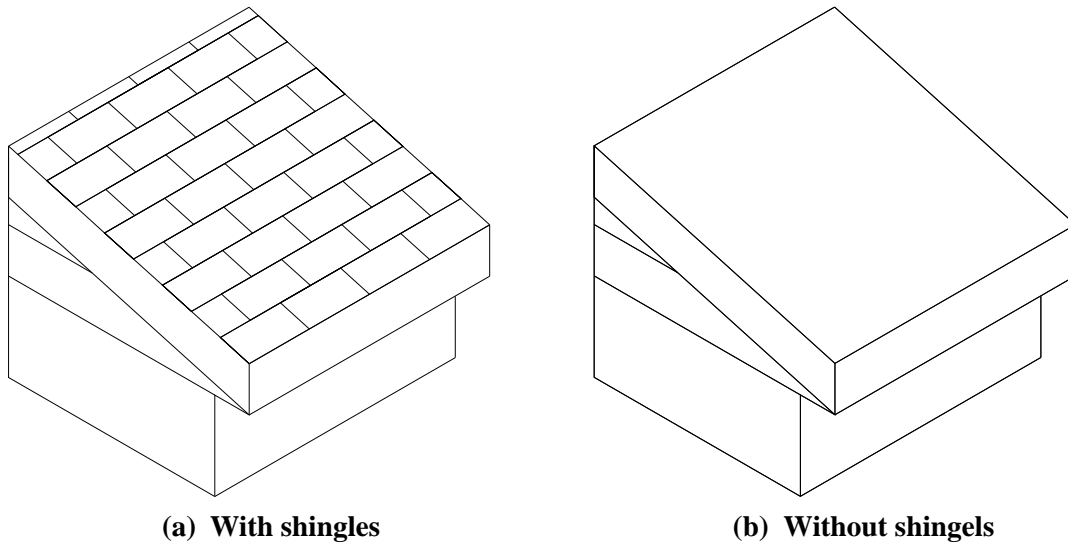
Figure 5.1. Three dimension schematics of the partial roof and wall models
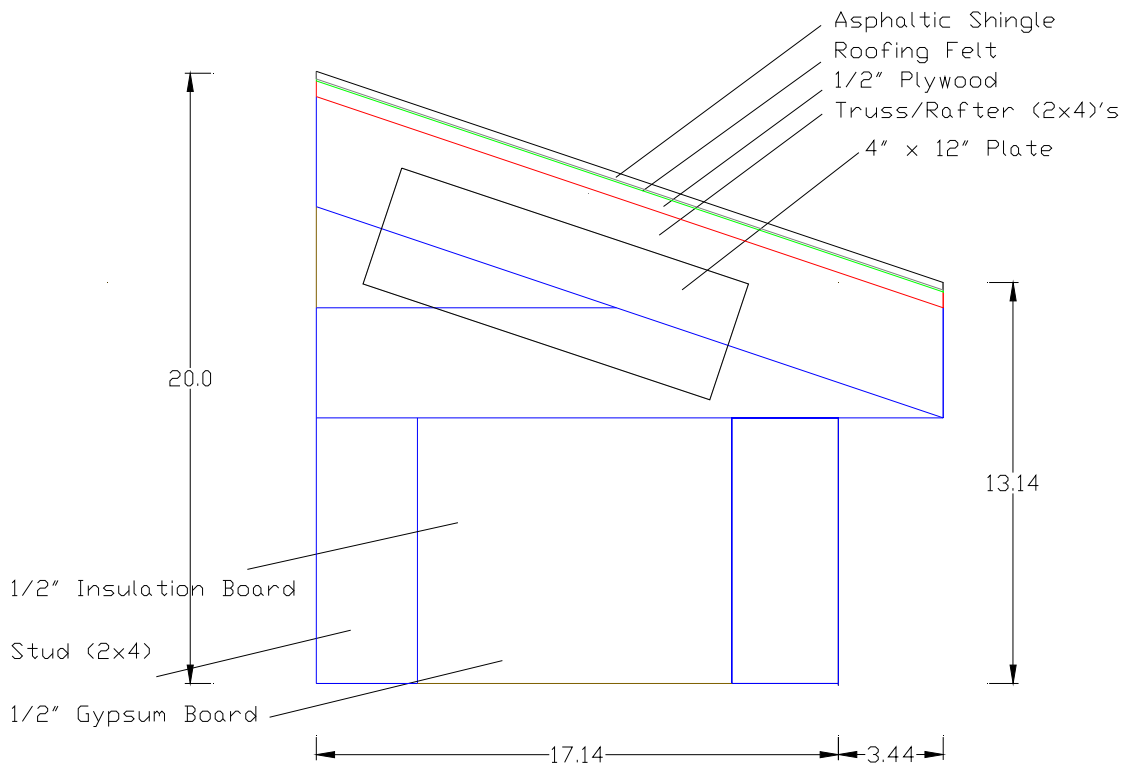
Figure 5.2. Side view of the partial roof and wall model with shingles (All dimensions are in inches)
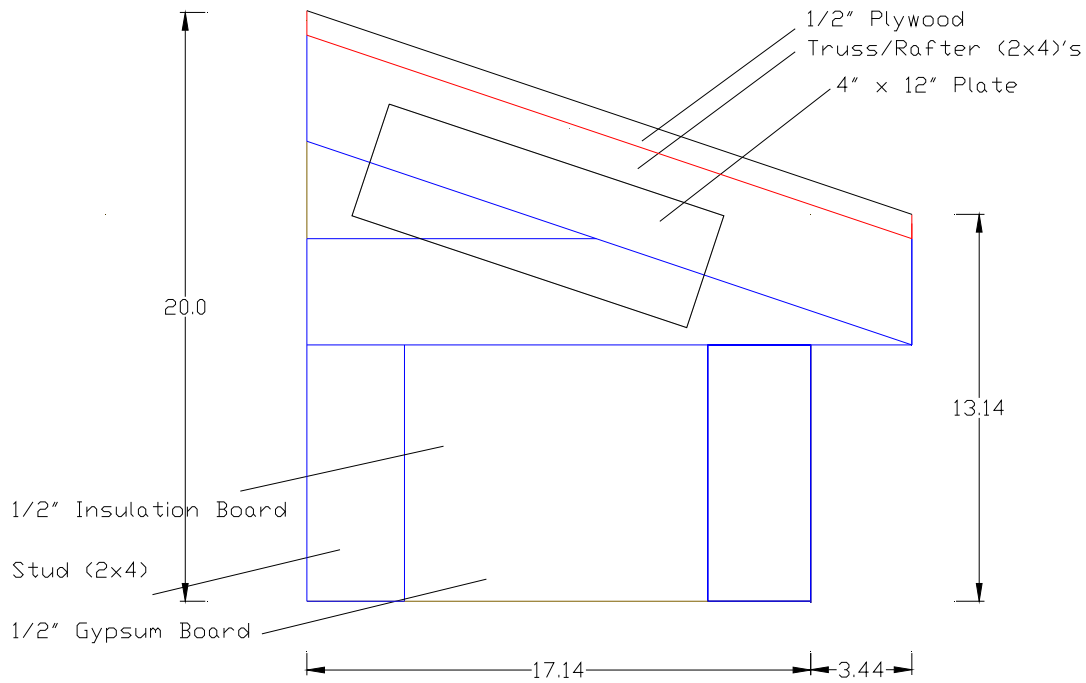
Figure 5.3. Side view of the partial roof and wall model without shingles (All dimensions are in in.)

(a) With shingles (b) Without Shingles

Figure 5.4. Each partial roof and wall model as erected in the AABL Wind and Gust Tunnel

5.1.2 Locations of Pressure Ports

As shown in Figure 5.5, each partial roof and wall model contained 27 pressure ports. Three of the 27 ports were connected to Setra Model 265 single-port pressure transducers. The other 24 pressure ports were connected to two DSA pressure transducers. Four rows of ports in Figure 5.5, each containing three pressure ports, were selected to better understand the possibility of interpolating pressure between

pressure port data. Three rows of ports in Figure 5.5, each containing five pressure ports, were selected to compare data from the Setra pressure transducer with data from the DSA pressure transducer. It was hypothesized that pressure data in the middle third region of the model would stay relatively constant throughout each individual row and conclusions could be made based on this assumption. Furthermore, the outer ports of each row could be compared to test the above assumption that pressure was relatively constant in the middle third region of the test section.
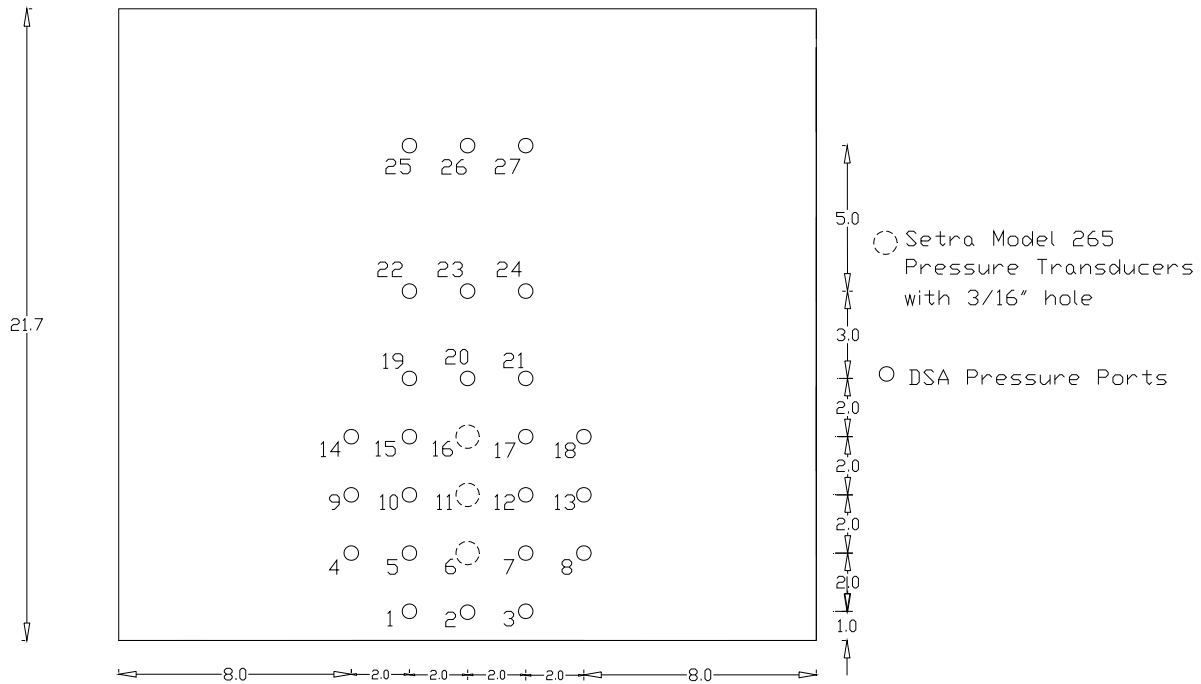
Figure 5.5. Pressure port locations on the top face of the partial roof and wall models

5.2 PRESSURE PORT PROTECTION DEVICE

The PPPD was erected in the field to protect the single-port pressure transducers from moisture. As shown in Figure 5.6, the PPPD has two caps to prevent rain water from entering the pressure recording system.   At the bottom of the PPPD in Figure 5.6 are two open tubes. One tube connects to the Setra model 265 pressure transducer with a flexible tube. The other tube is capped to collect any water from the system that the two top caps fail to reject. Approximately two inches from the top of the PPPD are two twist caps. These caps are twisted on their respective sides of the roof to securely fasten the PPPD to the roof surface.
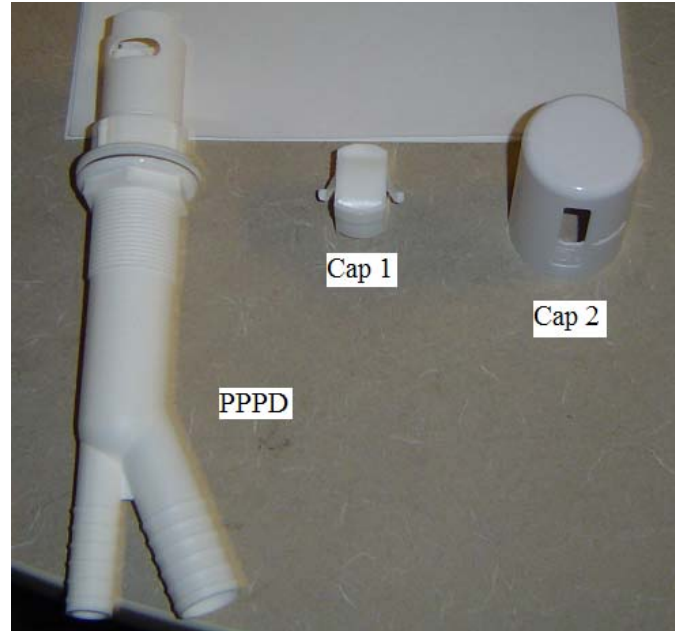
Figure 5.6. Disassembled pressure port protection device with pressure port on the side of cap 2

Interestingly, the pressure port itself is located on the side of the PPPD rather than the top. It is this physicality that caused concern about the use of the PPPD and the correlation between the measured data surface pressure on the roof. If pressure is measured normal to the port, then a port on the side of the PPPD would generate pressure readings dependent on the direction of the wind. The results and discussion portion of this chapter will further address this issue.

5.3 TESTING

Four tests were conducted on the model with a shingle surface and four tests on the model with a no shingle surface to test the effect of surface roughness on pressure measurements. To test the effect of port size on pressure measurements, two partial roof and wall models for test one contained regular size ports, while two partial roof and wall models for tests two, three, and four each contained three larger ports. Also, each of the two models for test three included one PPPD, while the models for tests one and two included no PPPDs to test the effect of a PPPD on pressure measurements. Finally, each of the two models for test four included three PPPDs to test the effect of multiple PPPDs on pressure measurements. All tests were run using a suburban boundary layer wind flow. Although this wind flow is different than the coastal boundary layer flow that the building is subject to in the field, the reason for using the suburban boundary layer flow was to maximize the turbulence of the wind flow.

When the tests were finished, it was discovered that the protrusion of the PPPD from the roof caused enough obstruction in the wind flow to generate incomparable data at all pressure port locations. Thus, the test plan was changed.

The new test plan was to focus entirely on the PPPD. Pressure ports 9 through 13, as illustrated in Figure 5.5, were instrumented and pressure data was collected. First, no PPPD was installed and pressure data was collected. Second, the PPPD was installed at Port 11, but Caps 1 and 2, as shown in Figure 5.6 were not attached. Third, Cap 1 was attached. Fourth, Caps 1 and 2 were attached and Cap 2 was rotated to the windward side (0°). Following the fourth test, Cap 2 was rotated in increments of 45 degrees with each test. Figures 5.7 shows the PPPD with no caps, Cap 1, and both caps, rotated at 0°.

| (a) No caps | (b) One cap | (c) Both caps |
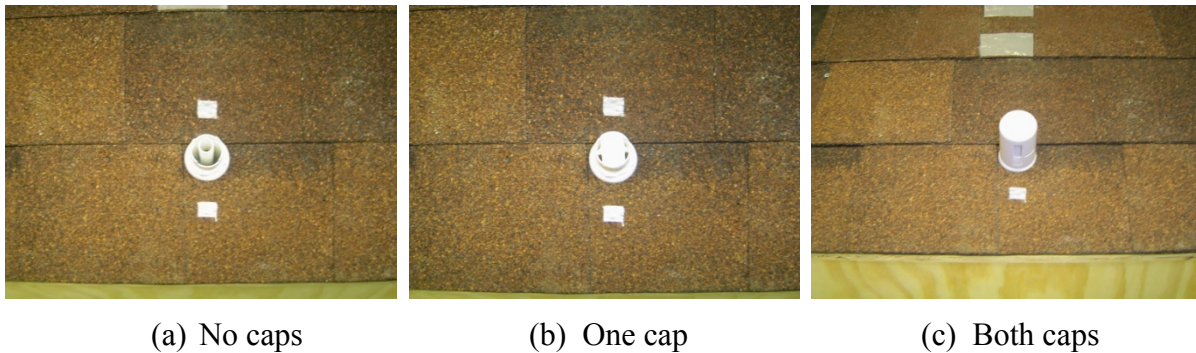
Figure 5.7. Pressure port protection device on partial roof and wall model with shingles

5.4 RESULTS AND DISCUSSION

The results of the partial roof and wall model tests are displayed graphically in Figures 5.8 through 5.13. Figures 5.8, 5.9, and 5.10 each display one row of pressure data as measured on the smooth surface partial roof and wall. Each data point in Figures 5.8 through 5.10 is the average port pressure recorded during five test runs and each test run involved the collection of 6000 data points over a time interval of 20 seconds. As shown in Figure 5.5, the four ports off center are connected to the lab pressure transducer while the middle port of each row is connected to the field pressure transducer. As stated earlier, it was hypothesized that the five ports should measure relatively equal pressure because they are all located in the middle third region of a symmetric model. The three figures show minimal difference between lab and field pressure transducer data, reaffirming the conclusion made after the first model test that the single-port pressure transducer is as accurate as the lab pressure transducer.
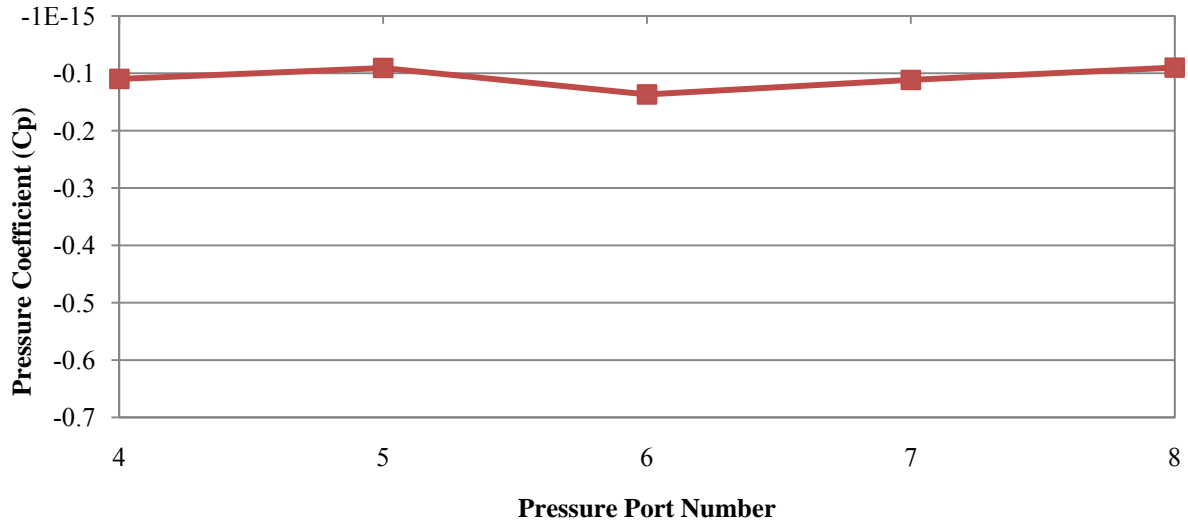
Figure 5.8. Field and lab pressure transducer readings for ports 4 through 8
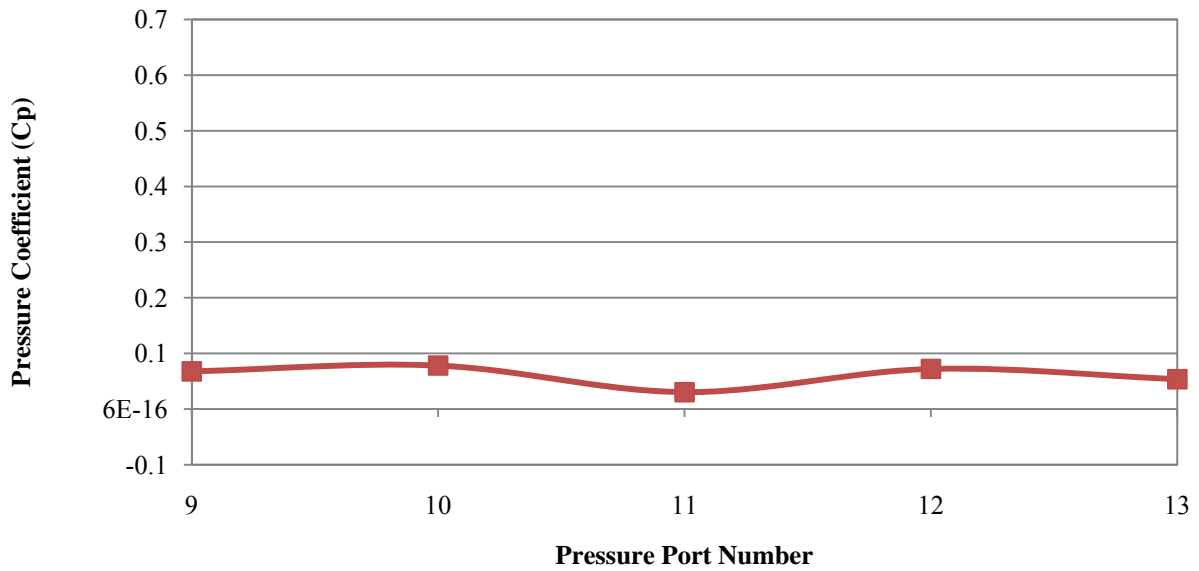
Figure 5.9. Field and lab pressure transducer readings for ports 9 through 13
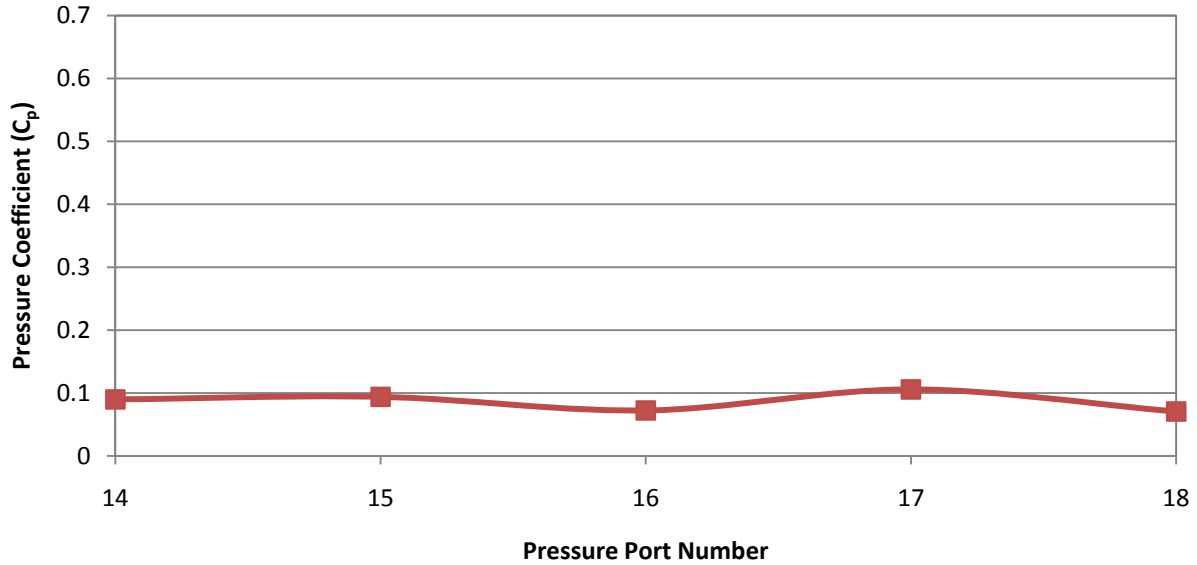
Figure 5.10. Field and lab pressure transducer readings for ports 14 through 18

Figure 5.11 illustrates the effect of surface roughness on pressure readings. The figure shows pressure data from ports 25, 26, and 27. Data was collected for both the smooth and shingle surface. The three ports are located seven rows beyond the leading edge of the model, so small pressure coefficients were expected for both cases. But for the shingle surface case, a leading edge of the shingles was located 1/8 in. toward the 0° (windward) side of the pressure ports, generating pressure readings of much larger magnitude than the smooth surface case. Thus, it was concluded that all elements of the test model including shingles must be scaled when tested in the wind tunnel.
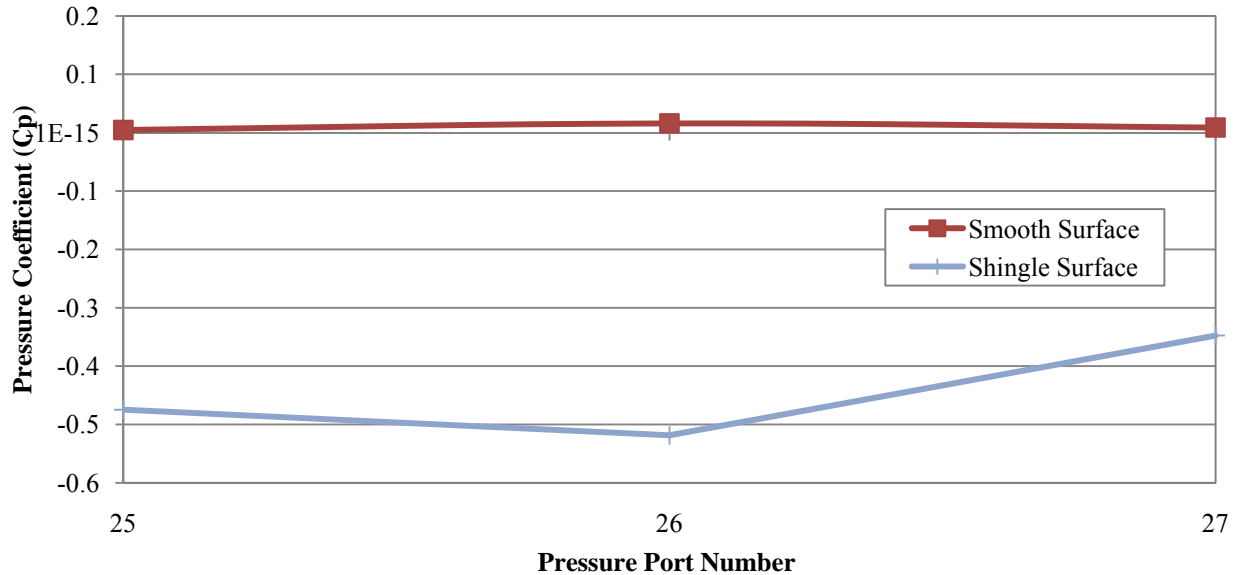
Figure 5.11. Effect of the shingled surface on pressure readings

The final tests on the roof and wall model were performed on the smooth surface model and pertained to the effect of the PPPD on pressure readings. Ports 9, 10, 11,12, and 13 were first tested without the PPPD and the data was recorded as the "expected values." The PPPD was then installed eight different ways at Port 11 for eight consecutive tests. First no caps were installed on the PPPD, then Cap 1 was installed, followed by the installation of Cap 2. The data collected at ports 9 through 13 for the aforementioned tests is displayed in Figure 5.12. Next, Cap 2 was rotated in increments of 45°, from 0 to 180° in an attempt to represent the reality of wind approaching the PPPD from any angle, and data was collected at each increment and displayed in Figure 5.13.

Reviewing Figures 5.12 and 5.13 suggests that recorded data was relatively consistent at each port other than the tested port, Port 11. This observation is important because it reassures the fact that all fluctuating data from Port 11 was caused by controlled changes to the port. Conclusions from Figure 5.12 at Port 11, where the PPPD was tested, are that 1) no pressure coefficients were close to the expected values, 2) the pressure coefficient measured with no caps installed was equal to the pressure coefficient with one cap installed because with only Cap 1 mounted on the PPPD, the port was still normal to the roof surface as is shown in Figure 5.7, and 3) the installation of Cap 2 caused a significant change in the pressure coefficient sign and magnitude because with the installation of Cap 2, the pressure port orientation was changed from normal to the roof surface to directly facing the wind, hence the large positive coefficient. The conclusion from Figure 5.13, at Port 11, is that not only did the installation of Cap 2 affect pressure data, but the sign and magnitude of pressure is directly related to the cap orientation. Based on Figures 5.12 and 5.13 it is evident that the PPPD adversely affects the port pressure readings.
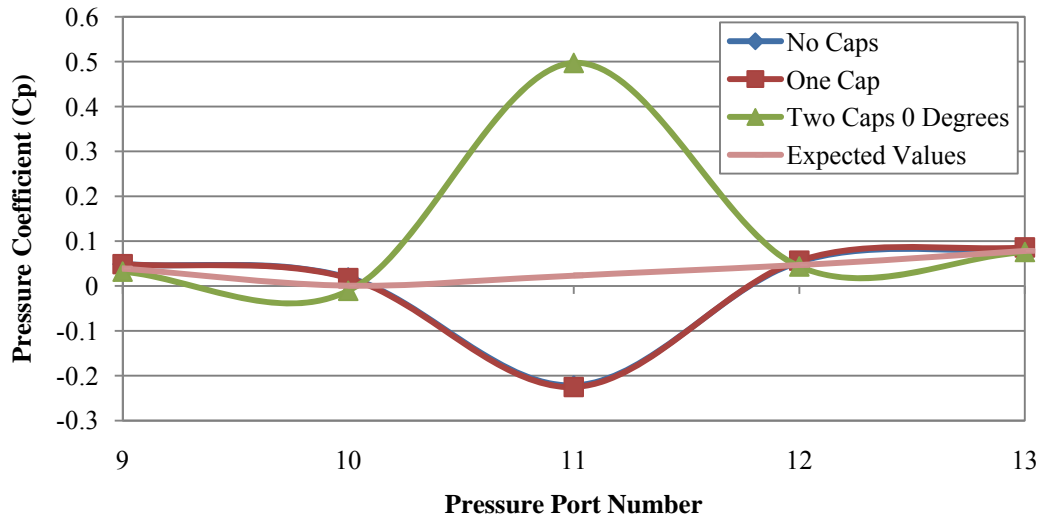
Figure 5.12. Effect of the PPPD, with and without the water prevention caps, on pressure readings
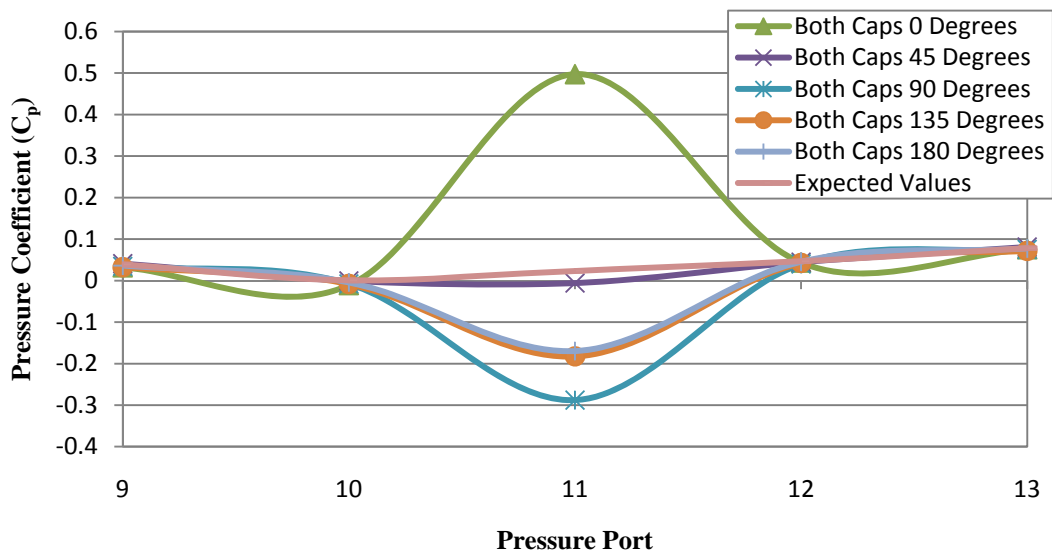
Figure 5.13. Effects of the PPPD, with both caps and different port orientations, on pressure readings

Due to the above results, three important recommendations were made for the building and testing of the fourth model, a model of the low rise building itself. Firstly, it was decided that the model would be built with a smooth surface to prevent inaccurate pressure readings due to the shingle edges. Secondly, a scaled version of the PPPD needs to be tested in the wind tunnel. Thirdly, a model of the low rise building itself and not a partial model must be instrumented and tested to better understand the possibility of interpolating pressure readings between ports.

Chapter 6: Wind Tunnel Test 4 of the Low-rise Building

To develop a basic understanding of the pressure distribution on the roof of the low-rise building described and to expand on data from the first three tested models, a 1:16 model of the field structure was constructed and tested in the AABL Wind and Gust Tunnel at Iowa State University. Between the eave, roof, and inside of the wood model, a total of 202 pressure ports were located. To duplicate the boundary layer profile on the test structure in the field, a coastal boundary layer wind profile was simulated in the wind tunnel and reference wind speed was measured and used to calculate pressure coefficients at pressure port locations. The model and ports were used in four different tests to: 1) affirm Model 2 fundamental variable observations; 2) study the wind angle effect on the magnitude and distribution of pressure on the roof; 3) determine pressure reading effects due to a scaled version of the PPPD; and 4) compare uplift force calculated from pressure data with measured uplift force values.

6.1 TEST MODEL

The low-rise building model was built according to a cross sectional area of the wind tunnel test region of 8352 square inches, with a wind tunnel blockage limitation set at eight percent of the cross sectional area for any orientation of the model.

6.1.1 Dimensions and Materials

In the field, the low-rise building walls have an eave height of 10 ft, hip roof edges are 48 ft by 32 ft, and the roof pitch is 1:3, as shown in Figure 6.1. Using a 1:16 scale, the model was 7.5 in. tall up to the eave with hip roof edges of 3 ft by 2 ft and a roof pitch of 1:3, as illustrated by the model shown in Figure 6.2. The model was constructed of 1/4 in. plywood. Assembly of the model was divided into three stages. First, the four wall pieces were glued together, as shown in Figure 6.3.1. Next, the four eave pieces were glued together and that piece was glued to the wall frame, as shown in Figure 6.3.2. Finally, the four hip roof pieces were glued to each other and then to the eaves. In the end, as shown in Figure 6.3.3, a quality model of the low-rise building was completed.

Figure 6.1. Low-rise field test structure constructed in Pensacola, Florida (FPL, 2006)
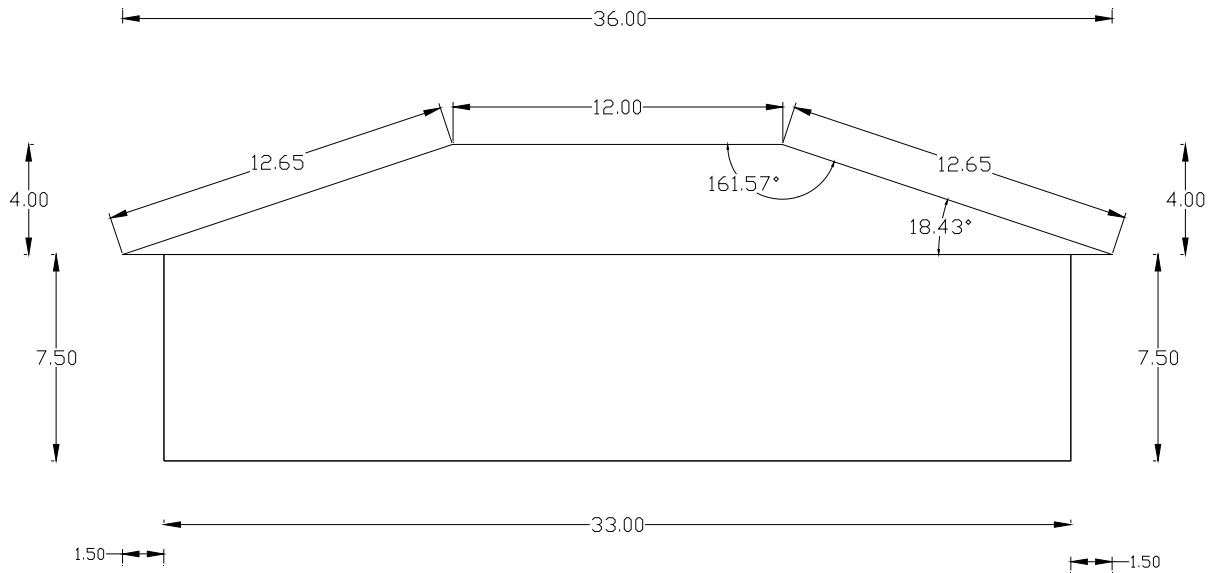
Figure 6.2. Side profile of the model test structure dimensions (Unless otherwise noted, all dimensions are in inches)

Figure 6.3a. 1/16 – Scale model of the low-rise test building after gluing the walls

Figure 6.3b. 1/16 – Scale model of the low-rise test building after gluing the walls and eaves

Figure 6.3c. 1/16 – Scale model of the low-rise test building after gluing the walls, eaves, and roof

6.1.2 Pressure Port Locations

As stated above, the low-rise building model was instrumented with 202 pressure ports. There were 190 pressure ports installed on the roof surface, 8 underneath the eaves, and 4 near the corners inside the model to measure internal pressure. In Figure 6.4, the circles represent model pressure port locations that coincide with ports on the field structure. These pressure port locations were chosen for the model to compare point pressure measurements between the field structure and the model. For the remainder of the text, these ports will be referred to as the circle ports. Circles with an addition symbol in the middle, as shown in Figure 6.4, are port locations that were strategically added to the model to determine an optimal number of pressure ports needed to measure the entire pressure distribution on the roof. For the remainder of the text, these ports will be referred to as circle-plus ports. Also, in Figure 6.4, the dashed ellipses represent model eave pressure ports, while the four internal ports are not displayed in the figure. Eave and internal pressure ports were installed to better compare pressures with the uplift force as was measured with the JR3 force balance to determine the accuracy of using pressure data to quantify uplift force in the wind tunnel. Next, the ports encased with a triangle, as shown in Figure 6.4, were used to perform fundamental variable tests to verify Chapter 4 conclusions. Finally, the ports surrounded by a square were the locations where a scaled version of the PPPD was installed as recommended in the Chapter 5 conclusions. In the end, all 202 pressure ports were used to complete all Model 4 tests.

Note that the roof and eave pressure port locations are labeled 1 through 198 in Figure 6.4. Also, because the roof is symmetrical, the corner region of the roof instrumented with approximately 64 pressure ports represents all four corner regions. Meanwhile, the roof region between ports 4, 11, 129, and 137 also represents a similar region on the opposite side of the roof. To better understand the pressure distribution in these two roof regions, and thus, in all six roof regions, a high concentration of ports was placed in the two regions. Each pressure port was located in the center of a 1.5 in. x 1.5 in. roof region or in some instances, the center of adjacent 1.5 in. squares as shown in Figure 6.4.
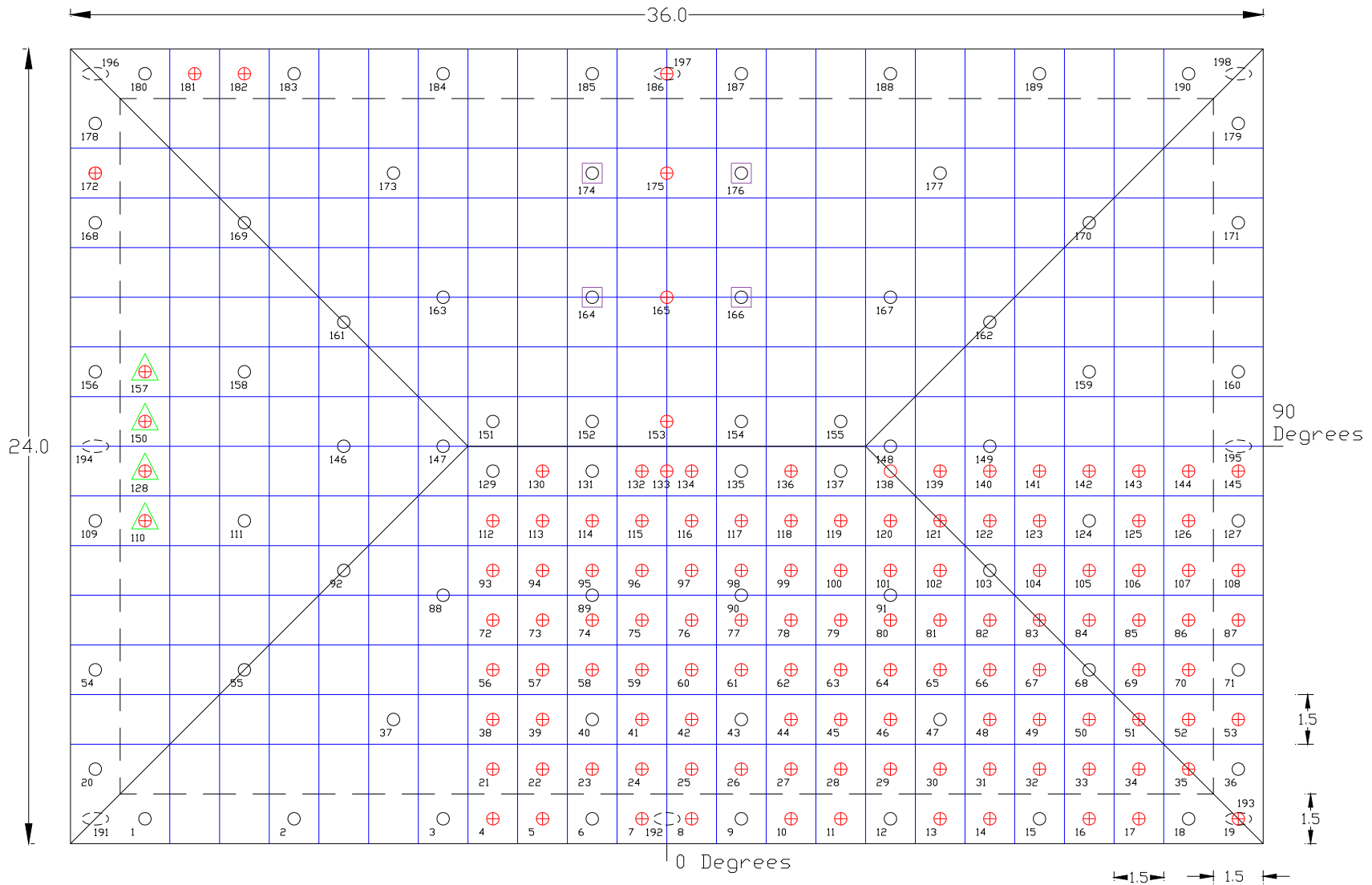
Figure 6.4. Top view of the low-rise building model showing the pressure port locations (All dimensions are in inches)

6.2 TESTING

Testing of the low-rise building model was completed in stages, using a reference velocity value produced by a coastal boundary layer wind flow. The wind tunnel's coastal boundary layer wind flow was chosen because it is a quality representation of the wind flow in the field. Accordingly, it was foreseen that the reference values of velocity and static pressure would correlate closely to field reference values because the field test structure is located in the Pensacola, FL, coastal boundary layer terrain. Actual recorded reference values from the wind tunnel and theoretical field reference values are shown in Section 6.2.2.

6.2.1 Boundary Layer

To produce the coastal boundary layer wind flow in the AABL Wind and Gust Tunnel, rows of chains were placed on the floor of the wind tunnel (Jones, 2008). Figure 6.5 depicts the terrain upstream of the model. As shown, the wind interacts with the chains and then encounters the low-rise building model. The wind profile generated at the test section location due to its interaction with the aforementioned chains is shown in Figure 6.6. The Cobra Probe was used to measure the wind profile. The Power Law exponent value is the exponent used to fit a curve to the velocity profile in Figure 6.6 was found to be approximately 0.13, which closely corresponds to 0.11 as suggested for the coastal terrain in Simiu and Scanlan (1996).
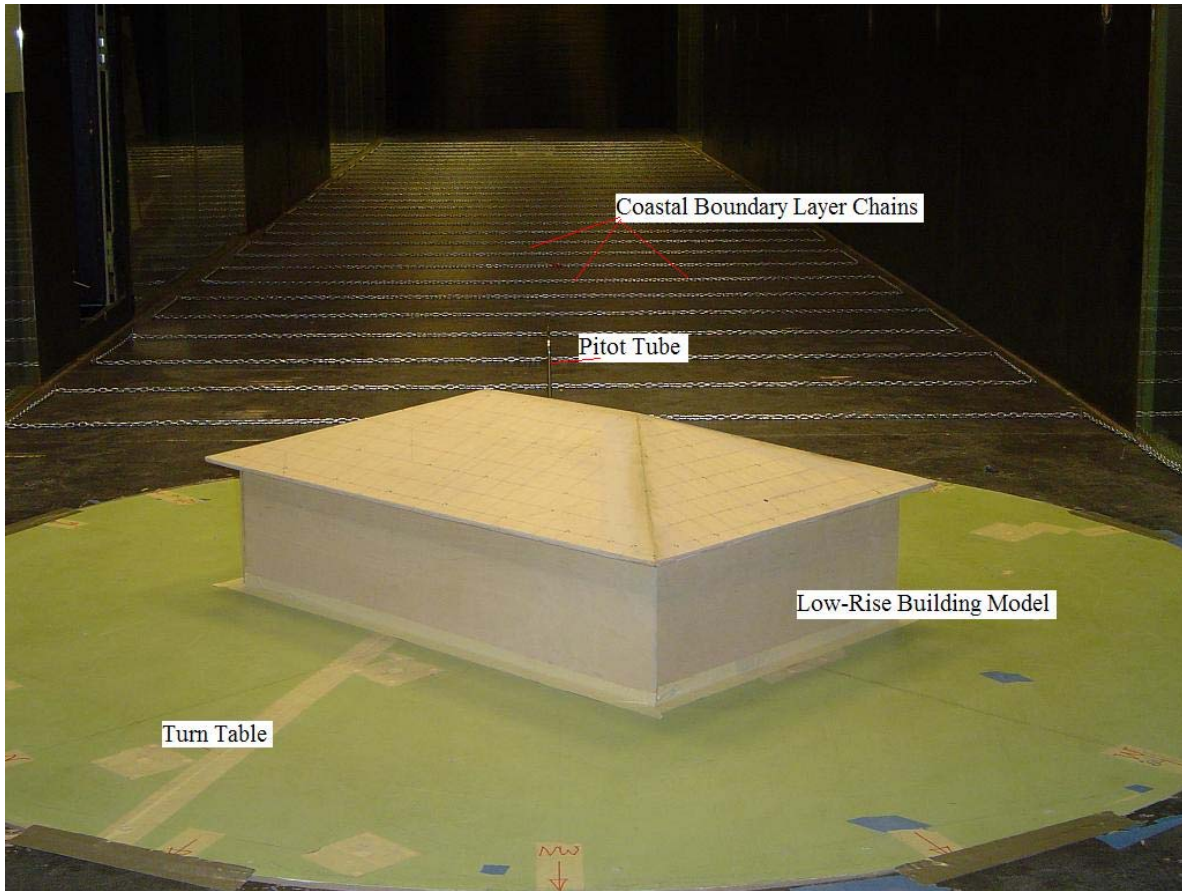
Figure 6.5. Low-rise building model as tested in Iowa State's AABL Wind and Gust Tunnel
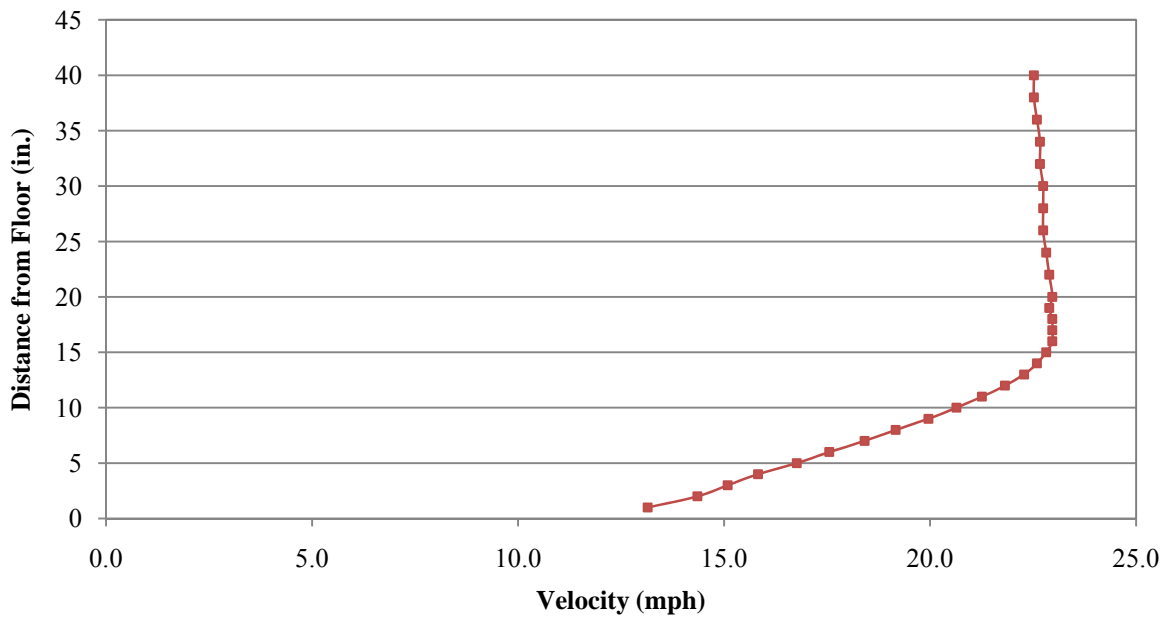
Figure 6.6. Coastal boundary layer profile as measured in the wind tunnel by the cobra probe

6.2.2 Miscellaneous Reference Values

In the case of the low-rise building model pressure tests, the ZOC and Setra transducers measured the total port pressure less the static pressure. Static pressure was inputted to the transducers through a circuit connection between the transducers and the pressure ports on the floor, ceiling, and wall surfaces of the wind tunnel at the location of the model. While testing with the ZOC, pressure data was relayed from the transducer to the computer in units of Pascal. For the Setra transducer, pressure data was recorded in Voltage and Figure 6.7 shows the calibration line used to convert the voltage to pressure (in. H_2O). The calibration line was formed with a pressure chamber and a voltage reader by connecting the pressure transducer to the chamber and the voltage reader. One variable of the calibration line is the known pressure applied to chamber through a hose and a pump and the other variable is the voltage as measured by the voltage reader. For the actual tests, the Setra transducer is connected to voltage reader and thus, the voltage output must be converted to a pressure value.

The reference barometric pressure at the time of the low-rise building model tests ranged from 29.70 to 30.10 in. Hg (i.e., 100576 to 101930 Pa). Reference temperature in the tunnel ranged from 72.8 to 78.4º F (i.e., 295.8 to 298.9º K). The gas constant used in the dynamic pressure equation was 124.71 J/(mol·K) (287.05 J/(kg·K)). Sections 2.1 and 4.2.3 explain how the above values were used to calculate the corresponding pressure coefficients at the locations of pressure ports. Because the height of the model was almost equal to the thickness of the boundary layer as shown in Figure 6.6, the velocity of 19.3 mph (8.63 m/s), at the eave height, was used as the reference velocity for the tests.

Note that the discrepancy between the model scale (1:16) and the boundary layer thickness scale (1:720) was expected to produce pressure coefficients relatively small in magnitude because the reference velocity, located in the denominator portion of Eq. 2.2, is larger than it would be at the reference 33 ft height. Thus, pressure port values should only be compared relative to other port values on the model and should all be a factor of the pressure port values in the field.
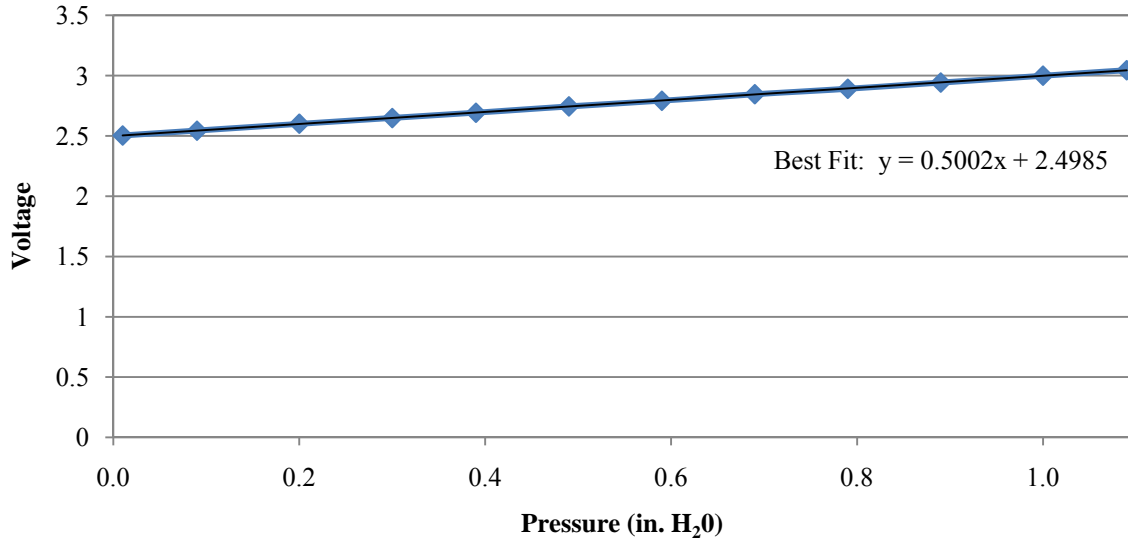
Figure 6.7. Graph showing the best fit curve and the corresponding equation used to calibrate the Setra pressure transducer data

6.2.3 Test Descriptions

A basic variable test, pressure distribution test, scaled PPPD test, and pressure/force comparison test were the four low-rise building tests. For the first low-rise building model test, the fundamental variables discussed in Chapter 4 were tested on the roof of the model to verify Chapter 4 conclusions. Ports encased with a triangle in Figure 6.4 were designated as the fundamental test ports. Port 110 was the tube length test port, where varying tube lengths of 24 in., 36 in., 48 in., 60 in., and 72 in. were tested. Pressure port 128 was the tube diameter test port, where varying tube diameters of 1/32 in., 1/25 in., 1/16 in., 3/32 in., and 1/8 in. were used. Port 150 was the port diameter test port, where varying port diameters of 1/32 in., 1/25 in., 1/16 in., 3/32 in., and 1/8 in. were tested. Finally, port 157 was the pressure transducer test port, where the ZOC and the Setra transducers were examined. Note that the chosen wind angle of attack was 270º, which was normal to the row of fundamental test ports. The results for these fundamental tests are presented in Section 6.3.1.

To perform the second low-rise building model test, all of the circle and circle-plus ports, as shown in Figure 6.4, were connected to the ZOC pressure transducer. The model was then subjected to a wind flow from 0 to 90º at an increment of 10º, and pressure data was recorded. Reference values explained below and recorded pressure data were used with Eq. 2.2 to calculate the pressure coefficient results summarized in Section 6.3.2. The purpose of the second test on the low-rise building model was to better understand the pressure distribution on the roof.

For the third low-rise building model test, a scaled version of the PPPD was constructed as recommended in Section 5.4. The scaled PPPD was mounted to the model at the pressure port locations

surrounded by squares, as shown in Figure 6.4. In the field, the PPPD has a height of 2-1/2 in., a diameter of 1-5/8 in., and a port area of 3/8 in.^{2}. Based on the 1:16 scale, the model PPPD was designed with a height of 5/32 in., a diameter of 13/128 in., and a port area of 3/2048 in^2, as shown in Figure 6.8. First the model was subjected to a wind flow at 90, 120, 135, 150, and 180° and the pressure data was recorded. Then the scaled PPPDs were mounted at four locations on the roof and the model was again subjected to wind flow at 90, 120, 135, 150, and 180° directions and the pressure data was recorded. Results for the scaled PPPD tests are discussed in Section 6.3.3.
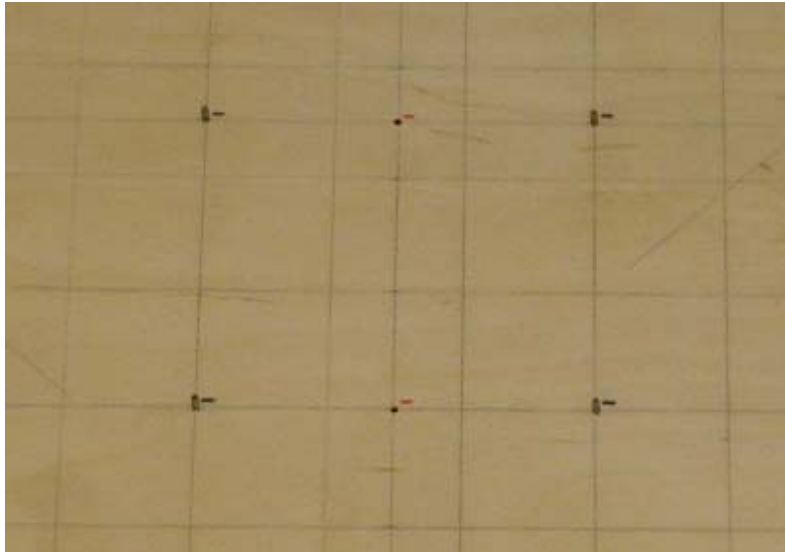
Figure 6.8. Four scaled versions of the PPPD mounted on the low-rise building model

To accomplish the fourth test, forces and pressures for wind directions of 0, 30, 60, and 90º on the low-rise building model were measured in an attempt to correlate wind pressure with uplift force. A wood base of 1 in. thickness was added to the model and the JR3, which measures forces and moments in three orthogonal directions, was attached to the base. The JR3 is shown in Figure 6.9. A layer of adhesive tape connected the perimeter of the model to the wind tunnel floor to prevent wind from entering into the model underneath its base, as shown in Figure 6.5. Pressure data were collected by the ZOC from all pressure port locations. A comparison of the pressure data collected by the ZOC and force data collected by the JR3 is discussed in Section 6.3.4.

Figure 6.9. JR3 used to measure the wind induced structural forces and moments at the base of the test model

6.3 PRESSURE DISTRIBUTION RESULTS

This section presents results of the four low-rise building model tests. Shown first are the effects of the basic variables, followed by the distribution of pressure on the roof. The scaled PPPD results are then discussed, and finally, a comparison of the pressure data and the force data is presented. Note that each test run consisted of collecting 10000 data points at each port over a 20 second time interval except for the Setra transducer test runs, which consisted of collecting 6000 data points over a 20 second time interval. This was because the lab view program used to record voltage seemed to produce more accurate data from test run to test run if 6000 data points were collected. Also, unless otherwise noted, each test consisted of averaging data from five test runs.

6.3.1 Effects of Basic Variables

Figures 6.10 through 6.17 present the data collected during the first test on the low-rise building model, which examined basic variable tests. Figure 6.10 shows the pressure coefficients recorded at each port on the 270° side of the hip roof during test runs 1 through 25. The reason each port in Figure 6.10 has five data points is because there were five changes to each fundamental variable. Also, the average of data from five quality runs within each test run was the recorded data, hence the reason for 25 total runs. In Figure 6.10, the four port numbers with asterisks coincide with the variable test ports so variation of pressure data was expected at only these port locations. Port 110 was the port used to test tube length variable, port 150 was the port used to test the port diameter variable, port 128 was used to test the tube diameter variable, and port 157 was used to test the two transducers. As shown in Figure 6.10, some

pressure port data was consistent at other ports from test run to test run, while other port data varied considerably. The inconsistent port data shows that, despite reattaching the model to a fixed base, removing the model between test runs to change the variables can lead to fluctuating pressure data at all port locations. The remaining graphs explain if the pressure coefficients follow a pattern.

*Basic variable test port
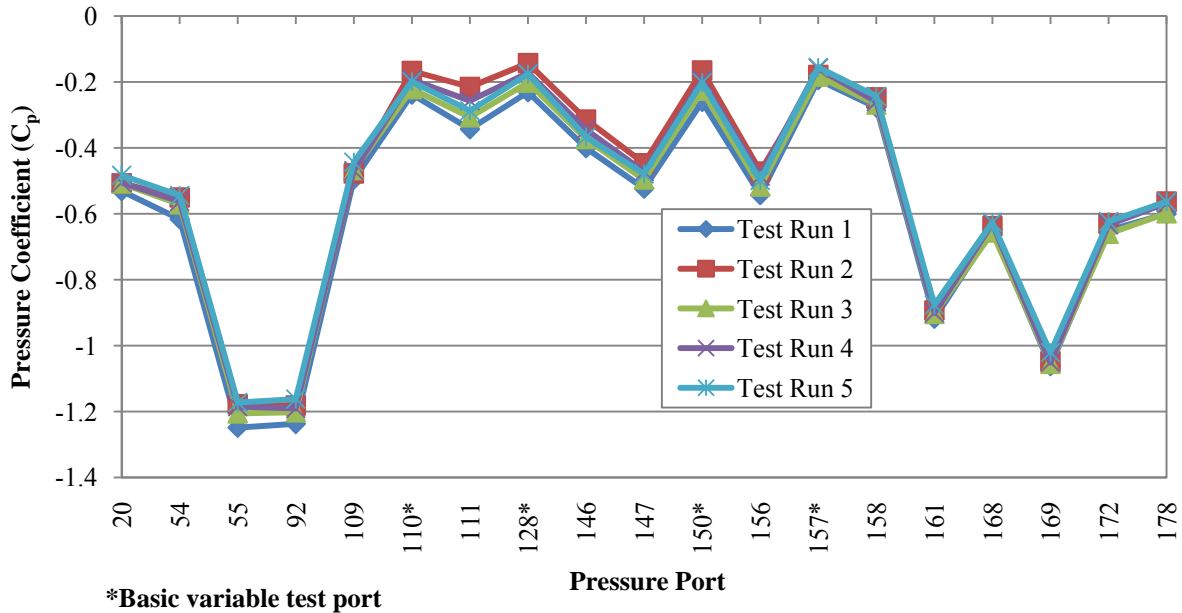
Figure 6.10. Pressure port coefficient values recorded during the fundamental variable tests

Figures 6.11 through 6.14 illustrate the pressure coefficients measured as a result of change in port diameter, tube diameter, tube length, and transducer type. For the first three graphs, each individual data point was referenced to the same port value for that graph in an attempt to show a trend. No increasing or decreasing trend lines exist in Figures 6.11 through 6.13 as the port diameter, tube diameter, and tube length were gradually increased. However, Figure 6.14 shows relatively similar readings between the ZOC and Setra, confirming that the Setra transducer used in the field is comparable to the ZOC transducer used in the laboratory.
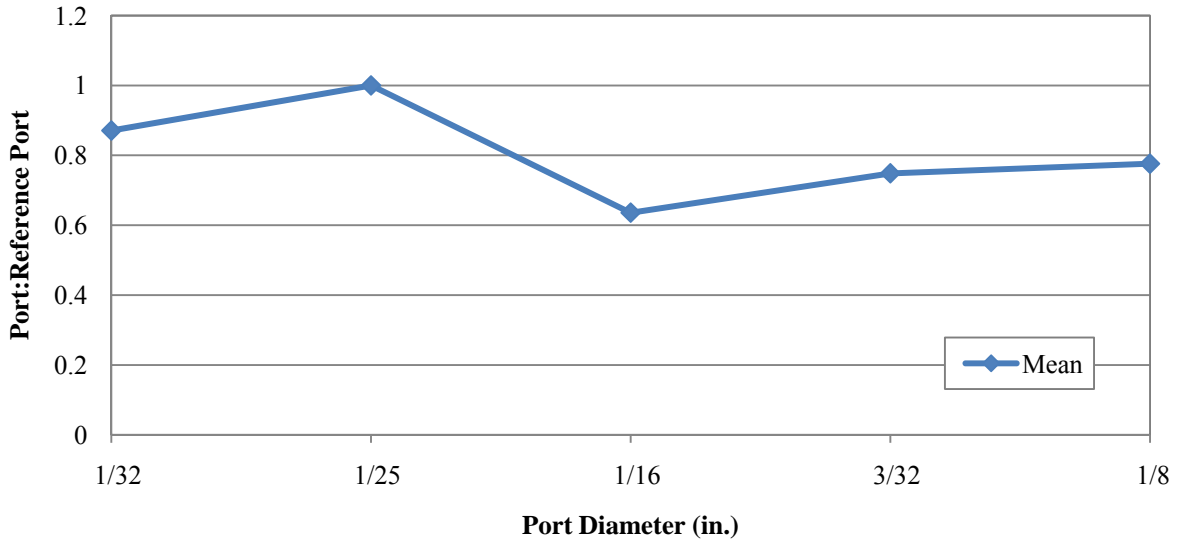
Figure 6.11. Pressure data trend observed for the port diameter change using 1/25 in. as the reference diameter
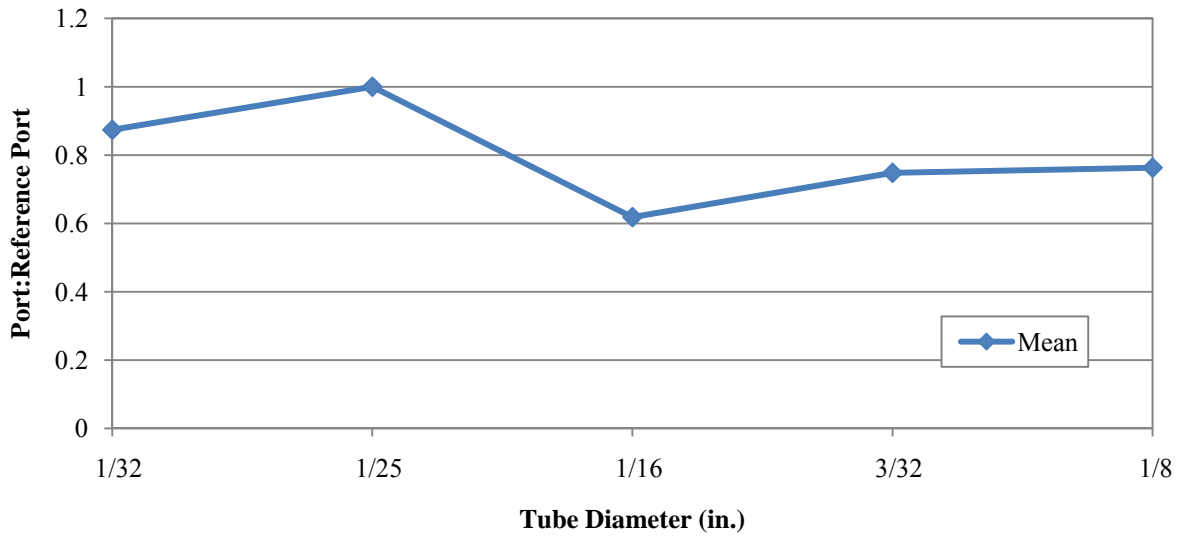
Figure 6.12. Pressure data trend observed for the tube diameter change using 1/25 in. as the reference diameter
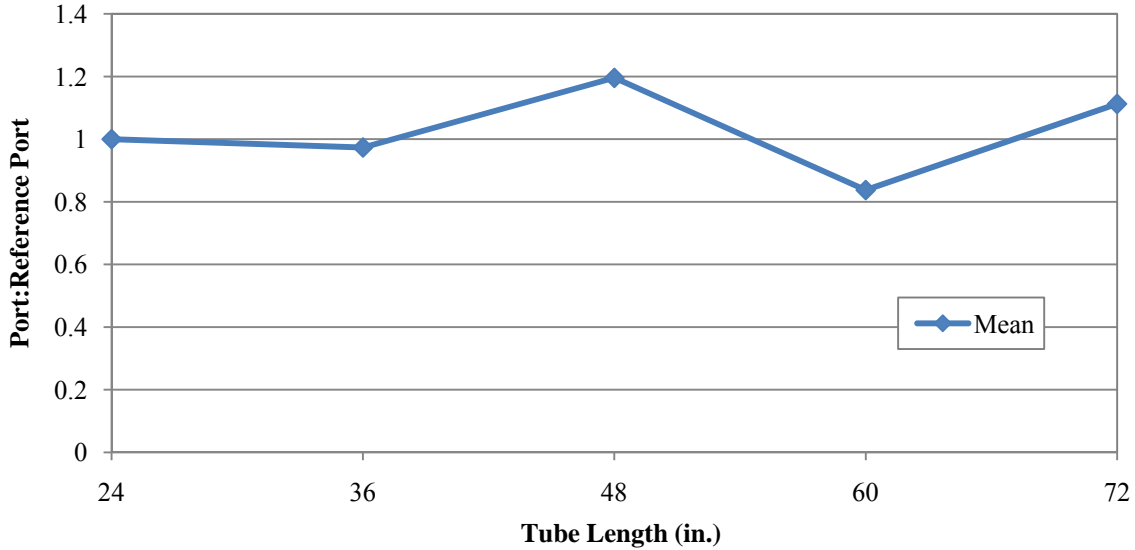
Figure 6.13. Pressure data trend observed for the tube length change using 24 in. as the reference length
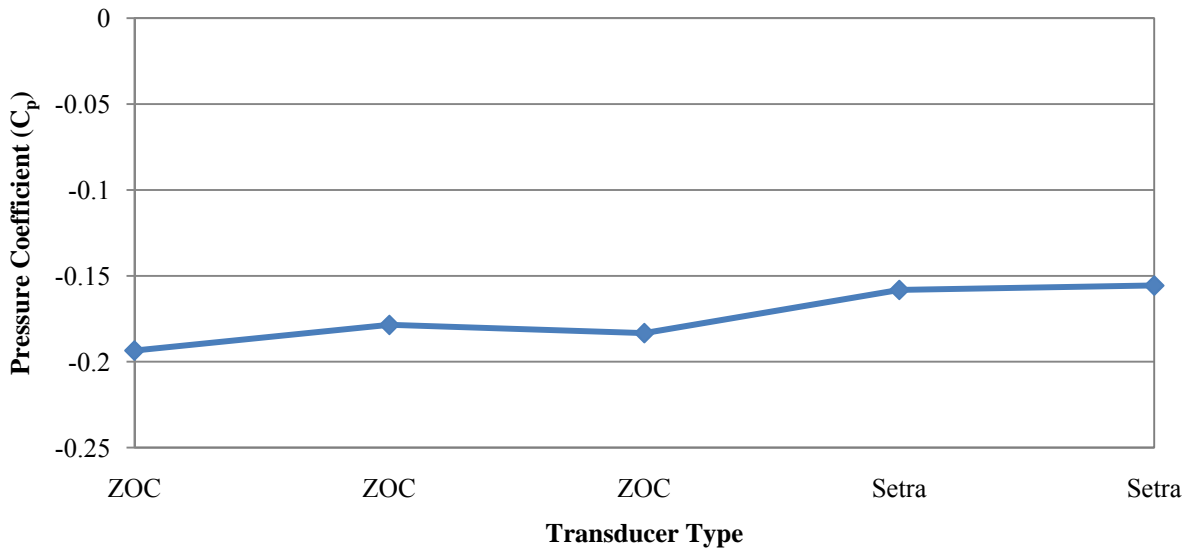
Figure 6.14. Comparison of the ZOC and Setra pressure coefficient mean values

After compiling the mean value pressure coefficients for the ZOC and Setra transducers as shown in Figure 6.14, further investigation of the data was done. Figure 6.15 shows the 6000 pressure coefficient data points that were recorded by each transducer during a 20 second time interval. According to Figure 6.15, it is apparent why the mean values are relatively similar, but what is needed to further evaluate the data is the power spectral density function as shown in Figure 6.16. A comparison of the mean values and power spectral density functions suggest that that ZOC does perform at a greater

precision level than the Setra. The Setra transducer is adequate for mean values, but less precise for fluctuating values.
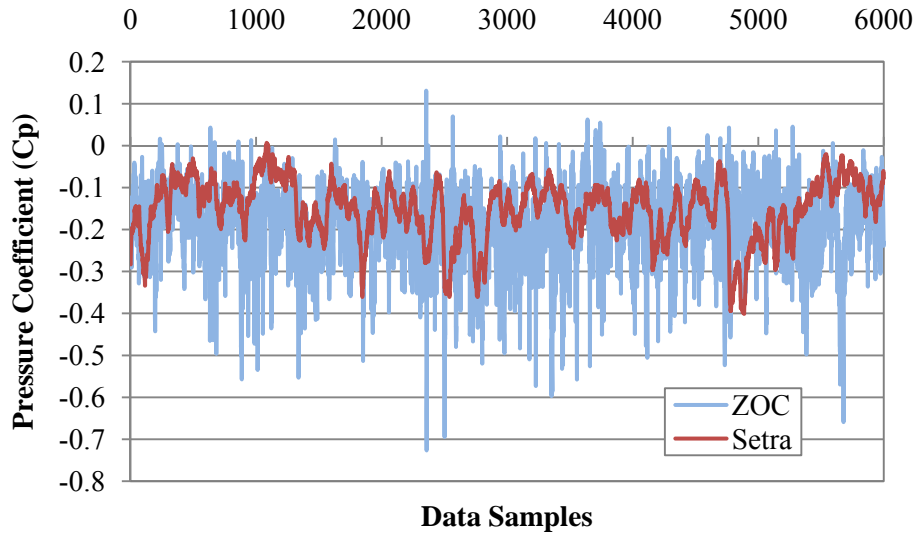
Figure 6.15. Comparison of time series data for the ZOC and Setra pressure coefficient data
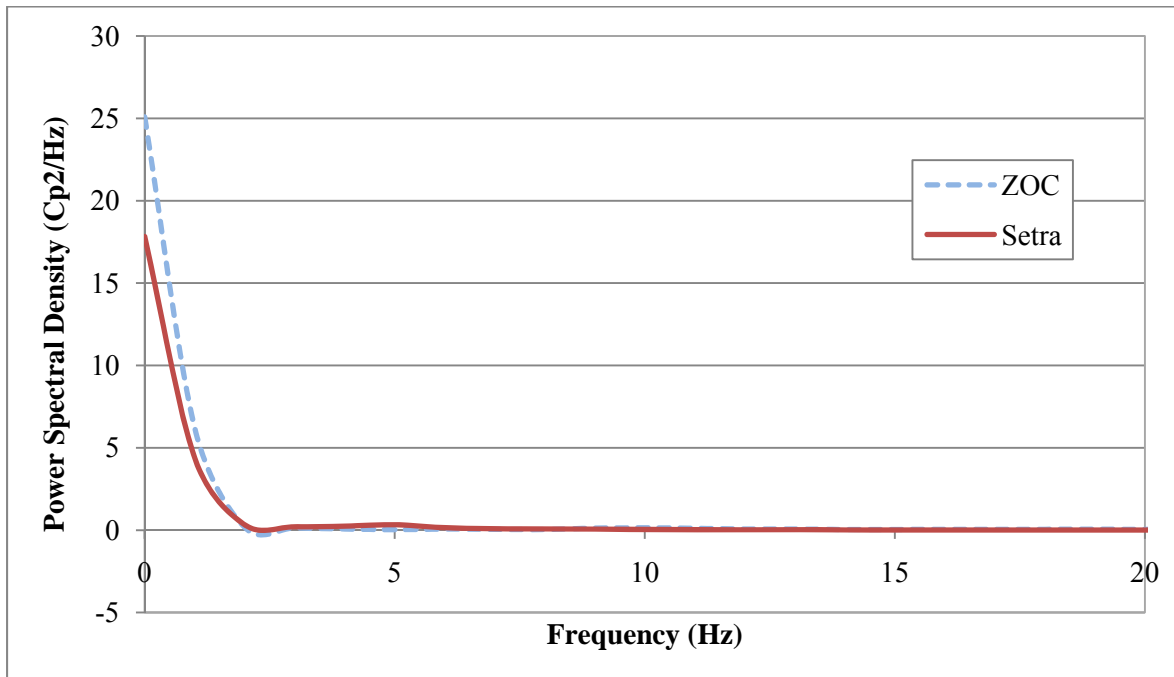
Figure 6.16. Comparison of the Power Spectral Density function for the ZOC and Setra data

Finally, Figure 6.17 clarifies why no trend line is evident in Figures 6.11 through 6.13. As alluded to above, Figure 6.17 shows the pressure data is more susceptible to the test run number than the tube length, tube diameter, or port size. Aside from the tube length and port size for the first five test

runs, each variable shows a similar trend from test run to test run, proving that removing the model from the base, changing the test variable, and attaching the model back to the base was affecting the pressure data more than the actual effects of the variables.

In the end, no tube length, tube diameter, or port size effects on pressure data conclusions can be reached based on the data produced by the low-rise building model. As discussed in Section 4.3, the expected results were that the pressure coefficients would decrease in magnitude as the tube length, tube diameter, and port diameter increased. Note that if test run 2 is neglected in Figure 6.17, then the tube length and tube diameter data comes closer to agreeing with the aforementioned expected results. Alternatively, no trend was observed on the roof of Model 2 as discussed in Section 4.3 and no trend is observed on the roof of the partial roof and wall model as shown in Figure 6.17.
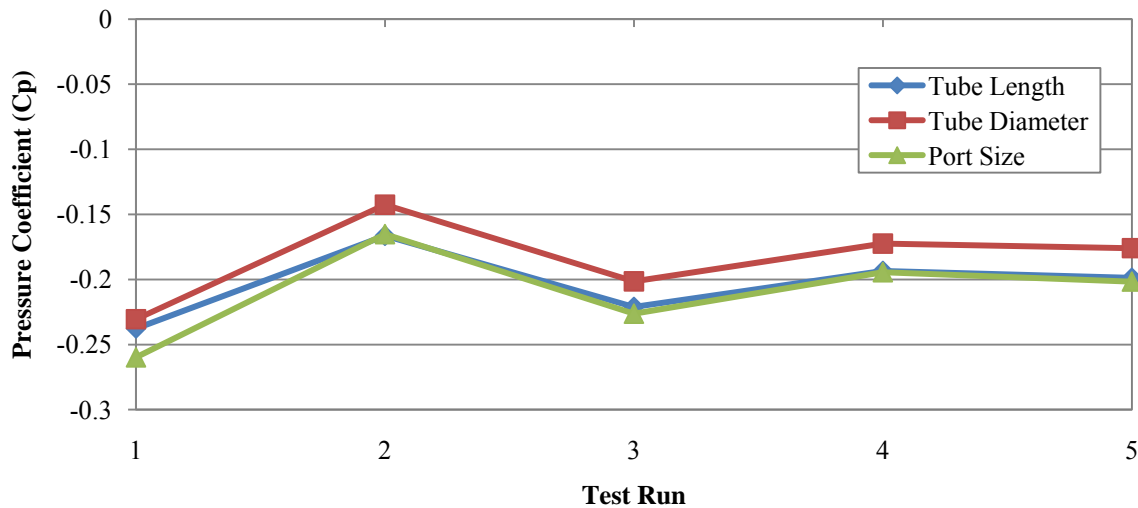
Figure 6.17. Graph illustrating the pressure coefficient data as a function of test number and testing variable

6.3.2 Roof Pressure Distribution

In Figures 6.18 through 6.28 are illustrations of the pressure distribution on the hip roof of the low-rise building model for eleven different model orientation cases. Pressure data was recorded by the ZOC while the reference values, as stated in Section 6.2.2, were used to calculate the pressure coefficients. Again, because of the relatively large model, small boundary layer thickness in the wind tunnel, and the reference velocity taken at eave height, pressure coefficient magnitudes should be compared with other coefficients on this model and not other models or the low-rise building itself. Essentially, the coefficients in Figures 6.18 through 6.28 should be used to create: 1) a visual of the wind flow over the low-rise building model; and 2) an optimal pressure port arrangement used to understand the pressure distribution on the hip roof for any wind angle of attack. Section 6.3.4 further explains the optimal pressure port arrangement. Also, the installation of pressure ports near the roof edges required precise work and evaluation of data after assembling the low rise building model showed that three of the ports were damaged during installation and thus were labeled "NA."

1	2	3	4	5	6	7	8	9	10	11	12	13	14	15	16	17	18	19	20	21	22
NA	-0.32	-0.33	-0.34		-0.41			-0.43		-0.46	NA			-0.43			-0.40			NA	
-0.26																					-0.26
-0.25				-0.35			-0.37		-0.38		-0.37				-0.37						
-0.25		-0.43																	-0.44		-0.24
					-0.36		-0.35		-0.36		-0.35			-0.36							
			-0.40														-0.40				
-0.29		-0.29																		-0.29	-0.28
						-0.34		-0.33		-0.33		-0.34		-0.34							
			-0.38		-0.63							-0.70		-0.38							
						-0.32	-0.28	-0.27		-0.27		-0.24	-0.28	-0.33		-0.50	-0.38	-0.37	-0.35	-0.34	-0.35
-0.39		-0.38				-0.26	-0.25	-0.22	-0.21	-0.20	-0.24	-0.25	-0.31	-0.39	-1.10	-0.56	-0.45	-0.39	-0.37	-0.38	-0.39
			-1.00			-0.23	-0.20		-0.16	-0.17		-0.19	-0.23		-0.45	-1.25	-0.58	-0.47	-0.42	-0.40	-0.46
					-0.26				-0.16			-0.16			-0.26						
						-0.19	-0.15		-0.14	-0.13		-0.18	-0.19		-0.32	-0.51	-1.19	-0.59	-0.49	-0.45	-0.46
-0.51		-1.41				-0.14	-0.14	-0.12	-0.13	-0.12	-0.12	-0.14	-0.17	-0.21	-0.24	-0.32	-0.48	-1.27	-0.62	-0.51	-0.52
				-0.18		-0.13	-0.11	-0.08	-0.10	-0.11	-0.11	-0.12	-0.14	-0.15	-0.19	-0.23	-0.32	-0.49	-1.38	-0.63	-0.56
-0.58						-0.15	-0.16	-0.12	-0.14	-0.16	-0.15	-0.16	-0.17	-0.16	-0.19	-0.21	-0.27	-0.35	-0.46	-1.24	-0.57
	-0.51		-0.56		-0.48	-0.48	-0.46	-0.40	-0.46	-0.44	-0.41	-0.43	-0.49	-0.45	-0.49	-0.56	-0.56	-0.62	-0.63	-0.55	-0.92

Figure 6.18. Pressure coefficients on the hip roof of the low-rise building model as measured in the wind tunnel with a wind attack orientation of 0°

Figure 6.19. Pressure coefficients on the roof of Model 4 with a wind attack orientation of 10°

Figure 6.20. Pressure coefficients on the roof of Model 4 with a wind attack orientation of 20°

Figure 6.21. Pressure coefficients on the roof of Model 4 with a wind attack orientation of 30°

Figure 6.22. Pressure coefficients on the roof of Model 4 with a wind attack orientation of 40°

Figure 6.23. Pressure coefficients on the roof of Model 4 with a wind attack orientation of 45°

Figure 6.24. Pressure coefficients on the roof of Model 4 with a wind attack orientation of 50°

NA	-0.23	-0.24	-0.20		-0.27		-0.32	-0.35	NA		-0.47		-0.51			NA		
-0.16																		-0.90
-0.22				-0.19			-0.29	-0.31	-0.36			-0.48						
-0.16		-0.34													-1.31			-0.86
					-0.25		-0.34	-0.41	-0.44			-0.79						
				-0.58									-1.53					
-0.16		-0.31													-0.33			-0.73
				-0.71	-1.08	-0.91	-1.12	-1.30	-1.15		-0.96	-0.80		-0.35				
						-0.64	-0.67	-0.61	-0.64	-0.59	-0.69	-0.66	-0.47		-0.29	-0.26	-0.18	-0.20 -0.65
-0.24		-0.63				-0.54	-0.49	-0.47	-0.43	-0.46	-0.48	-0.44	-0.46	-0.35	-0.44	-0.29	-0.23 -0.15 -0.09 -0.15	-0.60
			-0.66		-0.37	-0.42	-0.47	-0.34	-0.33	-0.39		-0.30	-0.35	-0.38	-0.22	-0.24	-0.32 -0.17 -0.09 -0.06 -0.06	-0.57
						-0.38	-0.30		-0.33	-0.28			-0.35	-0.26		-0.14	-0.16 -0.21 -0.07 -0.04 -0.03	-0.52
-0.28		-0.92				-0.31	-0.34	-0.30	-0.26	-0.25	-0.21	-0.23	-0.27	-0.16	-0.11	-0.11	-0.11 -0.15 -0.04 0.01	-0.35
				-0.23		-0.31	-0.26	-0.22	-0.21	-0.24	-0.18	-0.22	-0.21	-0.10	-0.10	-0.06	-0.05 -0.06 -0.09 0.03	-0.26
-0.33						-0.43	-0.38	-0.23	-0.32	-0.34	-0.20	-0.30	-0.29	-0.09	-0.05	-0.08	-0.03 0.00 -0.01 -0.07	-0.01
	-0.42			-0.48		-0.43	-0.56	-0.47	-0.46	-0.59	-0.52	-0.38	-0.41	-0.55	-0.27	-0.26	-0.23 -0.16 -0.12 -0.09 0.06	-0.04

Figure 6.25. Pressure coefficients on the roof of Model 4 with a wind attack orientation of 60°

NA	-0.19	-0.20	-0.19		-0.24		-0.32	-0.36	NA		-0.51		-0.55			NA		
-0.18																		-0.89
-0.20				-0.24			-0.30	-0.33	-0.36			-0.50						
-0.15		-0.39													-1.32			-0.85
					-0.29		-0.33	-0.37	-0.42			-0.71						
				-0.52									-1.50					
-0.17		-0.28													-0.33			-0.73
				-0.60	-0.86	-0.76		-0.79	-0.74		-0.61	-0.79	-0.79	-0.37				
						-0.57	-0.55	-0.46	-0.48		-0.46	-0.54	-0.55	-0.46		-0.29	-0.26 -0.18 -0.19	-0.65
-0.25		-0.56				-0.48	-0.42	-0.40	-0.35	-0.39	-0.40	-0.38	-0.43	-0.42	-0.61	-0.33	-0.23 -0.19 -0.14 -0.15	-0.63
			-0.63		-0.35	-0.38	-0.43		-0.29	-0.36		-0.33	-0.38		-0.34	-0.50	-0.23 -0.17 -0.12 -0.12	-0.62
						-0.35	-0.27		-0.30	-0.27		-0.35	-0.27		-0.25	-0.28	-0.44 -0.19 -0.12 -0.09	-0.56
-0.28		-0.68				-0.29	-0.32	-0.28	-0.25	-0.24	-0.21	-0.24	-0.29	-0.20	-0.20	-0.21	-0.23 -0.37 -0.15 -0.08	-0.43
				-0.24		-0.29	-0.24	-0.20	-0.20	-0.24	-0.17	-0.23	-0.23	-0.16	-0.17	-0.18	-0.18 -0.19 -0.37 -0.09	-0.36
-0.34						-0.37	-0.33	-0.17	-0.28	-0.30	-0.18	-0.29	-0.30	-0.14	-0.13	-0.13	-0.14 -0.13 -0.16 -0.33	-0.15
	-0.33			-0.36		-0.32	-0.41	-0.32	-0.30	-0.44	-0.38	-0.22	-0.26	-0.42	-0.18	-0.16	-0.16 -0.16 -0.12 -0.13 -0.12	-0.29

Figure 6.26. Pressure coefficients on the roof of Model 4 with a wind attack orientation of 70°

Figure 6.27. Pressure coefficients on the roof of Model 4 with a wind attack orientation of 80°

Figure 6.28. Pressure coefficients on the roof of Model 4 with a wind attack orientation of 90°

In summarizing Figures 6.18 through 6.28, the pressure coefficients are relatively symmetrical about the 0 and 90° line for the 0 and 90° cases as shown in Figures 6.18 and 6.28, which suggests that the pressure instrumentation recorded pressure accurately. As expected, the majority of pressure coefficients are negative, showing a suction pressure throughout the roof. The critical pressure regions are near the edges, corners, and ridges as discussed in Chapter 2. More specifically, the largest magnitude pressure coefficients are located near the ridges for the 0 and 90° cases as shown in Figures 6.18 and 6.28 and near the top and edges of the roof for the 30, 40, 45, 50, and 60° cases as shown in Figures 6.21 through 6.25. Finally, the middle portion of the leeward roof side is most susceptible to experiencing large magnitudes of pressure when the wind angle of attack is oriented between 40 and 50° as shown in Figures 6.22 through 6.24, while the edges of the leeward roof are most susceptible to experiencing large magnitudes of pressure when the wind angle of attack is oriented near 20° as shown in Figure 6.20.

6.3.3 Pressure Port Protection Device

For the scaled version tests of the pressure port protection device (PPPD) as noted previously, five low-rise building model orientations were tested without the PPPDs followed by the same five low-rise building model orientation tests with four PPPDs erected at pressure port locations 164, 166, 174, and 176 identified in Figure 6.4. The main objectives of the PPPD tests were to understand the effects of the PPPD on its own port reading as well as surrounding port readings and confirm the results with results discussed in Chapter 5. Figures 6.29 through 6.38 show the low-rise building model loaded with a wind attack orientation of 90°, 120°, 135°, 150°, and 180°, both with and without PPPDs.
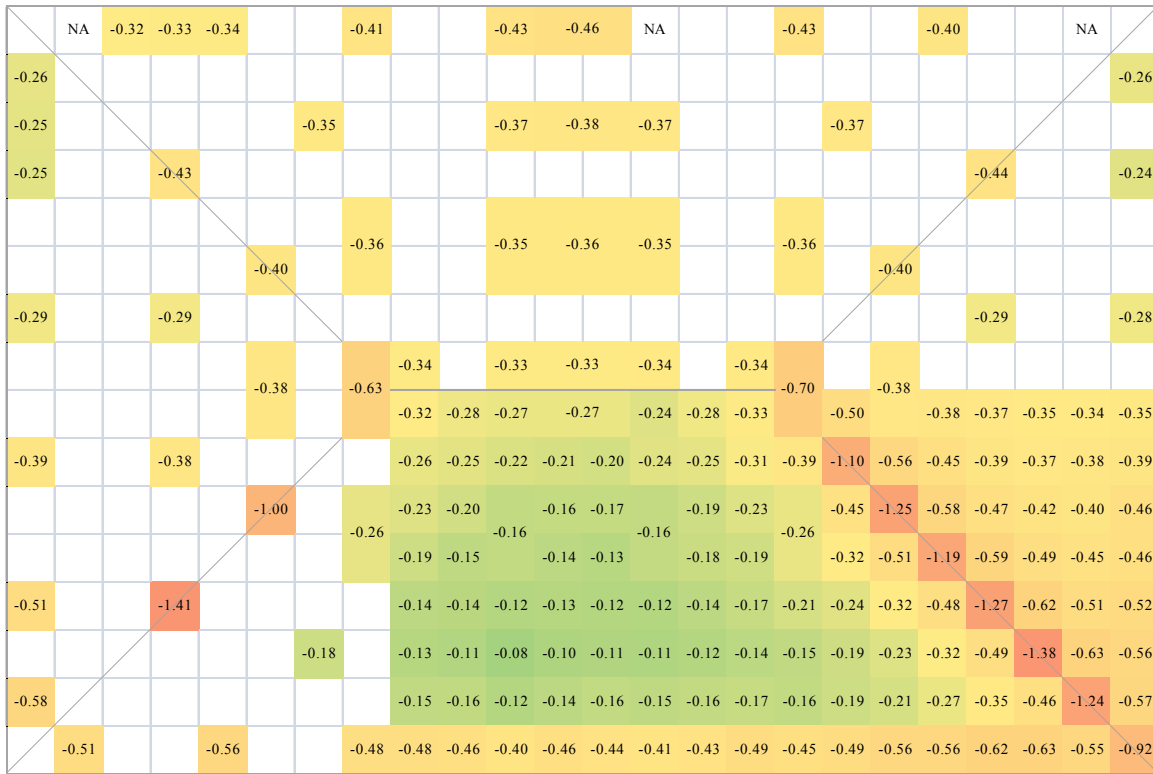
Figure 6.29. Pressure coefficients on the hip roof of the low-rise building model as measured in the wind tunnel with a wind attack orientation of 90° without attaching any PPPDs
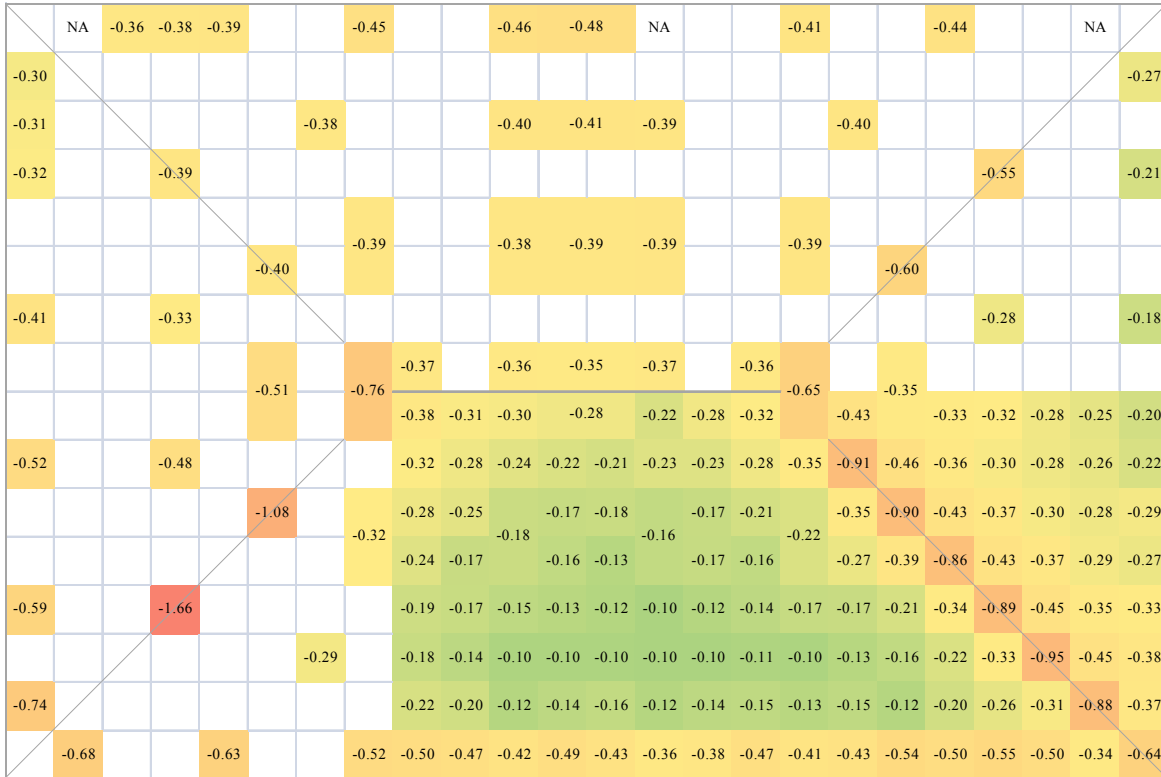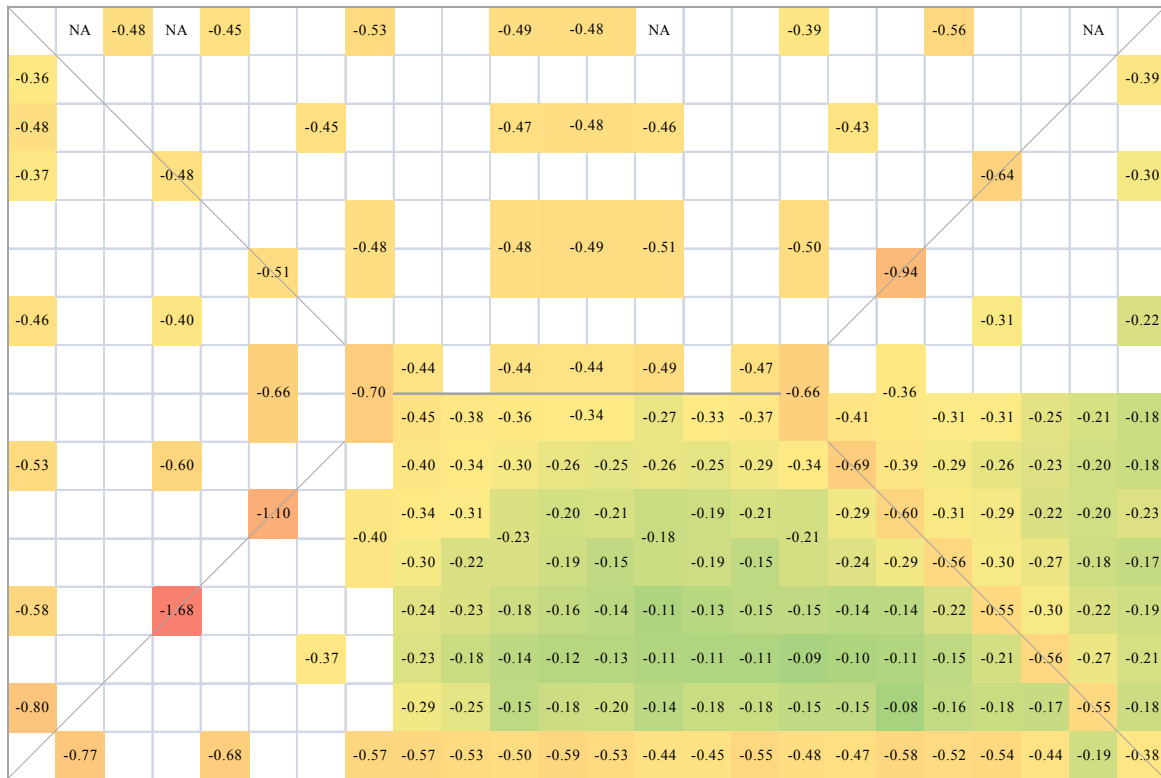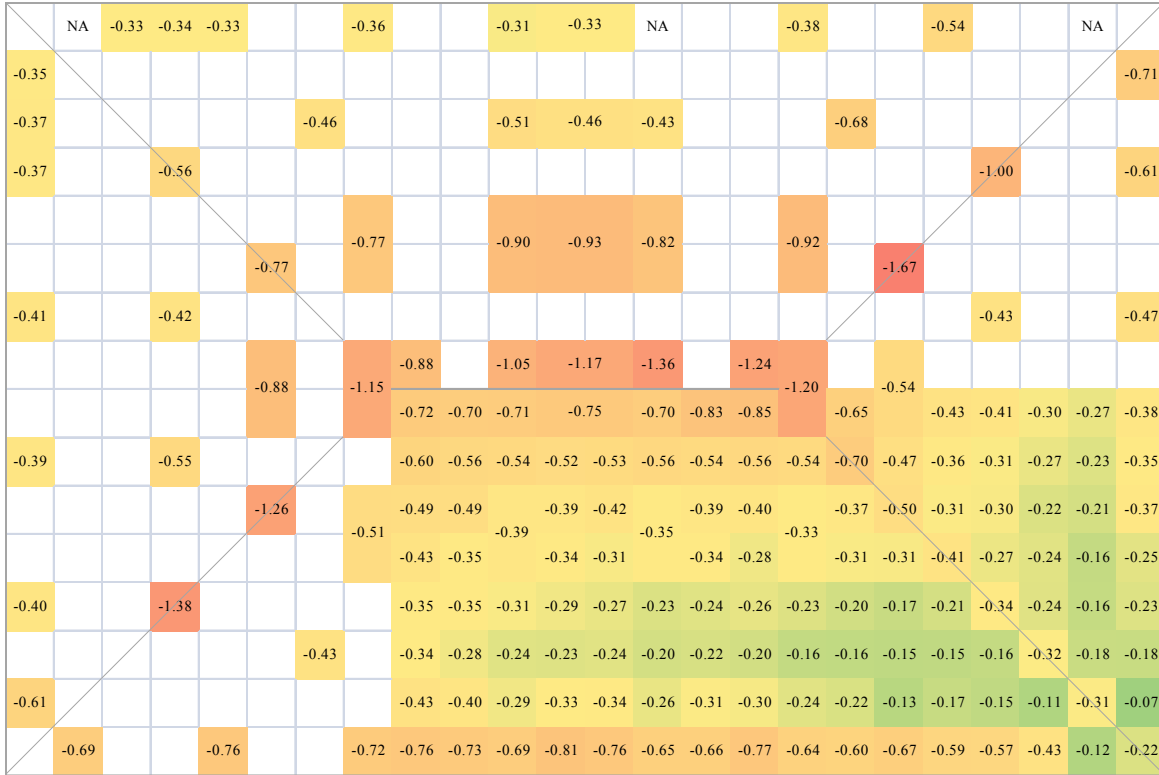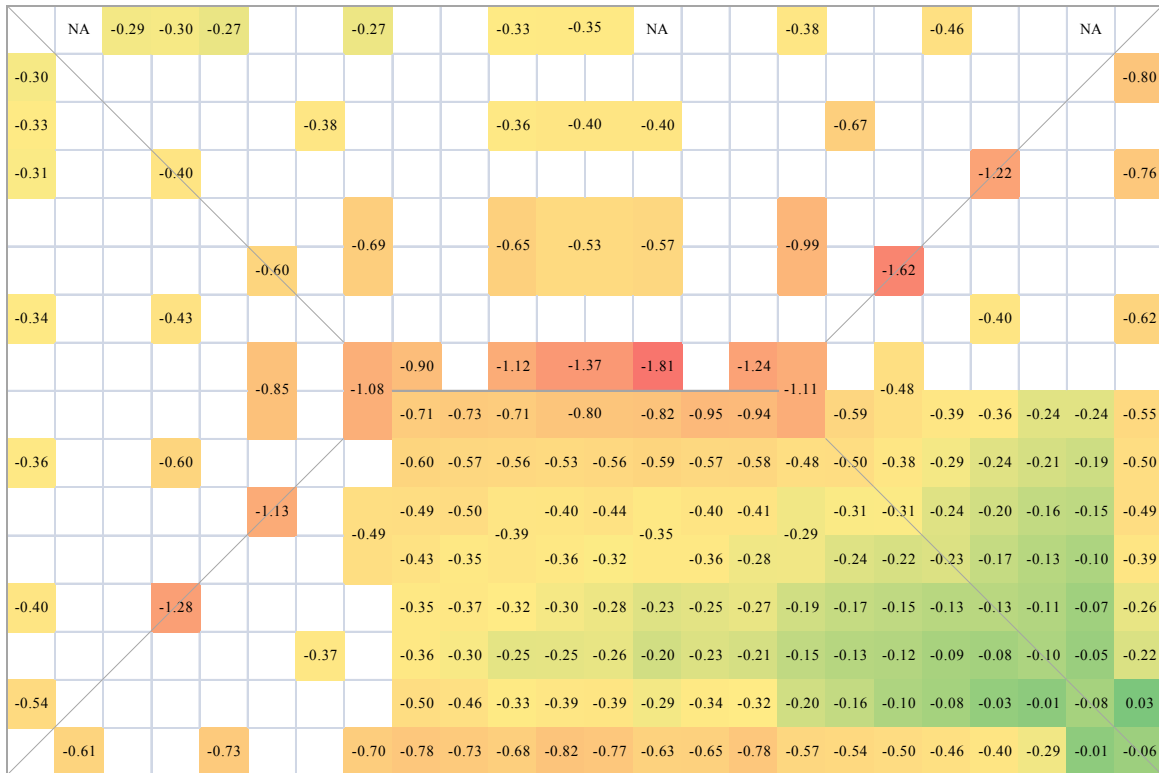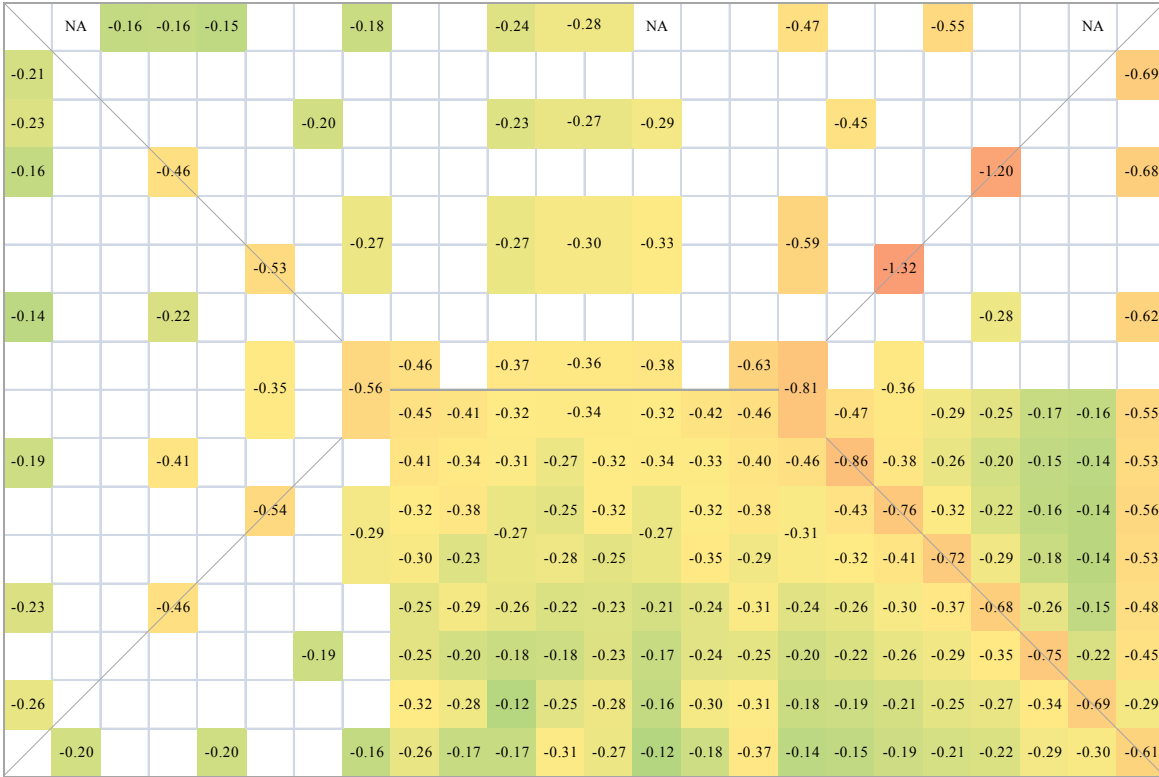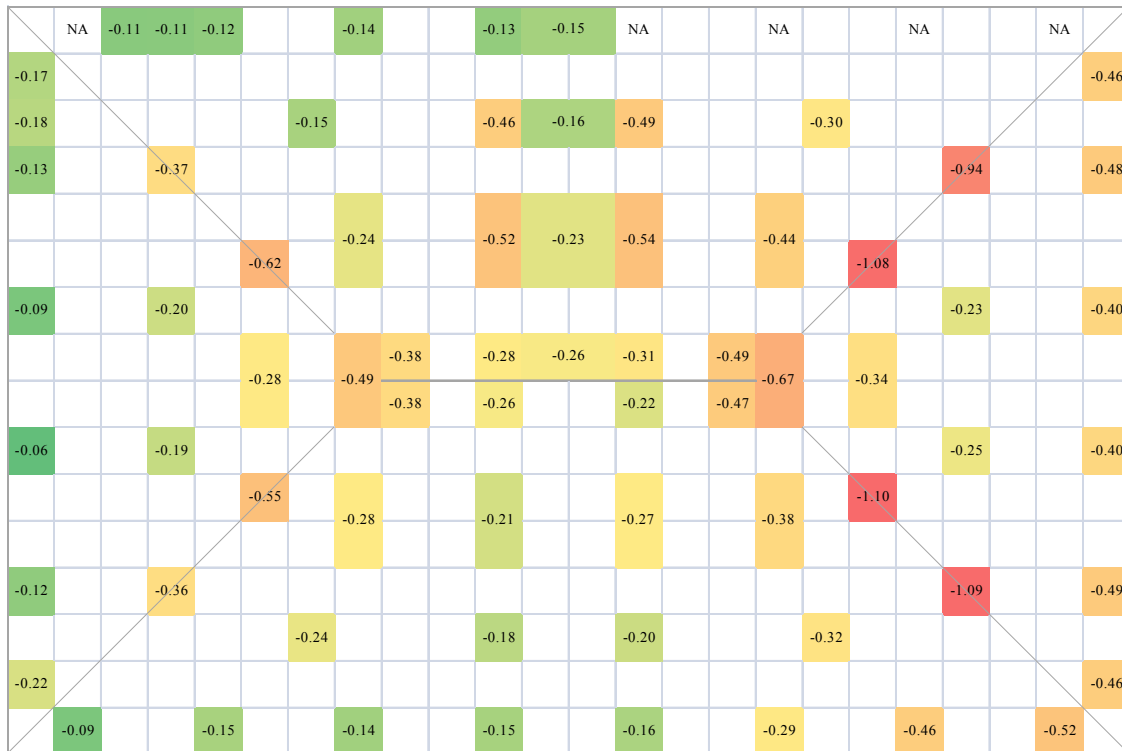
Figure 6.30. Pressure coefficients on Model 4 with a wind attack orientation of 90° and four PPPDs

Figure 6.31. Pressure coefficients on Model 4 with a wind attack orientation of 120° and no PPPDs

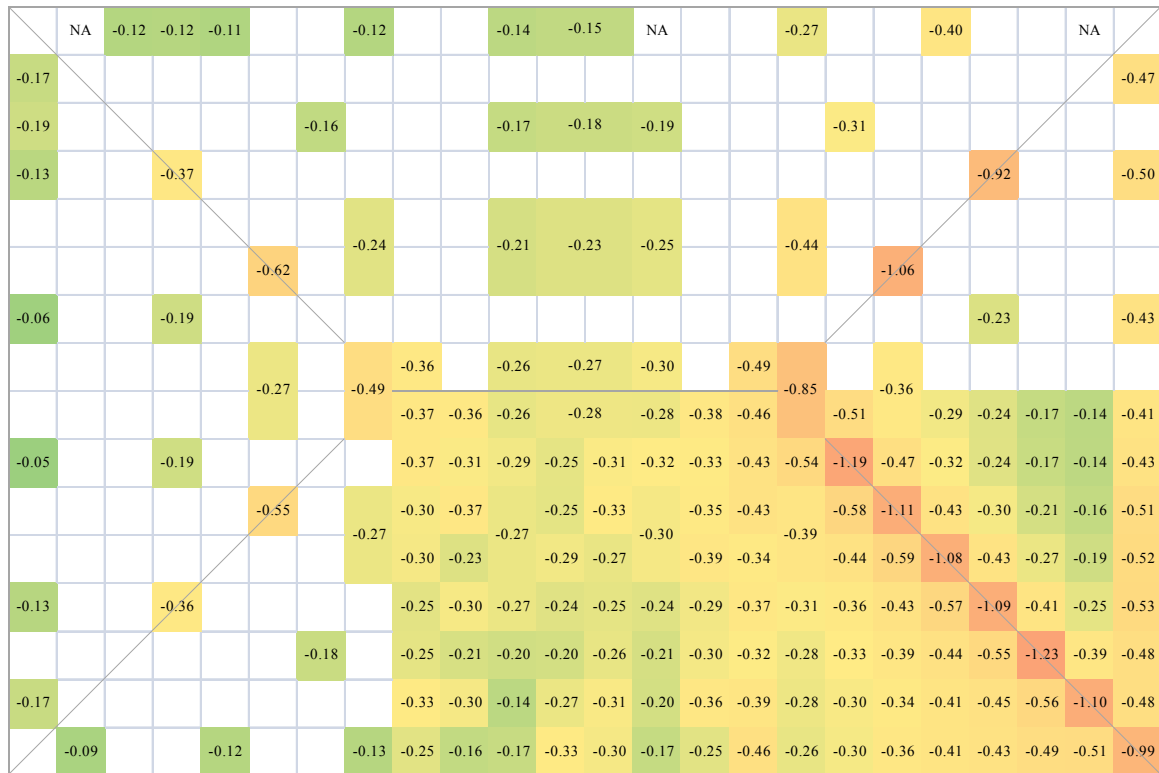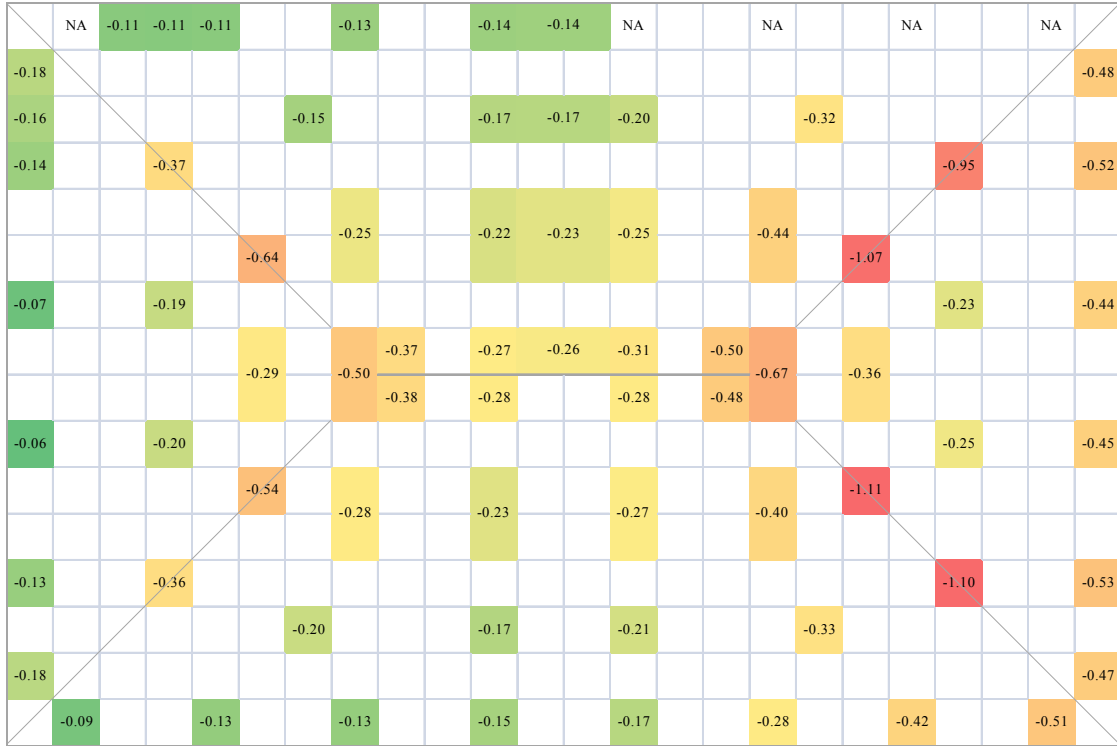**Figure 6.32. Pressure coefficients on Model 4 with a wind attack orientation of 120° and four PPPDs**

Figure 6.33. Pressure coefficients on Model 4 with a wind attack orientation of 135° and no PPPDs

Figure 6.34. Pressure coefficients on Model 4 with a wind attack orientation of 135° and four PPPDs
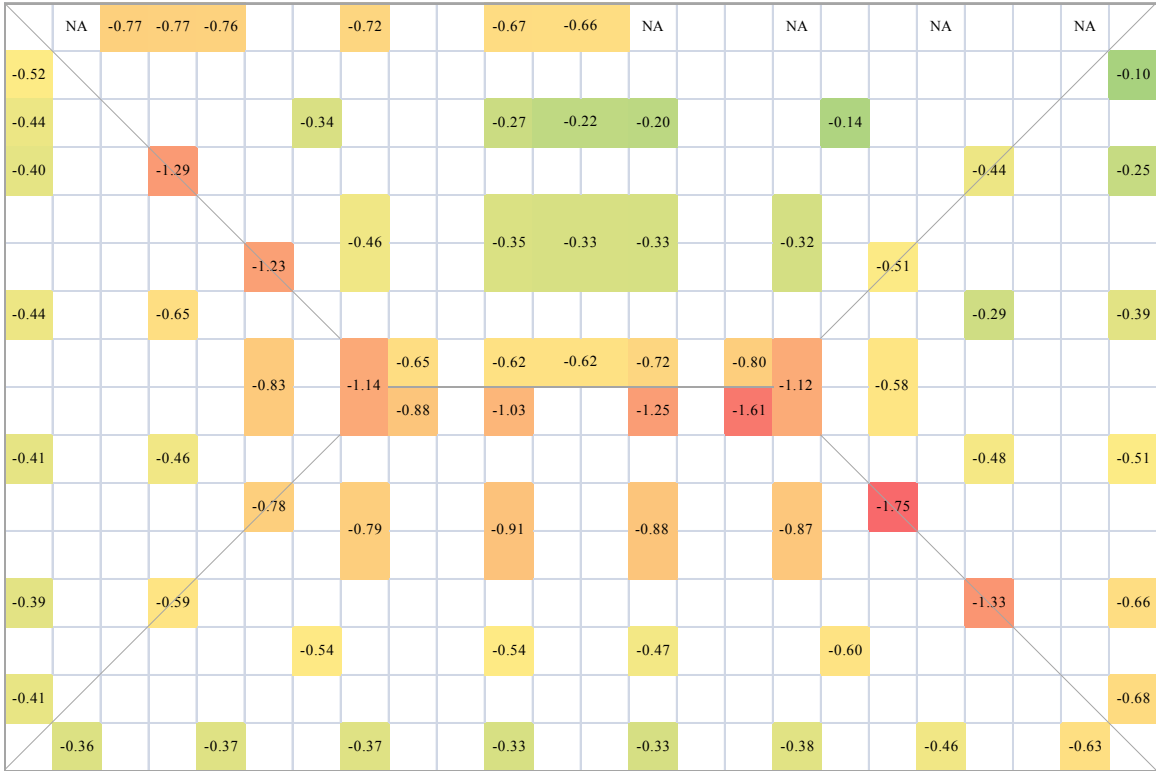
Figure 6.35. Pressure coefficients on Model 4 with a wind attack orientation of 150° and no PPPDs
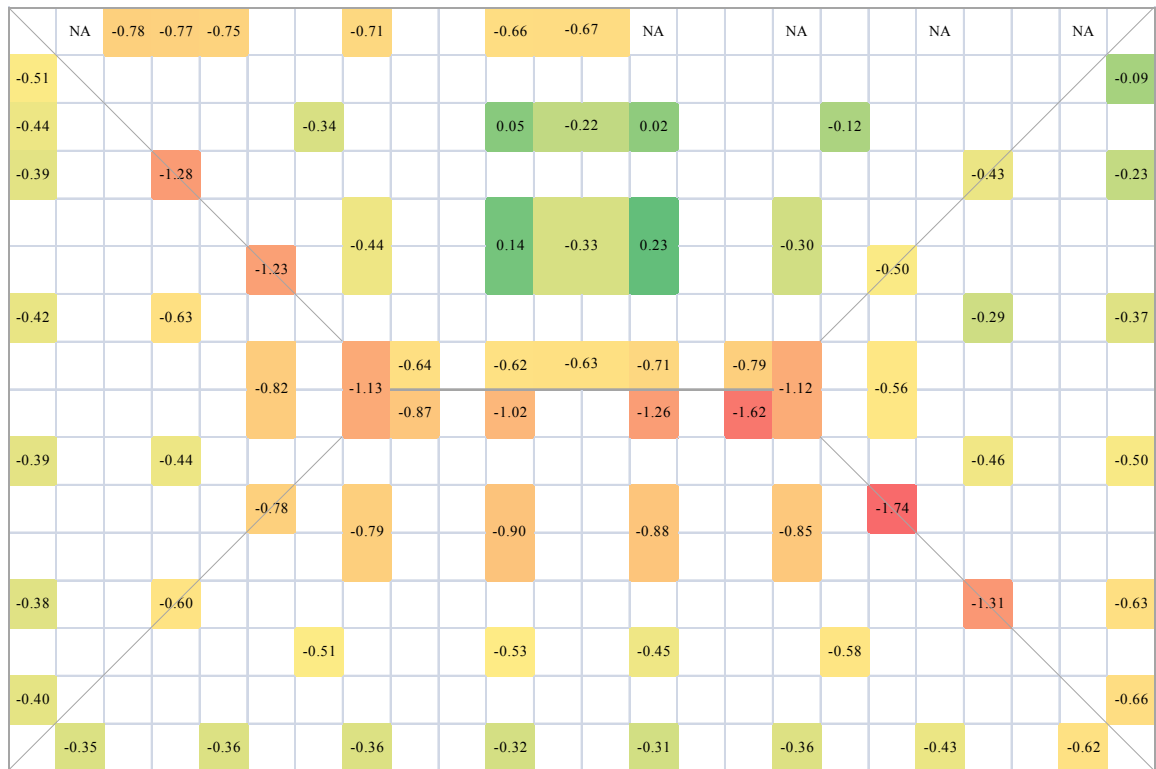
Figure 6.36. Pressure coefficients on Model 4 with a wind attack orientation of 150° and four PPPDs
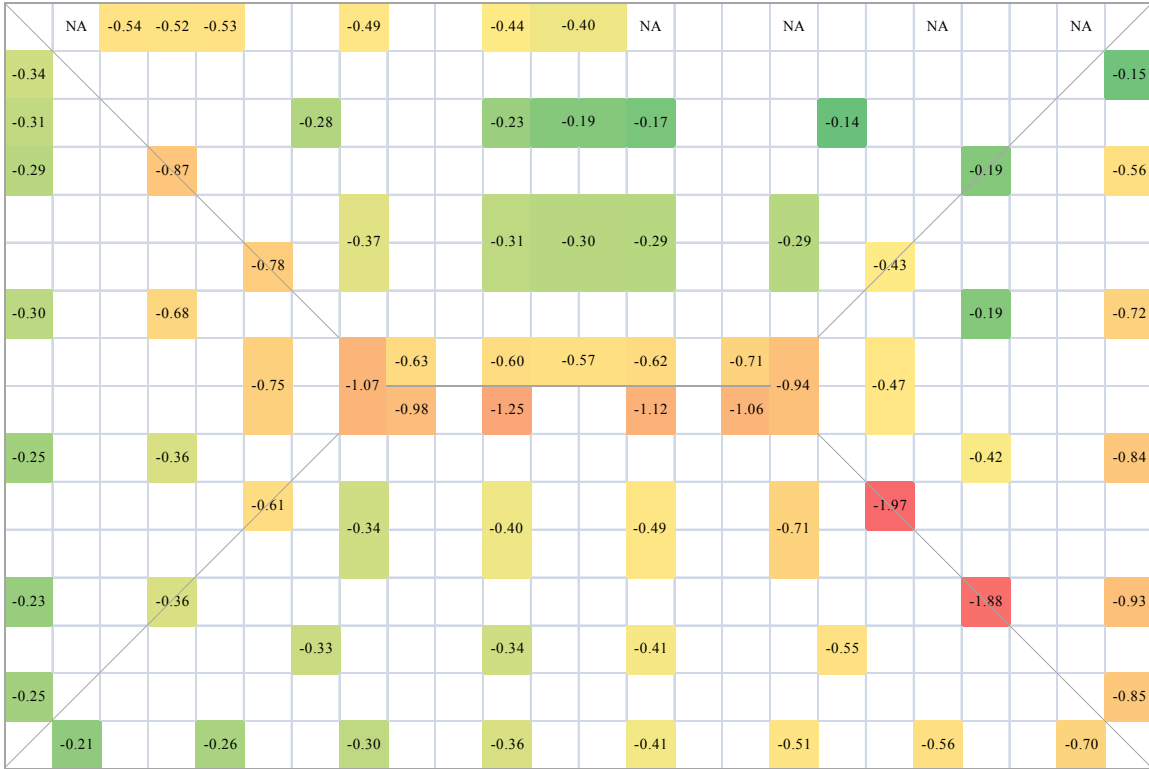
Figure 6.37. Pressure coefficients on Model 4 with a wind attack orientation of 180° and no PPPDs
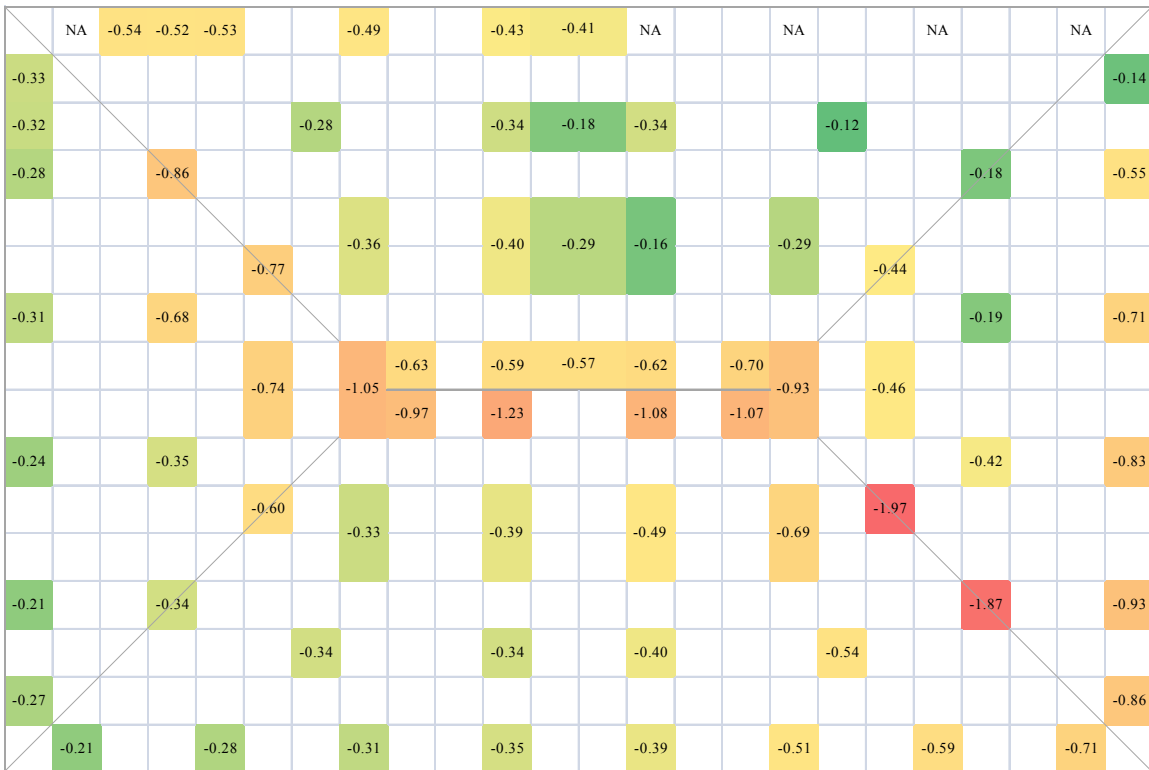

Figure 6.38. Pressure coefficients on Model 4 with a wind attack orientation of 180° and four PPPDs
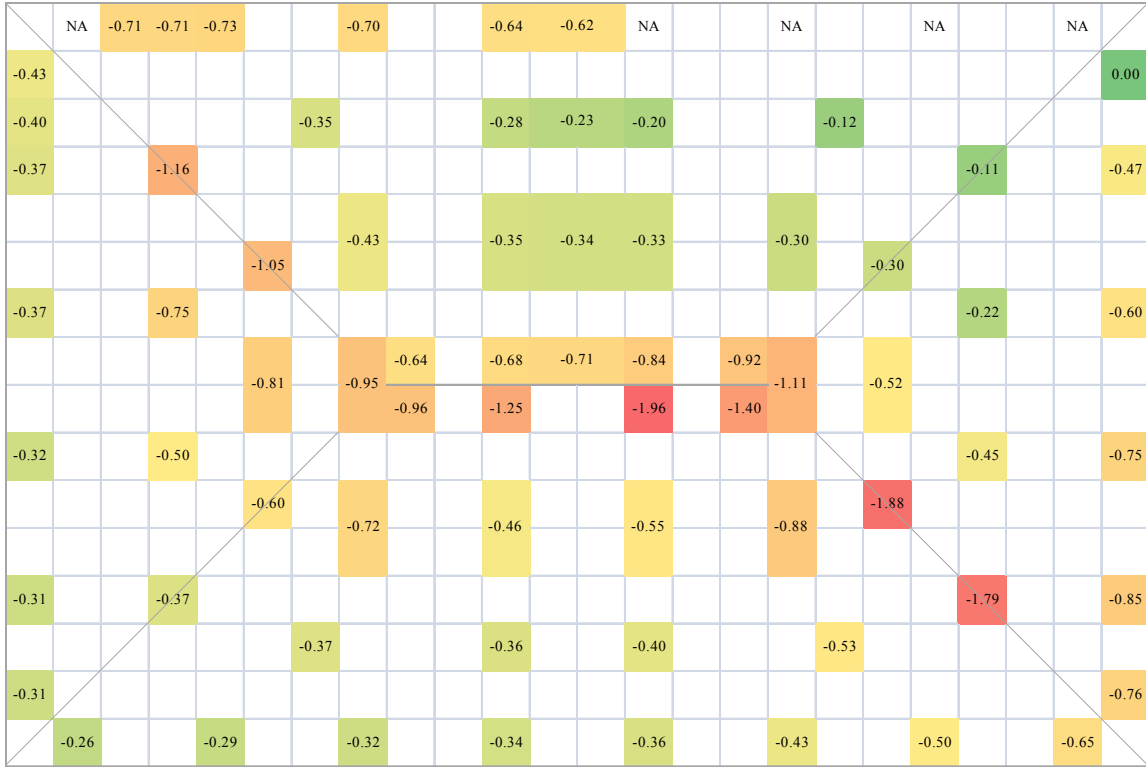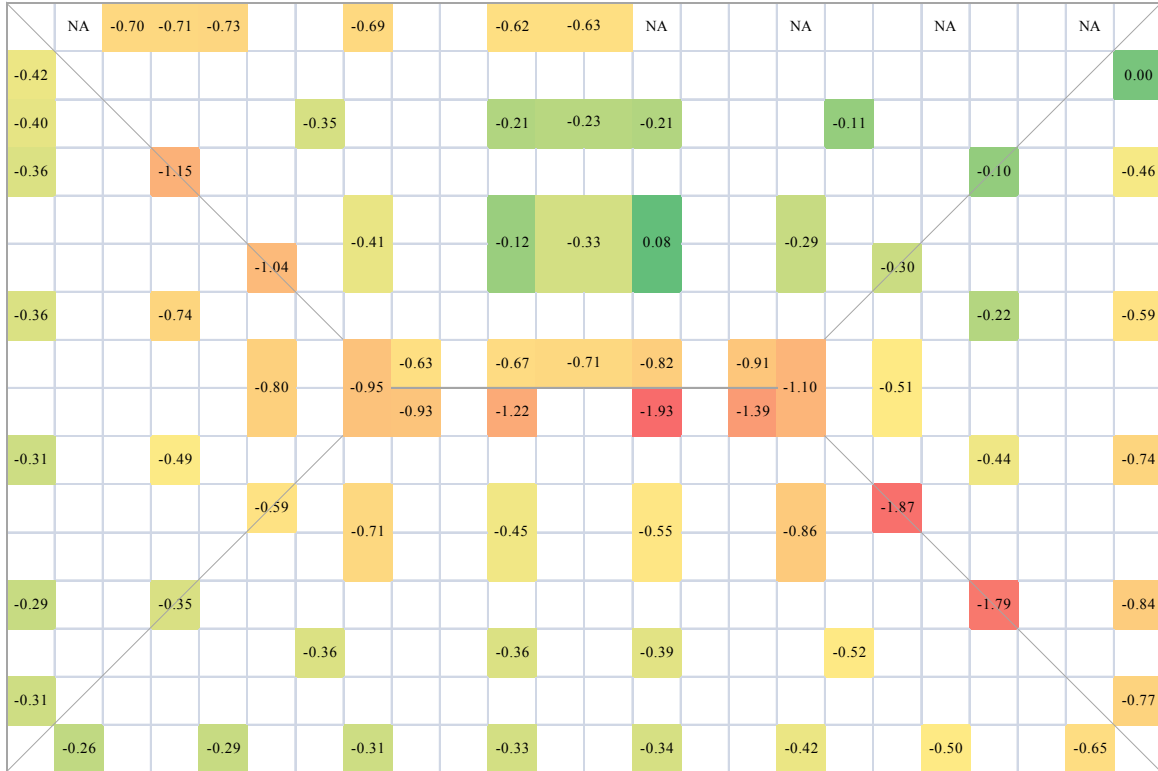
A comparison of figures with similar orientation among Figures 6.29 through 6.38 (i.e., Figures 6.37 and 6.38), shows that the protrusion of the PPPDs had minimal effect on the surrounding pressure port readings. However, the PPPD did significantly affect its own pressure port reading as stated in Section 5.4. For example, as shown in Figure 6.37, pressure ports 164, 166, 174, and 176 correspond to pressure coefficient readings of -0.16, -0.17, -0.14, and -0.11 respectively. In Figure 6.38, the same model orientation containing four PPPDs at the above port locations corresponds to pressure coefficient readings of 0.35, 0.33, 0.27, and 0.27 respectively, a significant variation in pressure magnitude. Also, previous discussions state that the pressure should be negative and thus the PPPD's causing of a positive pressure is inaccurate. A similar review of Figures 6.29 through 6.36 would reiterate the fact that the PPPDs adversely affected the pressure port data.

6.3.4 Pressures and Loads

After careful examination of the pressure data in Figures 6.18 through 6.28, an optimal tributary area layout was recommended for measuring pressure and is shown in Figure 6.39. Pressure data from the two densely populated regions of pressure ports in the corner region and in the center region of the low-rise building model was used to determine the optimal tributary areas. The two regions were examined in smaller parts according to the pressure distributions shown in Figures 6.18 through 6.28. Each part's average pressure was known by averaging data from all pressure ports within that region. Ports were then computationally removed from the part to see if the remaining ports could calculate a value close to the previously averaged value. This computational process was repeated until an acceptable pattern of ports within each part, for each wind angle of attack, was determined. In the end, the largest tributary area error was found to be 9% for the tributary area A7, as shown in Figure 6.40, for a wind angle of attack of 50°. The majority of the remaining tributary area errors fluctuated between 0 and ± 4%.

Near the hip roof ridges in Figure 6.39, like symbols designate tributary areas. Each symbol represents a 1.5 in. by 1.5 in. square section of the roof. For regions away from the roof ridges and edges in the figure, the tributary areas are outlined. Area partitions shown in Figure 6.39 are represented in Figure 6.40 with the letter A, followed by a number. Each number corresponds to a particular part or region of the hip roof. In total, Figures 6.18 through 6.28 suggested that the hip roof be divided into 84 regions, as shown in Figures 6.39 and 6.40.
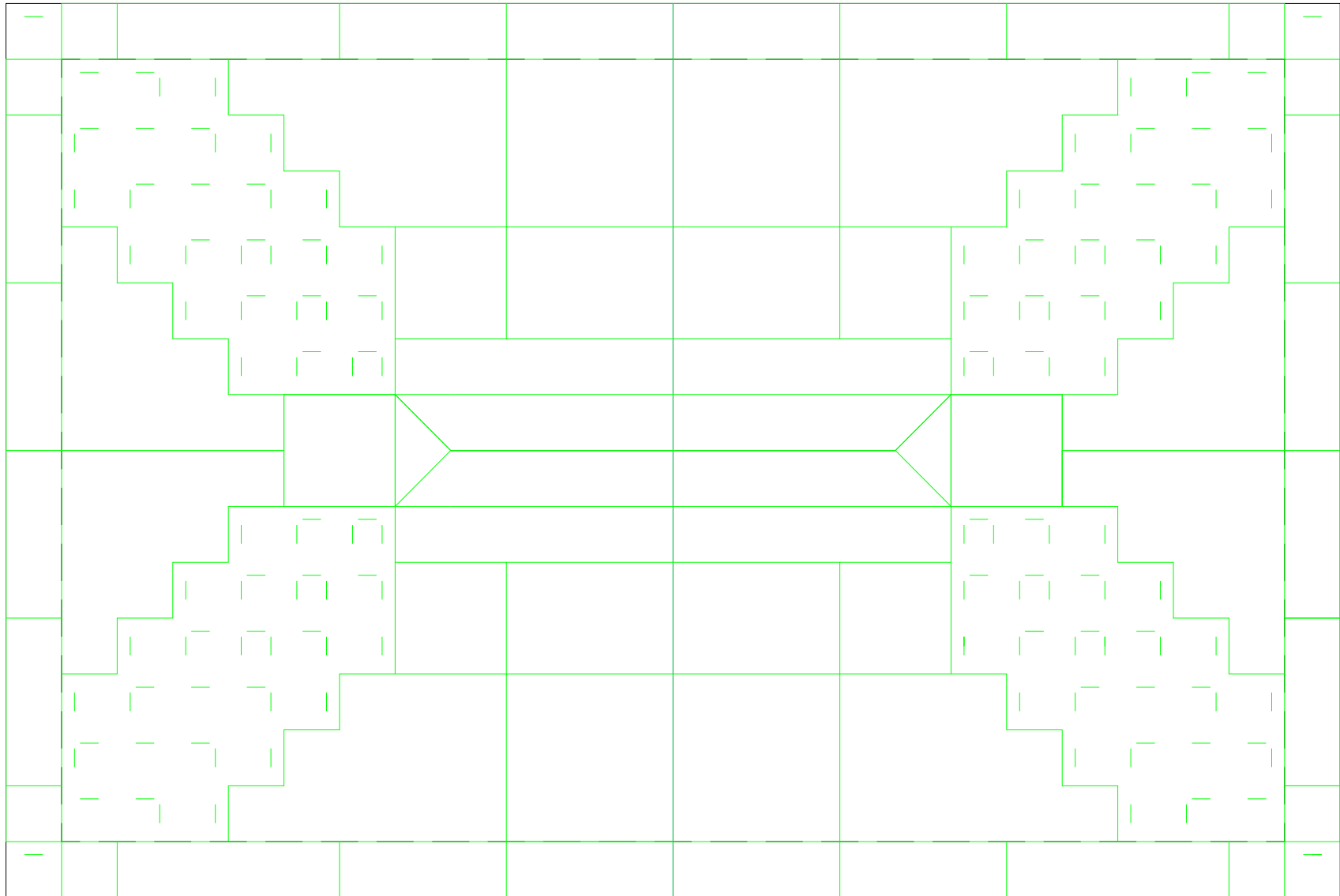
Figure 6.39. Optimal tributary area pressure distribution profile for the low-rise building

Shown in Figure 6.40 is the pressure data collected for the 8.5 mph, 0° case. Refer to Table 6.3 for the other wind load cases and model orientations tested. The pressure values shown in Figure 6.40 are displayed in Pascal units as measured by the ZOC. The values were converted to pounds per square inch and then multiplied by the regional area to obtain the calculated uplift forces shown in Table 6.2. Along with roof pressures, eave and internal pressure were factored into the total uplift force of Model 4. Figure 6.4 illustrates the locations of the eight eave ports and Table 6.1 displays the pressure value recorded by the ZOC at each port location. Table 6.1 also displays the four internal pressure port values as measured by the ZOC. The combination of area, roof, eave, and internal pressure data is shown in Table 6.2. After summing the roof, eave, and internal force data, the pressure values indicated an uplift force of 0.42 pounds due to a 0° wind directional force at 8.5 mph. Similar data was recorded and calculations were made to collect the uplift force data shown in Table 6.3.

A73	NA	A78	A78	-4.0	A78	A79	-4.8	A79	A80	-4.4	A80	A81	NA	A81	A82	-4.8	A82	A83	0.9	A83	A83	NA	A74
-2.8	A73	A59	A66	A69	A69	A69	A69	A69	A70	A70	A70	A71	A71	A71	A72	A72	A72	A72	A72	A67	A64	A74	-3.3
A65	A52	A73	A59	A66	A69	-4.4	A69	A69	A70	-4.7	A70	A71	-3.7	A71	A72	A72	-3.9	A72	A67	A64	A74	A57	A68
-2.5	A51	A52	-5.4	A59	A66	A69	A69	A69	A70	A70	A70	A71	A71	A71	A72	A72	A72	A67	A64	-4.9	A57	A58	-2.6
A65	A46	A51	A52	A53	A59	A66	-4.0	A60	A61	-4.1	A61	A62	-4.2	A62	A63	-4.6	A67	A64	A56	A57	A58	A49	A68
A45	A46	A46	A51	A52	-4.5	A59		A60	A61		A61	A62		A62	A63		A64	-5.2	A57	A58	A49	A49	A50
-3.9	A46	A46	-3.4	A51	A52	A53	A54	A54	A54	A54	A54	A55	A55	A55	A55	A55	A56	A57	A58	-3.3	A49	A49	-3.1
A45	A46	A46	A46	A46	-3.8	A39	-6.3	-4.2	A47	-4.3	A47	A48	-4.3	A48	-4.0	-6.9	A44	-4.1	A49	A49	A49	A49	A50
A35	A27	A27	A27	A27		A39		-3.9	A41	-2.4	A41	A42	-1.0	A42	-3.8		A44		A34	A34	A34	A34	A36
-3.7	A27	A27	-3.8	A25	A22	A28	A37	A37	A37	A37	A37	A38	A38	A38	A38	A38	A33	A23	A26	-4.4	A34	A34	-4.2
A35	A27	A27	A25	A22	-10.3	A12	-2.8	A29	A30	-1.6	A30	A31	-2.4	A31	A32	-2.9	A19	-10.8	A23	A26	A34	A34	A36
A21	A27	A25	A22	A28	A12	A13		A29	A30		A30	A31		A31	A32		A18	A19	A33	A23	A26	A34	A24
-4.9	A25	A22	-12.5	A12	A13	A14	A14	A14	A15	A15	A15	A16	A16	A16	A17	A17	A17	A18	A19	-12.5	A23	A26	-5.9
A21	A22	A1	A12	A13	A14	-3.8	A14	A14	A15	-1.5	A15	A16	-1.1	A16	A17	A17	-2.4	A17	A18	A19	A10	A23	A24
-7.4	A1	A12	A13	A14	A14	A14	A14	A14	A15	A15	A15	A16	A16	A16	A17	A17	A17	A17	A17	A18	A19	A10	-6.8
A1	-5.2	A3	A3	-7.7	A3	A4	-6.6	A4	A5	-4.9	A5	A6	-4.1	A6	A7	-5.8	A7	A8	-8.5	A8	A8	-7.0	A10

Figure 6.40. Tributary areas and measured pressure values used to calculate the uplift force on the low-rise building model oriented at 0° when subjected to a wind load corresponding to 8.5 mph at eave height

Table 6.1. Eave and internal pressure values used to calculate uplift force on the low-rise building model oriented at 0° when subjected to a wind load corresponding to 8.5 mph at eave height

Port	Eave Pressure Ports								Internal Ports			
	191	192	193	194	195	196	197	198	199	200	201	202
Pressure (Pa)	-3.5	1.1	-7.1	-7.7	-5.6	-5.2	-5.7	-3.4	-1.4	-1.5	-0.3	0.7

Table 6.2. Roof, eave, and internal tributary areas, pressure values, forces, and total uplift force

	A1	A2	A3	A4	A5	A6	A7	A8	A9	A10	A11	A12	A13	A14	A15	A16	A17	A18	A19	A20
Area (in²)	9.5	2.4	9.5	7.1	7.1	7.1	7.1	9.5	2.4	9.5	2.4	11.9	9.5	28.5	21.3	21.3	28.5	9.5	11.9	2.4
Avg. Pressure (Pa)	-12.5	-5.2	-7.7	-6.6	-4.9	-4.1	-5.8	-8.5	-7.0	-12.5	-7.4	NA	NA	-3.8	-1.5	-1.1	-2.4	NA	NA	-6.8
Avg. Pressure (psi)	0.00	0.00	0.00	0.00	0.00	0.00	0.00	0.00	0.00	0.00	0.00	-	-	0.00	0.00	0.00	0.00	-	-	0.00
Force (lb)	-0.02	0.00	-0.01	-0.01	0.00	0.00	-0.01	-0.01	0.00	-0.02	0.00	-	-	-0.01	0.00	0.00	-0.01	-	-	0.00

	A21	A22	A23	A24	A25	A26	A27	A28	A29	A30	A31	A32	A33	A34	A35	A36	A37	A38	A39	A40
Area (in²)	7.1	11.9	11.9	7.1	9.5	9.5	23.7	7.1	9.5	14.2	14.2	9.5	7.1	23.7	7.1	7.1	11.9	11.9	9.5	2.4
Avg. Pressure (Pa)	-4.9	NA	NA	-5.9	NA	NA	-3.8	-10.3	-2.8	-1.6	-2.4	-2.9	-10.8	-4.4	-3.7	-4.2	NA	NA	-3.8	-6.3
Avg. Pressure (psi)	0.00	-	-	0.00	-	-	0.00	0.00	0.00	0.00	0.00	0.00	0.00	0.00	0.00	0.00	-	-	0.00	0.00
Force (lb)	0.00	-	-	-0.01	-	-	-0.01	-0.01	0.00	0.00	0.00	0.00	-0.01	-0.01	0.00	0.00	-	-	0.00	0.00

	A41	A42	A43	A44	A45	A46	A47	A48	A49	A50	A51	A52	A53	A54	A55	A56	A57	A58	A59	A60
Area (in²)	10.7	10.7	2.4	9.5	7.1	23.7	10.7	10.7	23.7	7.1	9.5	11.9	7.1	11.9	11.9	7.1	11.9	9.5	11.9	9.5
Avg. Pressure (Pa)	-3.2	-2.4	-6.9	-4.1	-3.9	-3.4	-4.2	-4.1	-3.3	-3.1	NA	NA	-4.5	NA	NA	-5.2	NA	NA	NA	-4.0
Avg. Pressure (psi)	0.00	0.00	0.00	0.00	0.00	0.00	0.00	0.00	0.00	0.00	-	-	0.00	-	-	0.00	-	-	-	0.00
Force (lb)	0.00	0.00	0.00	-0.01	0.00	-0.01	-0.01	-0.01	-0.01	0.00	-	-	0.00	-	-	-0.01	-	-	-	-0.01

	A61	A62	A63	A64	A65	A66	A67	A68	A69	A70	A71	A72	A73	A74	A75	A76	A77	A78	A79	A80
Area (in²)	14.2	14.2	9.5	11.9	7.1	9.5	9.5	7.1	28.5	21.3	21.3	28.5	9.5	9.5	2.4	2.4	2.4	9.5	7.1	7.1
Avg. Pressure (Pa)	-4.1	-4.2	-4.6	NA	-2.5	NA	NA	-2.6	-4.4	-4.7	-3.7	-3.9	-5.4	-4.9	-2.8	-3.3	NA	-4.0	-4.8	-4.4
Avg. Pressure (psi)	0.00	0.00	0.00	-	0.00	-	-	0.00	0.00	0.00	0.00	0.00	0.00	0.00	0.00	0.00	-	0.00	0.00	0.00
Force (lb)	-0.01	-0.01	-0.01	-	0.00	-	-	0.00	-0.02	-0.01	-0.01	-0.02	-0.01	-0.01	0.00	0.00	-	-0.01	0.00	0.00

	A81	A82	A83	A84		
Area (in²)	7.1	7.1	9.5	2.4		
Avg. Pressure (Pa)	NA	-4.8	0.9	NA		
Avg. Pressure (psi)	-	0.00	0.00	-	**Roof Force**	
Force (lb)	-	0.00	0.00	-	-0.39	

	E1	E2	E3	E4	E5	E6	E7	E8	Internal Ports
Area (in²)	6.8	45.0	6.8	27.0	27.0	6.8	45.0	6.8	864
Avg. Pressure (Pa)	3.5	-1.1	7.1	7.7	5.6	5.2	5.7	3.4	-0.6
Avg. Pressure (psi)	0.00	0.00	0.00	0.00	0.00	0.00	0.00	0.00	-0.0001
Force (lb)	0.00	-0.01	0.01	0.03	0.02	0.01	0.04	0.00	-0.078

Uplift Force (lb)
0.42

**Table 6.3. Three model orientations and four wind velocities used to produce twelve uplift forces**

Model Orientation (°)	0	45	90	0	45	90	0	45	90	0	45	90
Eave Velocity (mph)	8.5	8.5	8.5	18	18	18	28	28	28	38	38	38
Uplift Force (lb)	0.42	0.62	0.45	2.59	3.03	2.25	6.68	7.35	5.54	12.32	13.56	10.37

Unfortunately, the JR3 force data was deemed inadmissible because the largest recorded uplift force by the JR3 was 0.5 pounds for any orientation and wind velocity, which is considerably less than the 15 pounds the JR3 is capable of measuring. It was concluded that the model dimensions were too large for one JR3 located in the center of the model to capture uplift force accurately. Thus, the tributary areas shown in Figure 6.39 were used in conjunction with the force calculation shown in Table 6.2 to calculate the uplift forces shown in Table 6.3. Equation 6.1 suggests the uplift force trend as the cross sectional area (B) and the velocity (U) are changed.

$$\overline{F_L} = (\frac{1}{2}\rho U^2)BC_L \qquad\qquad\qquad\qquad \text{(Eq. 6.1)}$$

Assuming the air density (ρ) and force coefficient of lift (C_L) were constant throughout the low rise building model tunnel tests, then according to Eq. 6.1 and as shown in Table 6.3, the mean lift force ($\overline{F_L}$) should have been largest in magnitude for the model orientation of 0° and eave velocity of 38 mph because this is when the amount of model area facing the wind and wind velocity were the greatest.

As a result of confidence in pressure data in Tables 6.1 through 6.3, Figures 6.41 and 6.42 have been drawn to show the recommended pressure port locations. Each tributary area contains the amount and location of pressure ports needed to accurately quantify the pressure for that region for any wind angle of attack. As discussed in Chapter 2 and shown in Figure 6.42, a more dense array of pressure ports is needed near the roof edges, ridges and corners than are needed elsewhere on the roof. As previously stated, pressure fluctuates considerably near these roof areas. Note that four pressure ports from the original model have been removed, while 28 roof and 8 eave ports have been added as shown in Figure 6.41 and 6.42. The 28 roof pressure ports are represented as circle-pluses and the 8 eave pressure ports are represented as dashed ellipses in Figures 6.41 and 6.42. In total, 92 roof pressure ports, 8 eave pressure ports, and 4 internal pressure ports are recommended for the low-rise building in the field to be able to correlate the load cell force data to pressure data.
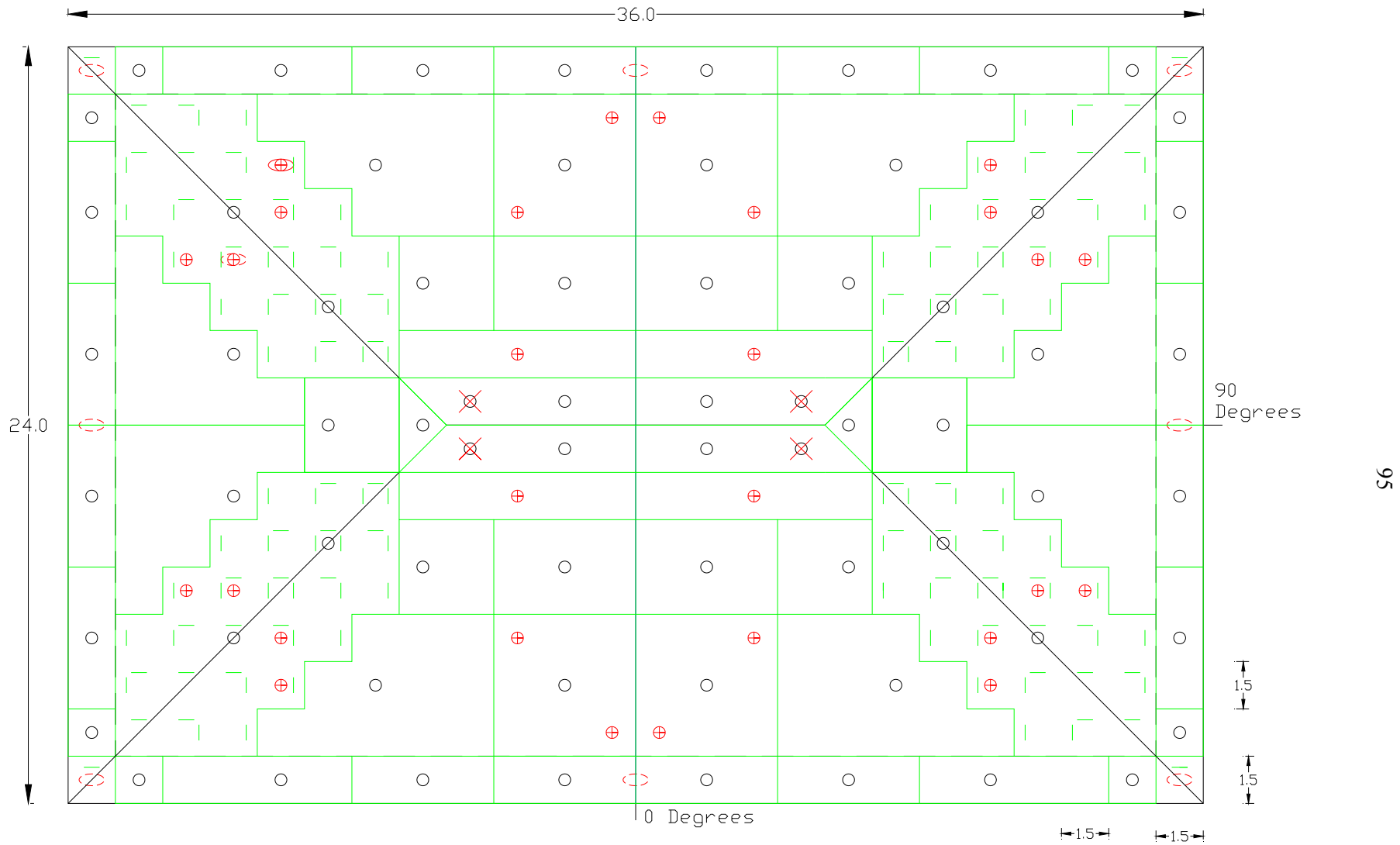
Figure 6.41. Illustration of the 92 roof pressure ports, corresponding tributary areas denoted by similar symbols or an outline, and 8 eave pressure ports (All dimensions are in in.)

Of the four low-rise building model tests, two produced conclusive results. The results from the roof pressure distribution and the pressure port protection device tests are conclusive. The results from the fundamental variable and pressure and load tests are not conclusive. Sections 6.3.1 through 6.3.4 explained the low rise building model results and how each objective for the model was satisfied or not satisfied. As was shown throughout Chapter 6, all of the data collected was important and informative, but only some of the data produced conclusive results.

Chapter 7: Summary, Conclusions, and Recommendations

Following a summary of the work completed in this report, conclusions drawn from the study and recommendations are presented in this chapter.

7.1 SUMMARY

Four different models were wind tunnel tested at ISU for this research project. Model 1 was rectangular in shape with a length of 15 inches, a width of 12 inches, and a height of 4.5 inches. The model was tested in the Bill James Wind Tunnel where it was subjected to a free flow wind load. A total of 38 pressure ports were strategically placed on the model's front and top surfaces to better understand: 1) the pressure acquisition equipment, 2) the affects of single-port versus multiple-port pressure transducers, 3) the affects of port diameter size, and 4) the possibility of interpolating pressure data between ports.

Test model 2 was cubic in shape with a length, width, and height of 22 inches. The model was tested in the AABL Wind and Gust Tunnel at ISU and was subjected to a turbulent, suburban boundary layer wind load. A total of 77 pressure ports were strategically placed on the model's front and top surfaces to better understand the affects of: 1) pressure port diameter, 2) tube diameter, 3) tube length, 4) transducer type, and 5) surface roughness on pressure readings. Conclusions for Model 2 tests are stated below.

Model 3 was a partial roof and wall with a length of 20.58 inches, a width of 24 inches, a height of 20 inches, and a roof pitch of 1:3. It was tested in the AABL Wind and Gust Tunnel at ISU and was subjected to a suburban boundary layer wind load. A total of 27 pressure ports were placed on the model's roof surface to better understand the effects of: 1) pressure transducers used in the field, 2) surface roughness, and 3) the pressure port protection device (PPPD).

Test model 4 was a 1:16 model of the low-rise building located in Florida. It was a hip roof model with roof edge lengths of two feet and three feet and a roof pitch of 1:3. Tested in the AABL Wind Tunnel at ISU, the model was subjected to a coastal boundary layer wind load ranging from 0 to 90°. A total of 202 pressure ports, with 190 on the roof surface, eight under the roof eave, and four inside the model, were used to better understand: 1) the affects of the basic test variables, 2) the pressure distribution on the low-rise building, and 3) the affect of the PPPD on pressure readings. Also, a force measuring device (JR3) was attached at the base of Model 3 in an attempt to directly measure the uplift/downward force of the roof on the walls due to wind loading.

7.2 CONCLUSIONS

Conclusions drawn from different model tests are as follows:

Model 1:

    • There was a basic understanding of wind tunnel testing and pressure data analysis procedures.

    • The single-port pressure transducers were accurate.

    • Effect of pressure port diameter on pressure readings needed to be studied further.

    • The possibility of interpolating pressure data between ports needed further studying.

Model 2:

    • An increase in pressure port diameter, tube diameter, and tube length all corresponded to a decrease in pressure magnitude.

    • An increase in surface roughness corresponded to an increase in pressure magnitude.

    • Similar to results from Model 1, the single-port pressure transducers compared well to the multiple-port lab pressure transducer.

Model 3:

    • Setra pressure transducers used in the field compared well to the lab pressure transducer.

    • Failure to scale the shingles resulted in inaccurate pressure values for the surface roughness portion of the tests.

    • The PPPD adversely affected pressure readings.

Model 4:

    • Fundamental variable results were inconclusive.

    • Setra pressure transducers used in the field compared well to the lab pressure transducer for mean pressures but not so well for fluctuating pressures.

    • The PPPD adversely affected pressure readings.

    • Critical pressure regions on the hip roof were located near the corners, ridges, and edges of the low-rise building.

    • While some of the pre-existing pressure port locations were helpful to understand the pressure distribution, the distribution of ports could be more efficient and the recommendation for redistribution of ports is given below.

    • The relatively large size of the model caused inaccurate readings by the JR3 for load results.

7.3 RECOMMENDATIONS

First, the Setra pressure transducer, tube length, tube diameter, and port size used to measure pressure on the low-rise building in the field are adequate. Model tests proved that while there may be some data influence on pressure due to these variables, it is within 4.0 to 7.0% and not significant for mean pressures. Most importantly, the transducer type, tube length, tube diameter, and port size are consistent among all ports on the low-rise building in the field. Thus, the use of the aforementioned equipment should continue.

Secondly, the pressure port protection device, used in the field to prevent water from damaging the pressure transducer, caused inaccurate pressure readings. Data results for test models 3 and 4 suggested that the location of the port on the side of the PPPD caused the inaccurate readings. This observation was made after pressure port measurements changed significantly from positive to negative values as the model orientation changed. The significant pressure changes occurred because pressure transducers are designed to measure pressure normal to the pressure port.

In the laboratory, a typical pressure tube end is mounted flush with the surface, producing a pressure reading normal to the surface. But when using the PPPD, by design, the port is flush with the side of the PPPD, producing pressure readings normal to the side of the PPPD. For pressure readings normal to the roof surface, as desired, the port should be on the top of the PPPD, but then water is more likely to enter the pressure measuring system. It is therefore recommended that the PPPD not be used in the field because it gives erroneous readings. Finally, further thought needs to be put into design of a pressure port protection device that will protect the pressure transducer from the elements of nature without compromising the pressure readings.

Thirdly, a few more strategically located pressure ports are needed to accurately quantify the entire pressure on the roof of the low-rise building. Figure 6.41 illustrates exactly where these extra pressure ports are needed. In addition, with the ultimate goal of correlating measured roof pressure data to measured load cell data, it is highly recommended that eight eave pressure ports and four internal pressure ports be installed on the low-rise building in the field.

Finally, if the JR3 load cell is used to quantify roof loads on walls in future wind tunnel tests, one JR3 should be placed at each of the model's four corners.

Chapter 8: References

App, Gregory and Yingzhao Chen (2006, June).   The Database-Assisted Design of Low-Rise Buildings: Aerodynamic Considerations for a Practical Interpolation Scheme. *Journal of Structural Engineering*, 132, 909-917.

Baker, C.J. (2001, October). Unsteady Wind Loading on a Wall. *Wind and Structures*, 4(5), 413-440.

Bienkiewicz, Bogusz and Yawei Sun (1992). Local Wind Loading on the Roof of a Low-Rise Building. *Journal of Wind Engineering and Industrial Aerodynamics,* 45(1), 11-24.

Chen, U., G.A. Kopp, and D. Surry (2002, June). Interpolation of Wind-induced Pressure Time Series with an Artificial Neurla Network. *Journal of Wind Engineering and Industrial Aerodynamics*, 90(6), 589-615.

Chen, Y., G.A. Kopp, and D. Surry (2003, May). Interpolation of Pressure Time Series in Aerodynamic Database for Low Buildings. *Journal of Wind Engineering and Industrial Aerodynamics*, 91(6), 737-765.

Chen, Xinzhong and Nan Zhou (2007). Equivalent Static Wind Loads on Low-Rise Buildings Based on Full-scale Pressure Measurements. *Engineering Structures,* 29, 2563-2575.

Cook, N.J. (1990). "The Designer's Guide to Wind Loading of Building Structures," Part 1 Background, damage survey, wind data, and structural classification. London: Butterworths.

Cook, N.J. (1990). "The Designer's Guide to Wind Loading of Building Structures," Part 2 Static Structures. London: Butterworths.

Holmes, J.D. (1990). Analysis and Synthesis of Pressure Fluctuations on Bluff Bodies Using Eigenvectors. *Journal of Wind Engineering and Industrial Aerodynamics ,* 33, 219-230.

Holmes, J.D., R. Sankaran, K.C.,S. Kwok, and M.J. Syme (1997, July-October). Eigenvector modes of Fluctuation Pressures on Low-Rise Building Models. *Journal of Wind Engineering and Industrial Aerodynamics*, 69-71, 697-707.

Hoxey, R.P., A.P. Roverson, B. Basara, and B.A. Younis (1993, December). Geometric Parameters That Affect Wind Loads on Low-rise Buildings: Full-scale and CFD Experiment. *Journal of Wind Engineering and Industrial Aerodynamics*, 50(1-3), 243-252.

Hoxey, R.P, P.J. Richards, and J.L. Short (2002, March). A 6 mm Cube in an Atmospheric Boundary Layer Flow. Part I. Full-scale and Wind-tunnel Results. *Wind and Structures*, 5(2-4), 165-176.

Hurricane Camille. (n.d.) Retrieved September 27, 2009, from Wikepedia: http://en.wikipedia.org/wiki/Hurricane_Camille

Jones, Emily (2008). Experimental Simulation of Atmospheric Boundary Layers and Extreme Gust Events (Master's dissertation, Iowa State University, 2008). URL: http://proquest.umi.com.proxy.lib.iastate.edu:2048/pqdlink?did=1510558511&Fmt=7&clientId=6 0760&RQT=309&VName=PQD

Letchford, C.W. and K.C. Mehta (1993, December). Distribution and Correlation of Fluctuating Pressures on the Texas Tech Building. *Journal of Wind Engineering and Industrial Aerodynamics,* 50, 225-234.

Levitan, Marc and Kishor Mehta (1992, October). Texas Tech Field Experiments for Wind Loads Part 1. Building and Pressure Measuring System. *Journal of Wind Engineering and Industrial Aerodynamics*, 43(3), 1565-1576.

Levitan, M.L., K.C. Mehta, W.P. Vann, and J.D. Holmes (1991, July-August). Field Measurements of Pressures on the Texas Tech Building. *Journal of Wind Engineering and Industrial Aerodynamics*, 38 (2-3), 227-234.

Major Hurricanes to Enter the Gulf Coast. (n.d.) Retrieved April 20, 2009, from Geocities: http://www.geocities.com/hurricanene/gulfcoast.htm

Mehta, Kishor and Douglas Smith(2004). Full-Scale Measurements for Wind Effects on Buildings. *Engineering Construction and Operations in Challenging Environments Earth and Space 2004: Proceedings of the Ninth Biennial ASCE Aerospace Divisions International Conference, Engineering, Consturctions and Operations in Challenging Environments Earth and Science 2004: Proceedings of the Ninth Biennial ASCE Aerospace Division International Conference, 2004,* 190-194.

Model 265 Very Low Differential Pressure. (n.d.). Retrieved August 15, 2008, from Setra: http://www.setra.com/tra/pro/p_hv_265.htm

National Hurricane Center. (2009). Hurricane Research Division. Retrieved May 4, 2009, from Web site: http://www.aoml.noaa.gov/hrd/tcfaq/tcfaqHED.html

Okada, Hisashi and Young-Cheol Ha (1992, October). Comparison of Wind Tunnel and Full-scale Pressure Measurement Tests on the Texas Tech Building. *Journal of Wind Engineering and Industrial Aerodynamics*, 43(4), 1601-1612.

Robertson, A.P., R.P. Hoxey, J.L. Short, W.A. Ferguson, and S. Osmond (1996). Full-scale Testing to Determine the Wind Loads on Free-standing Walls. *Journal of Wind Engineering and Industrial Aerodynamics*, 60(1-3), 123-137.

Sh. Ahmad and K. Kumar (2002, November). Wind Pressures on Low-rise Hip Roof Buildings. *Wind and Structures,* 5(6), 493-514.

Simiu, E. and Scanlan, R.H. (1996). Wind Effects on Structures: Fundamentals and Applications to Design. Third Edition. New York: John-Wiley and Sons, Inc.

Stathopoulos, T. (1980, May). PDF of Wind Pressures on Low-Rise Buildings. *Journal of Structural Division*, 106(5), 973-990.

Tamura, Y., H. Kikuchi, and K. Hibi (2001, December). Extreme Wind Pressure Distributions on Low-rise Building Models. *Journal of Wind Engineering and Industrial Aerodynamics*, 89(14-15), 1635-1646.

Tieleman, Henry W. (2003, December). Wind Tunnel Simulation of Wind Loading on Low-rise Structures: A Review. *Journal of Wind Engineering and Industrial Aerodynamics* , 91, 1627-1649.

Tieleman, H.W., R.E. Akins, and P. R. Sparks (1980, July). Comparison of Wind-tunnel and Full-scale Wind Pressure Measurements on Low-rise Structures. *Journal of Wind Engineering and Industrial Aerodynamics*, 8(1-2), 3-19.

Wu, F., Sarkar, P.P. and Mehta, K.C. (2001). Full-Scale Study of Conical Vortices and Roof Corner Pressures. *Wind and Structures, An International Journal*, Vol. 4, No. 2, pp. 131-146.

Wu, F., Sarkar, P.P. Mehta, K.C. and Zhao, Z. (2001). Influence of Incident Wind Turbulence on Pressure Fluctuations near Flat-Roof Corners. *Journal of Wind Engineering and Industrial Aerodynamics*, Vol. 89, pp. 403-420.

Zhao, Z., Sarkar, P.P. and Mehta, K.C. and Wu, F. (2002). Wind-Flow Characteristics and their Loading Effects on Flat Roofs of Low-Rise Buildings. *Wind and Structures, An International Journal*, Vol. 5, No. 1, pp. 25-48.

Acknowledgements

A special thanks to my co-major professors, Dr. Sri Sritharan in the Civil Engineering department and Dr. Partha Sarkar in the Aerospace Engineering department for their advice and patience throughout my research project. I thoroughly enjoyed their classes, am thankful for Dr. Sri's research foresight and guidance, and am grateful for the knowledge and the once-in-a-lifetime opportunity from Dr. Sarkar to work in the wind tunnel.

I would like to thank the FPL group from Madison, Wisconsin for providing many of the resources and information needed for this research project. Their promptness in answering my questions and approving my design plans allowed me to move forward efficiently and effectively. Thanks for trusting me with your research.

I would like to thank my committee members Dr. Terry Wipf in the Civil Engineering department and Dr. Thomas Rudolphi in the Aerospace Engineering department. Also, I would like to thank Bill Rickard, Doug Wood, Wei Zhang, and Matt Hawkins for all their help in the lab. Without them, I would still be trying to comprehend the idea of recording wind pressure.

Finally, I would like to thank Amate House for the encouragement to follow my dream and study engineering at Iowa State, the DMACC Bears for letting me coach baseball during graduate school, my family for constant support and encouragement, my wife, Nikki, for her endless love and patience, and the Lord for blessing us with our daughter Macie and a rewarding three year experience at Iowa State.